Characterisation of Aluminium Matrix Syntactic

Foams under Static and Dynamic Loading

Thesis submitted in accordance with the requirement of the

University *of* Liverpool for the degree of

Doctor of Philosophy

By

Mohamed Ali Al Tenaiji

March 2014

ACKNOWLEDGMENTS

LIST OF PUBLICATIONS

1. Altenaiji M, Schleyer G and Zhao Y. Characterisation of Aluminium matrix syntactic foams under static and dynamic loading. Protect 2011: Performance, Protection & Strengthening of Structures under Extreme Loading, Lugano Switzerland, 2011.

2. Altenaiji M, Schleyer G and Zhao Y. Characterisation of Aluminium matrix syntactic foams under static and dynamic loading. Applied Mechanics and Materials. 2012;82:142-147.

3. Altenaiji M, Guan Z, Cantwell W and Zhao Y. Characterisation of aluminium matrix syntactic foams under dynamic loading. ICAM2013, Kuala-lumpur Malaysia, 2013.

4. Altenaiji M, Guan Z, Cantwell W, Zhao Y and Schleyer G. Characterisation of aluminium matrix syntactic foam under drop weight impact. Journal of Materials Design. 2014;59:296-302.

ABSTRACT

In this study, aluminium matrix syntactic foams reinforced with several types of ceramic micro-sphere were produced by pressure infiltration. The mechanical properties of a range of aluminium matrix syntactic foams were investigated in order to optimise the composition and structure to find the best configuration in terms of high energy absorption capability, and to validate the finite element predictions against the corresponding experimental results.

Initially, the compressive behaviour of six different types of aluminium matrix syntactic foam was evaluated. It was shown that the size of the ceramic micro-spheres, the grade of the aluminium matrix and the volume fraction of the aluminium matrix all have a significant influence on the compressive strength and energy absorption capability of the material. Then, the three-point bending and shear fracture properties of aluminium syntactic foams were evaluated. These tests indicated that density plays an important role in determining the stiffness, specific energy absorption and ultimate flexural strain. Here, it was found that the specific energy absorption related to shear was lower than that corresponding to flexure. Following this, the behaviour of the syntactic foams under low velocity impact was characterised and the underlying failure mechanisms were identified to evaluate their effective mechanical performance. It was found that the aluminium syntactic foams subjected to drop-weight impact have 20–30% higher plateau values than samples subjected to the equivalent level of quasi-static compression. Subsequently, the Split Hopkinson Pressure Bar technique was used to investigate the behaviour of the material at high strain-rates, which highlighted the material sensitivity of aluminium syntactic foams under high strain-rate loading.

Following this, terminal ballistic tests were conducted to determine the perforation resistance of the aluminium syntactic foams. The results showed that the syntactic foams have the ability to prevent the perforation of projectile velocities up to 120 m/s. Finally, blast tests were performed to investigate the influence of the charge mass and sample thickness on the dynamic response of the syntactic foams. The results showed that syntactic foams with a thickness of 14 mm have the capability to sustain a blast load of 4.82 Ns.

Finite element models were developed to simulate the structural behaviour of aluminium syntactic foams subjected to various quasi-static and dynamic loads. Here, an elasto-plastic model with both ductile and shear failure criteria was employed to predict the material performance. The rate-dependent response of the foam was considered by a stress-ratio based model to take strain-rate effects into account. The numerical simulations were compared with their corresponding experimental results with reasonably good correlation. In general, the essential features of the aluminium syntactic foams tested under different loading regimes were captured by the FE models, including load-displacement traces, deformation and failure modes.

CHAPTER 5: FINITE ELEMENT MODELLING

CHAPTER 6: FINITE ELEMENT SIMULATION RESULTS AND DISCUSSION

CHAPTER 7: Conclusions and Recommendations for Future Work

REFERENCES

LIST OF FIGURES

LIST OF TABLES

CHAPTER 1 : INTRODUCTION

This chapter contains a brief introduction to aluminium matrix syntactic foams, aluminium alloys and ceramic micro-spheres, along with their applications. Additionally, this chapter discusses matrix syntactic foam, which covers types of matrix and ceramic microspheres, the method of fabrication and the effect these parameters have on the material response under static and dynamic loading. Moreover, the chapter also discusses the motivation and scope of the research herein and the aims and objectives of the study, as well as gives a detailed outline of the thesis.

1.1   Background

The impact and shock resistance of engineering structures is currently of great interest to the engineering community and government agencies. This is primarily due to the urgent need to provide protection against possible terrorist attacks. Development of lightweight, strong and ductile materials to be used in making military vehicles for this purpose is a formidable challenge facing the materials community. Under blast or impact loading, a structure may undergoes large plastic deformations leading to partial or total failure. The important characteristics (Hanssen et al., 2002) of such a structural response are: i) deformation mode and failure mode; ii) impulse and shock wave transfer; and iii) energy absorption through plastic deformation.

Aluminium foams have become more important due to their physical and mechanical properties (Banhart, 2001). However, the foaming process can have a detrimental effect on the properties of the foam (Babcsan et al., 2007). Metal foams have applications

restricted to instances where compressive strength is not the primary design criterion due to their lower mechanical properties compared to the base metal, such that they cannot be used as load-bearing materials (Gibson and Ashby, 1999). An alternative method to enhance the Young's modulus and strength of the foam has been developed, which incorporates porosity in materials using hollow particles as fillers to produce a syntactic foam (Kiser et al., 1999). The difference between aluminium foam and aluminium matrix syntactic foam is that the hollow particles in the syntactic foam are infiltrated by the matrix, whereas the hollow particles in conventional foams are filled by air, as shown in Figure 1.1.
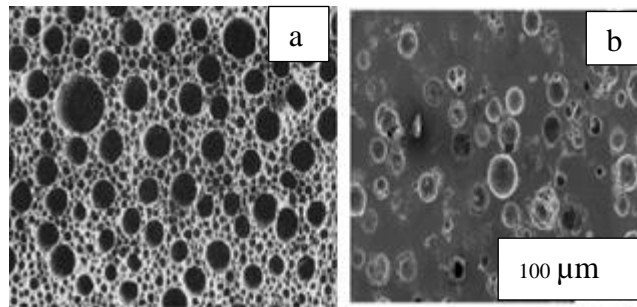
Figure 1.1. (a) Microstructure of aluminium foam; (b) microstructure of aluminium matrix syntactic foam.

The material used in this research is an aluminium matrix syntactic foam. Aluminium matrix syntactic foam is a type of composite material. It has a porous structure consisting of a metal matrix filled with ceramic microspheres. Metal matrix syntactic foam has a higher compressive strength than a polymer matrix syntactic foam and a superior energy absorption capacity to that of aluminium foam, primarily due to its higher plateau strength and densification strain. The compressive strength of the material is related to the energy absorption capability of foams and is usually quantified by using measurable

stress–strain relationships. Syntactic foams usually show a long and flat stress–strain curve after initial yielding. The cell walls experience a continuous plastic collapse at a critical value, known as the 'plateau stress', until the material reaches a nominal densification strain (ε_D). The best energy-absorbing material therefore must have the longest plateau before reaching this strain. These material specifications highlight the properties that should be chosen to withstand high strain-rate loading.

1.2   Aluminium Alloys

Aluminium alloys are alloys of which aluminium is a dominant metal. Typically, the alloying elements in aluminium alloys include zinc, silicon, manganese, magnesium and copper. Their strength to weight ratio makes them a preferred choice for aerospace and other industries, where weight needs to be minimised. Aluminium alloys possess a variety of characteristics that make them useful materials for engineering structures. For a particular application, choosing the correct alloy requires consideration of its corrosion resistance, weldability, workability, formability, ductility, density, tensile strength and mechanical stiffness. The versatility of its properties renders aluminium the most widely used metal after steel. Approximately 29 million tonnes of aluminium are produced worldwide every year. Three quarters of this material is produced as a new material, whereas the remainder is produced by recycling, thereby saving energy. Aluminium is one of the lightest metals, with a strength to weight ratio greater than that of steel.

Aluminium exhibits various properties resulting in it being used in transport, packaging, energy generation, food preparation and electrical transmission applications. The

excellent strength to weight ratio of aluminium alloy makes it a prime material for the construction of trains, military vehicles, ships and aircraft.

The properties that give aluminium its versatility for these applications are as follows:

- lightweight;

- corrosion resistance;

- electrical and thermal conductivity;

- ductility.

In addition to all the advantages that are offered by aluminium, it also has some drawbacks, which are as follows:

- it is not as strong as steel;

- it is easily oxidised;

- it is not hard and scratches easily;

- it is more expensive than steel.

1.3   Ceramic Micro-spheres

Ceramic micro-spheres have two different inner structures, either porous or hollow. Both types have the same effective density and porosity. The shape of each ceramic micro-sphere is different. The hollow ceramic micro-spheres have a perfect spherical shape, while porous ceramic micro-spheres have a roundish shape with a rough surface as shown in Figure 1.2 (Tao, 2010).
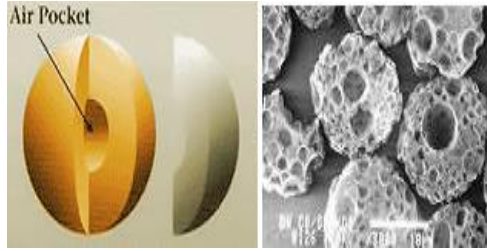
Figure 1.2. Hollow and porous ceramic microspheres (Walsh, 1997).

Ceramic micro-spheres are semi-transparent, with a fine particle size and a high strength. They are ideal for improving both hardness and filler loading, while at the same time providing gloss control. Ceramic micro-spheres offer a number of advantages owing to the following properties:

- low weight and volume;

- low thermal conductivity;

- transparency to UV down to 250 nm;

- high filler loadings due to their inert nature.

The main disadvantage of ceramic micro-spheres is their failure to absorb energy, which in turn affects their material properties.

1.4   Matrix Syntactic Foam

Matrix syntactic foams are composite materials that consist of a matrix incorporating porous or hollow ceramic particles. This type of foam is a new classification of materials that can be produced using several metals or polymer matrices and ceramic micro-spheres. It consists of a metal matrix with ceramic micro-spheres embedded in the matrix. A metal matrix can be composed of aluminium, steel, titanium or magnesium. The

ceramic micro-spheres can be a porous or hollow structure. In contrast, hollow metal spheres are rarely used. The size of the hollow ceramic micro-spheres determines the porosity of the matrix syntactic foam, as shown in Figure 1.3.
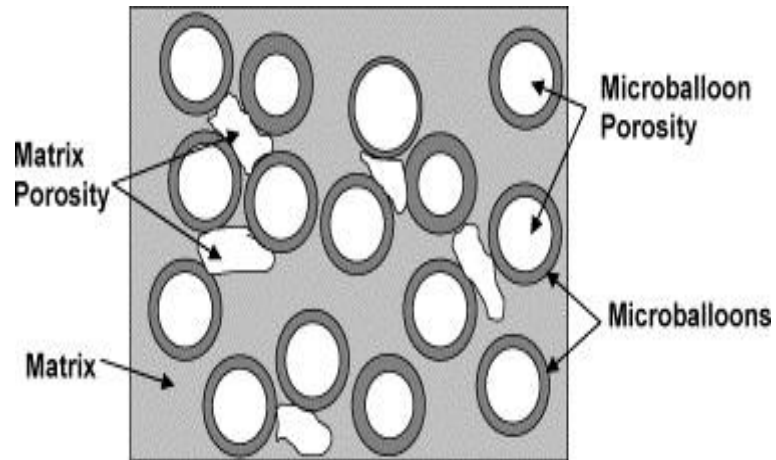
Figure 1.3. Schematic representation of the syntactic foam showing matrix porosities (Gupta and Ricci, 2006).

A matrix syntactic foam is considered as a light material with a high energy absorption capacity. Researchers (Rohatgi et al., 2011; Luong et al., 2013) have studied metal matrix syntactic foams, with a particular focus on the compressive behaviour and fabrication of these materials. The most commonly used method for manufacturing metal matrix syntactic foams is the melt infiltration (Tao and Zhao, 2009). In this method, molten metal is pressure-infiltrated in ceramic micro-spheres, as shown in Figure 1.4.
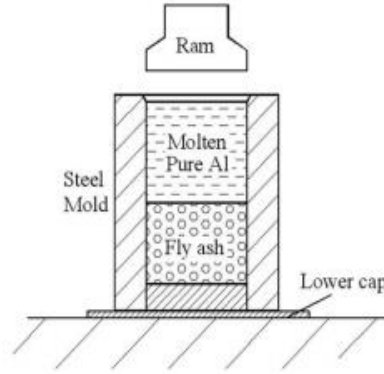
Figure 1.4. Schematic of the preparation of a metal syntactic foam by pressure infiltration (Zhang et al., 2009).

The volume fraction of the metal matrix to the ceramic micro-spheres has been studied by Orbulov (Orbulov and Majlinger, 2010). The volume fraction of the metal matrix can be reduced by embedding ceramic spheres with size distributions that are multimodal in nature. This increases the foam porosity. However, these types of foam deform under compression in a brittle mode, either by cracking or by shear, due to a high percentage volume of ceramic micro-spheres (Balch and Dunand, 2006). The brittle deformation can lead to a significant reduction in the plateau strength and energy absorption.

In comparison with fully dense alloys and metals, metal matrix foams show a high specific stiffness, a low density and a mechanical damping capacity, a high energy absorption capacity. This combination of characteristics makes metal foams an appealing choice for functional applications, as well as structural applications. Structural or functional applications of metal foams include sound-damping and fire-proof panels, foam sandwich cores, underwater buoyant structures and energy-absorbing packaging. Syntactic foams are a type of a composite foam. They consist of hollow spheres that are

embedded in a continuous matrix. These types of silica-alumina/aluminium spheres and alumina/aluminium spheres foams have a higher density as compared with the traditional aluminium foams that are manufactured, for example, by salt infiltration or gas entrapment in the melt. Moreover, they offer a high energy-absorption capability, isotropic mechanical properties and a high strength. Additionally, their closed cell geometry is appealing for its insulating and mechanical properties (Balch and Dunand, 2006).

Metal matrix syntactic foams are used in a variety of applications. For example, they are typically used in lightweight structures such as boat hulls, buoyancy modules for marine riser tensioners and autonomous underwater vehicles (AUV) in the marine industry, as shown in Figure 1.5 (Kudo, 2008).

Figure 1.5. Photograph of syntactic foam autonomous underwater
vehicle (Trellborg AEM).

Metal matrix syntactic foams are used as building materials such as acoustic isolation materials for rooms, artificial marble, wood and so forth. In addition, they are used in the automotive industry as bumpers for vehicles and as protective materials for the packaging industry, due to their high energy-absorption characteristics (Walsh, 1997). Other applications include blast mitigating materials, as shown in Figure 1.6, acoustically-

attenuating materials and radar-transparent materials. In addition, aluminium matrix syntactic foam is found to have a higher damping capacity than the matrix alloy (Rohatgi et al., 2011). Also, Zhang et al. (2009) suggest the use of aluminium matrix syntactic foams in crash energy absorption zones (Zhang et al., 2009).

Figure 1.6. Photograph of a syntactic foam blast mitigating material (Trelleborg AEM).

1.5   Motivation and Scope

Due to the limited knowledge of the characteristics of aluminium matrix syntactic foams under static and dynamic loading, this research aims to firstly undertake an experimental and finite element investigation into the response of such materials under quasi-static compression, three-point bending and shear loading. Following this, the dynamic response of the material will be studied under low and high velocity impact as well as under blast loading. The prediction of the load carrying capacity and energy absorption characteristics will be investigated.

1.6 Research Objectives

The main objective of this research is to investigate the best possible combination of aluminium matrix and ceramic micro-spheres for producing an energy-absorbing material that could be used in armoured vehicles. This objective will be achieved by fulfilling the following sub-objectives.

- **Fabrication of different types of aluminium matrix syntactic foams**

Identify the best combination of the aluminium matrix and ceramic micro-spheres for producing high energy absorption materials.

- **Characterisation of the syntactic foams under dynamic and static loading**

A series of experimental tests will be conducted to investigate the behaviour of aluminium matrix syntactic foams under static and dynamic loading, which include the energy absorption capability of the aluminium syntactic foams at very high strain-rate loading.

- **Use of the finite element (FE) analysis**

Finite element models will be developed to simulate the structural response of aluminium matrix syntactic foams under both static and dynamic loading. All models will be validated against the corresponding experimental results. It is expected that FE models will be used simulate a large number of cases which are not covered in the experimental work.

- **Studies on the effect of the tests on material parameters and performance**

Parametric studies using the validated FE models will be conducted on aluminium matrix syntactic foams. This is to analyse the effects of the sample dimensions, the size of the ceramic micro-spheres, the type of aluminium alloy, projectile velocity and explosive charge size on the response of the material.

1.7   Outline of the thesis

To achieve the objectives stated above, i.e. to acquire the best combination of aluminium matrix and ceramic micro-spheres for the synthesis of a high-strain rate energy absorbing material and to use numerical analyses to predict the response of aluminium matrix syntactic foams under quasi-static and dynamic loading, the thesis is divided into seven chapters as follows.

- Chapter 1 explains the significance of this work, as well as highlighting its main aim and the associated objectives for achieving the benefits of this study.

- Chapter 2 presents a literature review, focusing on relevant experimental work, theoretical analysis and numerical modelling of the aluminium matrix syntactic foam. Attention is focused on the characterisation of the material response under static and dynamic loading.

- Chapter 3 describes the experimental work conducted in this research. It is divided into three sections: the fabrication procedures to manufacture different types of aluminium matrix syntactic foams and the characterisation of the syntactic foams under quasi-static and dynamic loading.

- Chapter 4 presents and discusses the results obtained following tests on aluminium matrix syntactic foams.

- Chapter 5 describes the FE models using Abaqus/Standard and Abaqus/Explicit that are used in this research. This covers the simulations of the quasi-static and dynamic responses of aluminium matrix syntactic foams.

- Chapter 6 presents and discusses the simulation results obtained from numerical modelling on aluminium matrix syntactic foams.

- Chapter 7 presents the conclusions drawn from this study and the recommendations for future work.

CHAPTER 2: LITERATURE REVIEW

Over the past ten years, a wide range of polymeric and metallic cellular materials have been manufactured, with the goal of developing structures that are lightweight in nature. These are typically sandwich structures and are sufficiently strong. Such materials can be thought of as composites that are porous and constituted of spaces, which are connected with struts, shells or plates. Due to their high specific strength, low weight, good energy dissipation and high specific toughness features, they have found applications as the core in sandwich structures on a frequent basis. Commonly in such structures, the core should sustain crushing or indentation. On the other hand, the face-sheets offer bending strength to the structure. There are many studies available on the behaviour of metal foams in sandwich structures under different loading conditions; however, they are scattered throughout the literature. This chapter attempts to consolidate the literature in this field.

2.1   Cellular Materials

2.1.1   General

By definition, cellular materials are composites consisting of a solid material (e.g. a metal, or a polymer) and air in the formed cells. They consist of a network of solid ribs or plates, which are made up of lightweight materials that have the advantage of strength/weight ratio and stiffness/weight ratio over the solid material (Zhang, 2001). The properties of such materials are primarily dependent upon the shape and structure of the cells.

Man-made cellular materials can exist either in the form of a two-dimensional honeycomb structure or a three-dimensional foam. In nature, materials such as wood,

coral, leaves, bone and cancellous materials, etc. have a cellular structure. Such materials are usually efficient at absorbing energy and possess low densities. Primarily, the level of porosity within the material controls the energy absorption process.

Cellular materials and their properties have been explored extensively by researchers in previous decades (Gibson and Ashby, 1999). Over the past decade, metallic foams have been developed with a high porosity and have been used as engineering materials for the development of lightweight structures, typically sandwich-type structures, with adequate stiffness and strength (Davies and Zhen, 1983). Recently, there has been much research and numerous attempts to evaluate the properties, production methodologies and potential applications of such types of cellular material. These studies and researches have been widely reported in the literature (Davies and Zhen, 1983).

For the past ten years, a wide range of polymeric and metallic cellular materials have been created with the objective of developing lightweight structures (Zhu et al., 2010). The majority of these are sandwich structures. Cellular materials have high a strength and are lightweight with good energy-dissipation properties. For these reasons, they are often used as the core in a sandwich structure. In such structures, the core primarily sustains crushing or indentation, whereas the face sheets confer the structure with bending strength. Today, sandwich structures are used on a large scale in a broad variety of applications, such as packaging, ship manufacture, vehicle manufacture and in the defence industries. Cellular metals, which have microstructures and are stochastic in nature, can sustain enormous plastic deformation at a fixed level of stress (Zhu et al., 2010). Due to their extremely high energy absorption capabilities, such types of material are suitable for use as the core in a sandwich structure. Five types of cellular metal are

discussed in the following section, these being honeycombs, metal foams and textile and truss-based lattice materials.

Cellular materials can be classified into stochastic cells and periodic cells, depending on the topologies and geometry of their microstructure (Zhu et al., 2010). Stochastic cells have a random microstructure that can either be open or closed. On the other hand, periodic cells have two-dimensional channels, like a honeycomb structure or a three-dimensional structure, such as that of a truss or textile. The classification scheme of cellular materials is illustrated in Figure 2.1.
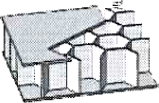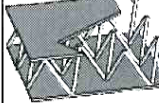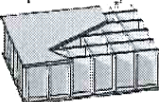
Figure 2.1. Hierarchical descriptions of cellular materials classification (Zhu et al., 2010).

2.1.1.1   Metal foams

Metal foams are amongst the most significant type of cellular materials. Metal foams are a new class of composite materials that have a low density. This class of materials

contains metals that have gas-filled pores as the solid material. The pores can be sealed in a similar way to that found in closed-cell devices. Additionally, the pores can be fashioned to form an interconnected network in a similar manner to open-cell foams. Metal foams have been reported to possess a range of physical and mechanical properties (Ashby et al., 2000). Cellular materials that have stochastic or periodic microstructures are configured to the core of sandwich panel structures (Zhu et al., 2010). The strength of a metal that is foamed has a proportional relationship to its density. A twenty percent dense material is twice as strong as ten percent dense material.

2.1.1.2   Syntactic foams

A syntactic foam is a type of composite material that has a low density and a higher strength and stiffness than metal foams. It can be produced by infiltrating molten metal into hollow ceramic spheres (Banhart, 2001).

2.1.1.3   Honeycombs

A honeycomb is composed of plates or sheets that form the edges of the unit cell. They can be configured in a different manner by rearranging the shape and size of the cells. The cells can be square, triangular, rectangular, hexagonal, circular or diamond shaped. Honeycomb materials can be used in heat exchangers, for energy absorption as well as in building constructions (Zhu et al., 2010).

2.1.1.4   Trusses and textiles

Trusses and textiles belong to a class of three-dimensional cellular materials. There are two types of cellular material with open-celled structures. A lattice material is composed

of struts that meet at a node, while textile structures consist of woven metal wires, which are bonded together, as shown in Figures 2.2 and 2.3, respectively.
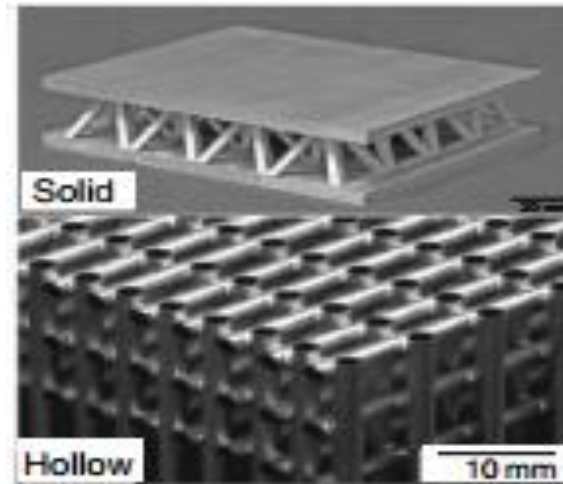
Figure 2.2. Solid and hollow lattice truss structures (Zhu et al., 2010).
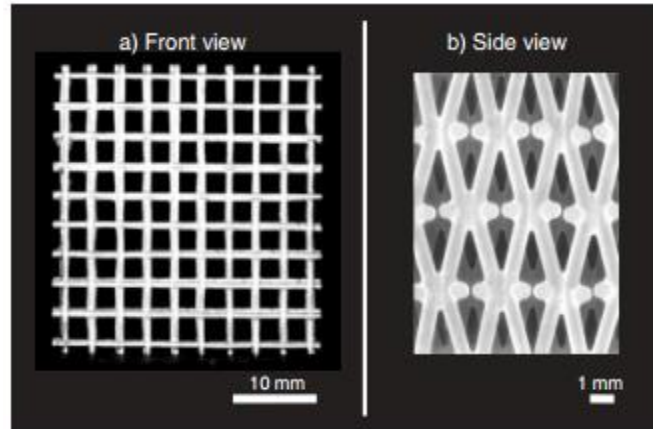
Figure 2.3. Two views of metal textile structures (Wadley, 2002).

Cellular materials can be used in a variety of applications. The choice of foam is based on the porosity (opened or closed cells), the size of the pores and the type of solid-material (metal, alloy, etc.). It has been noted that in the majority of applications the medium, which can be gaseous or liquid, needs to pass through the pores of the cellular material.

17

Therefore, these pores may need to have different degrees of connectivity. A few may require fully open cells to facilitate a high rate flow of fluid, whereas others may require partially open cells. On the other hand, in applications such as load-bearing structural applications, closed cells are required. The application of cellular materials is classified in accordance with the extent of connectivity required. Additionally, the applications are also classified depending on whether they are primarily structural or functional, as illustrated in Figure 2.4.
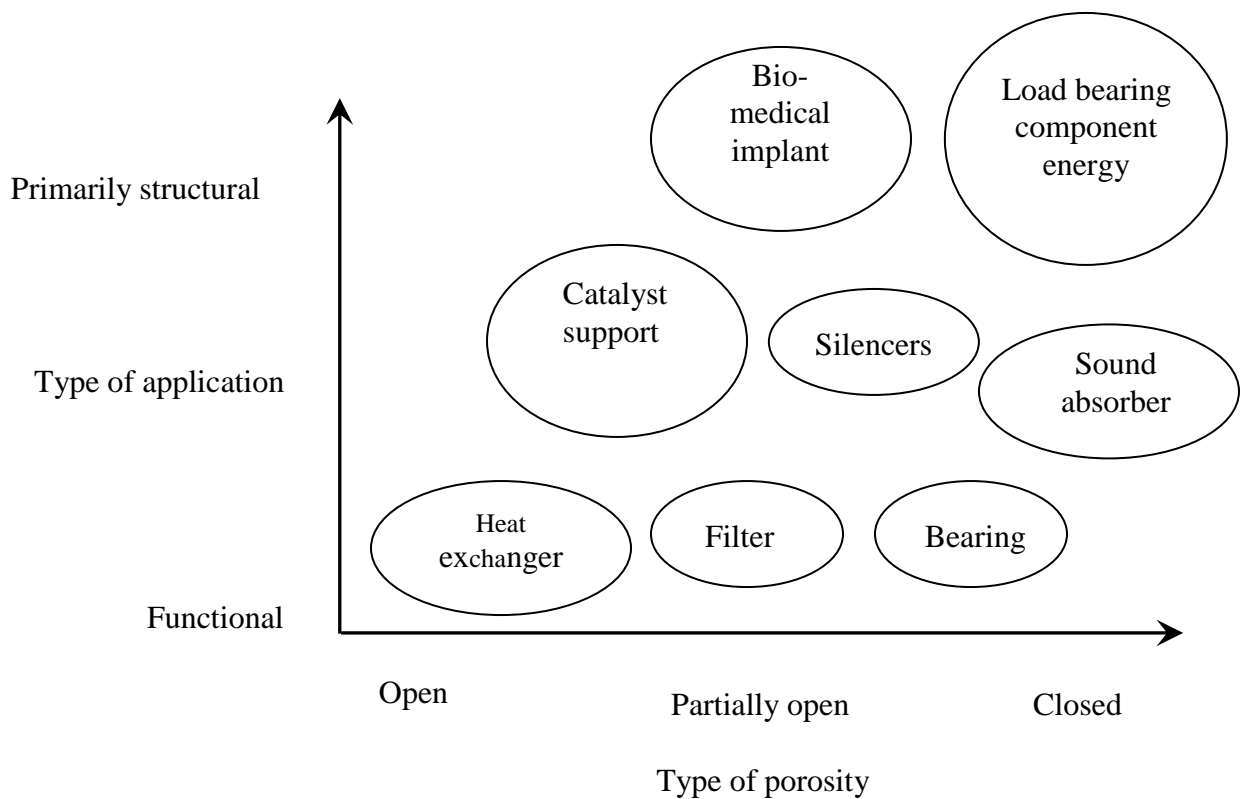
Figure 2.4. Classification of application of cellular materials (Banhart, 2001).

Cellular materials have many applications, such as in cooling machines, heat exchangers, filtration, the transferring and storage of liquids, the support of catalysts, fluid flow control, silencers, flame arresters, battery electrodes, water purification, electrochemical

and acoustic control (Banhart, 2001). For example, the radial heating element in an air heater is often made from porous Fe-Cr-Al foam (Cookson et al., 2006). In addition, Schwartz et al. (1998) reported that the replacement of honeycomb structures with an aluminium foam sheet enables high performance at low cost in aerospace applications.

2.1.2   Types of stochastic foams

Open-cell foams are three-dimensional cellular materials. These types of foams are made of cells with edges connected through open faces. The resulting foam is designated as being an open-cell foam, as shown in Figure 2.5.
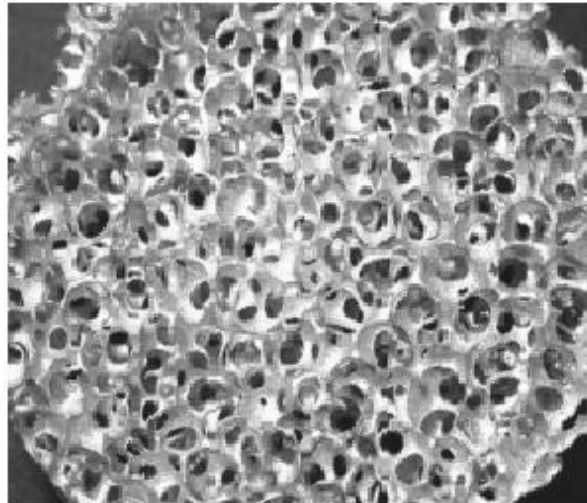
Figure 2.5. Open-cell aluminium metal foam (Chou and Song, 2002).

Closed-cell foams are three-dimensional cellular materials, in which the faces of the cells are in solid form, arranged in such a way that each cell is sealed off from its neighbours. In closed-cell foams, the passage of air, water and moisture vapour is prevented as shown

in Figure 2.6. It has been noted that closed-cell foams provide a greater stability and strength compared with open-cell foams (Malekjafarian and Sadrnezhaad, 2012).
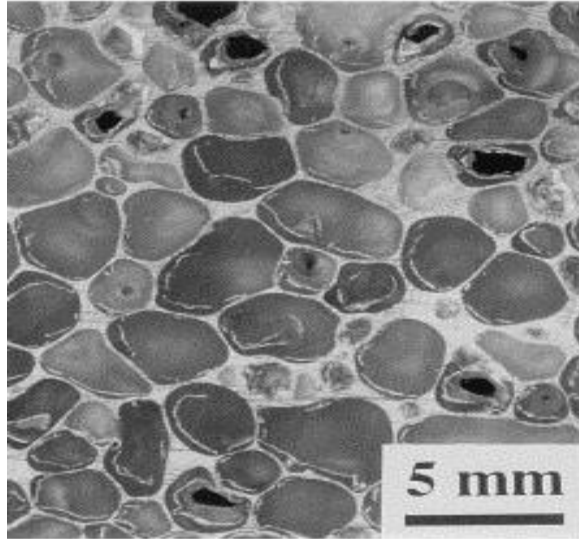
Figure 2.6. Closed-cell aluminium metal foam (Miyoshi et al., 1999).

2.1.3 Cell structures

The structures of the cells in a cellular solid material can vary. The structures can be perfectly organised, as in a honeycomb structure, or they can be organised in a disordered manner, such as in three-dimensional cellular solids materials, e.g. foams. The geometry of the cells refers to their shape and size. The majority of honeycomb types have a hexagonal shape. Therefore, the edge connectivity of such types of cell is six. Alternatively, honeycombs can have square or triangular cells, with an edge connectivity of four or three. Additionally, a random honeycomb structure has different sized cells. They can either be small, with as few as three sides, or as many as nine sides of connectivity (Gibson and Ashby, 1999).

The study of the geometry of three-dimensional cellular solids is more difficult than that of honeycomb cellular solids. In 1873, Plateau identified that, with this type of cell shape, it is possible to partition the space into an array of cells. Recently, computer modelling has been used to identify the unit cells in foams. In 1995, Weaire and Phelan (Phelan et al., 1995) identify the unit cells in a specified area per unit volume, as shown in Figure 2.7.
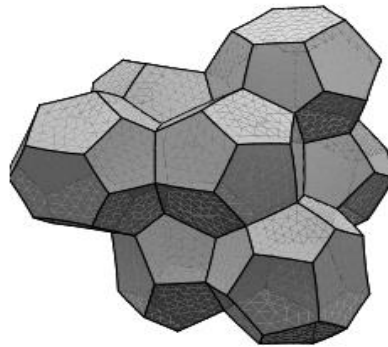
Figure 2.7. Eight cells, forming a fundamental unit of a Weaire-Phelan foam
(Phelan et al., 1995).

It has been determined that the face corrugations and the face curvature of foam cells can substantially reduce the peak stress and the modulus of the metal foam (Simone and Gibson, 1998). Additionally, variations in the thickness of the cell walls, wavy distortion of the cell walls and non-uniformity in the shape of the cells have a substantial impact on the mechanical properties of cellular solids (Grenestedt, 1998). It was concluded that planar cell walls have a higher stiffness than curved and serrated cells (Sugimura et al., 1997).

2.1.4   Characterisation of cellular materials

In order to characterise a cellular material, there is a need for a description of its cell type (closed or open), its relative density, as well as the mean cell diameter (Gibson and Ashby, 1999). Cellular materials can be characterised using many parameterss, such as the mean diameter of the cell, the raw material that constitutes the cells, its shape, size and its porosity and relative density (Wei et al., 2012). The constituents can be analyzed with the help of scanning electron microscopy (SEM), optical microscopy and X-ray tomography. The simplest method for measuring cell relative density or porosity is to measure the weight, assuming that the sample is of a pre-known volume (Gibson and Ashby, 1999). Furthermore, such foams can be characterised by their cell topology (open cells and closed cells). Characterisation of metal foams can be undertaken with the help of optical microscopy, provided that it is completely filled by an opaque epoxy before being polished. SEM is the most useful technique for characterising open-celled foams, whereas X-ray tomography is a useful technique for investigating the deformation modes in cellular solids (Ashby et al., 2000). The tomography technique is dependent on the low X-ray absorption characterisations of these materials, and it is a good technique to study dense and large specimens. Another benefit of tomography is that the deformation modes in the sample can be analyzed and monitored in a non-destructive manner (Maire et al., 2003).

The mechanical properties of cellular materials are different from those of solid materials, due to differences in their microstructures (Banhart, 2001). This section describes the compressive properties of cellular materials.

A stress–strain curve can be used to determine the Young's modulus, as well as the values of plateau strength and densification strain. An example of a general stress–strain curve for a cellular material under uni-axial compression is given in Figure 2.8. It shows the densification regime, the plateau strength and linear elastic region of the foam.
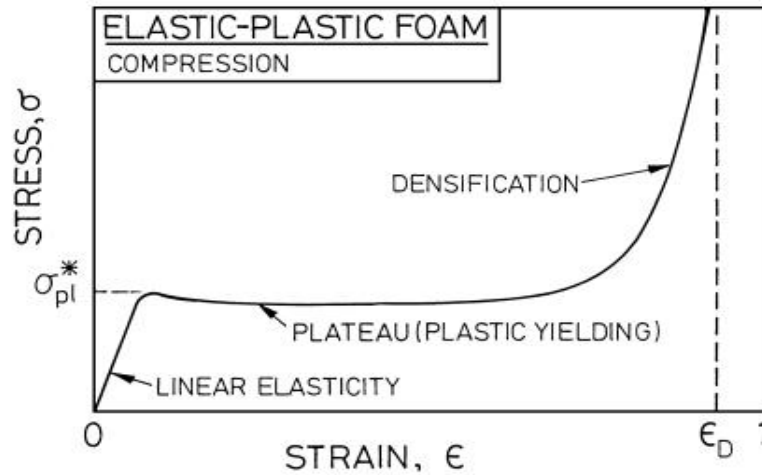
Figure 2.8. An example of a stress–strain curve for an elastic-plastic foam (Gibson, 2000).

The stress–strain curve for metallic foams shows three regimes of behaviour from the material. As can be observed in Figure 2.8, initially, the curve shows a linear dependence of stress on strain. Such a dependency is governed by the strength of the cell walls and the solid material. It is evident that the stiffness of the metallic foam increases with the increasing strength or stiffness of the cell walls (Ashby et al., 2000). It has been reported that the type and grade of the solid metallic alloy has a significant effect on the stiffness of metal syntactic foam (Orbulov and Ginsztler, 2012). It has been shown that metallic alloys with a higher yield strength offer a greater stiffness than other alloys. In this part of the loading phase, the material undergoes non-permanent deformation. The Young's

23

modulus of foams is calculated from the linear elastic region of the stress–strain curve. It is affected by the following parameters: cell wall bending, edge contraction, membrane stretching and the enclosed gas pressure (Siu, 1999; Surace et al., 2009; Zhao et al., 2005). The slope of the first loading region of the stress–strain curve is lower compared to the unloading curve; this is due to localisation of plasticity in the sample as the old yield point value is lower than the compressive strength of the metallic foam. This is illustrated in Figure 2.9 (McCullough et al., 1999).
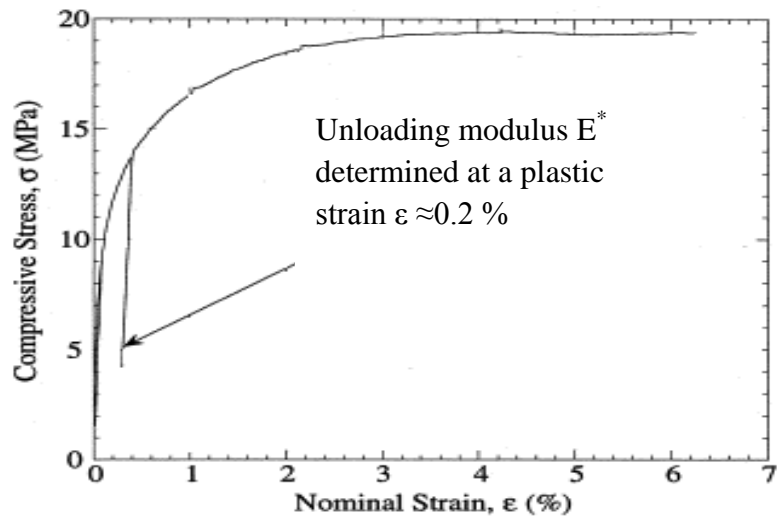
Figure 2.9. An example of a loading and unloading stress–strain curve for a cellular foam.

The unloading curve is therefore recommended for the measurement of Young's modulus (Gubicza et al., 1996). The second stage in the graph is a stress plateau, which shows the collapse of the cell walls, where buckling, yielding and brittle crushing of the foam takes place (Mondal et al., 2009). This stage starts when the material reaches its initial yield point. The shape of the plateau regime depends on whether the foam has open or closed cells. This stage continues until the cell walls have collapsed following the start of the

densification regime, where the stress begins to increase rapidly (Montanini, 2005). In the final stage, the densification strain depends on the porosity of the foam, because during the densification strain the pore space has squeezed (Tao, 2010). When the strength of the cell walls in an open cell foam exceeds the value of the fully plastic moment, it creates plastic hinges, which is when the densification stage starts. Stretching and bending of the cell walls then occurs during densification of the closed-cell foam. In addition to this, the presence of fluid within the cells also has an impact on the densification of closed-cell foams (Mills, 2007).

2.1.5   Energy absorption

Energy absorption is the capability of a material to convert kinetic energy into another form of energy such as heat, viscosity, visco-elasticity and visco-plasticity or even friction. The kinetic energy should be less than the maximum limit of energy absorption of the material in order to keep the object safe. Cellular materials typically have a good capability for energy absorption.

The two most significant parameters for porous materials in terms of energy absorption are densification strain and plateau strength (Sun and Zhao, 2003). The energy-absorbing capability of the material is measured by the length and height of the flat part of the stress–strain curve. The region below the plateau of the stress–strain curve represents the energy per unit volume that can be absorbed (Iannace et al., 2001). This is illustrated in Figure 2.10. When all the pores of the cells are closed, plastic deformation starts and the stress becomes equal to the plateau strength. The composition and type of the matrix material controls the energy-absorption process (Zhang and Zhao, 2007).
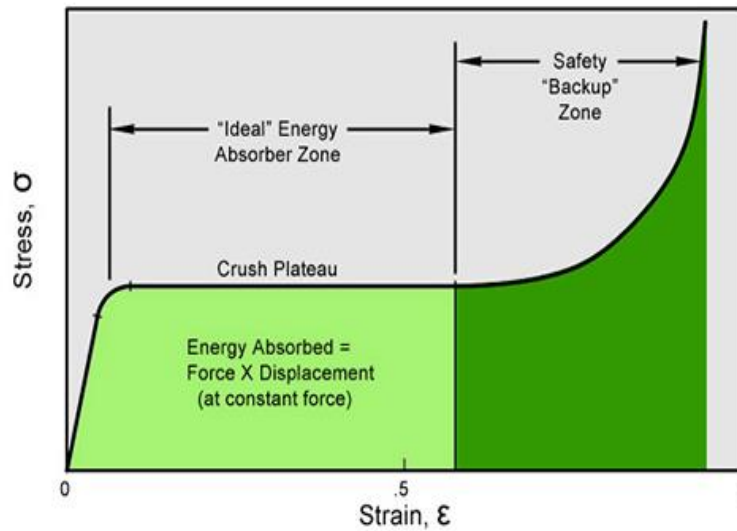
Figure 2.10. Stress–strain curve for an energy absorbing material
(ERG, Aerospace Corporation, 2011).

Foams have the capability to absorb kinetic energy more efficiently than their solid counterparts (Gibson and Ashby, 1999). It is also noted that the energy-absorbing capability of a foam depends on its porosity. In turn, the porosity controls the capability of the material to obtain the maximum densification strain. In addition, the plateau stress also depends on the porosity of the foam (Schneider et al., 1998). When the porosity of the foam increases, the plateau stress decreases. Consequently, the level of energy absorption is proportional to the porosity and the plateau stress (Sahu et al., 2013). On the other hand, the plateau stress is inversely proportional to the porosity. From the literature, it is concluded that energy absorption in a foam material can be maximised through a careful choice of the type and composition of the metal matrix.

2.1.6 Applications of cellular metallic materials

Metallic cellular materials are used in a wide range of applications, including the automotive industry, as shown in Figure 2.11, lightweight construction, the aerospace industry, the building industry, the railway industry, machine construction, sporting equipment and the biomedical industry. The industries in which they have found functional applications include the storage of liquids, the transfer of liquids, sparkers, battery electrodes, water purification, fluid flow control, acoustic control, heat exchangers as shown in Figure 2.12, cooling machines, supports for catalysts, flame arresters, electrochemical applications, silencers and filtration and separation.
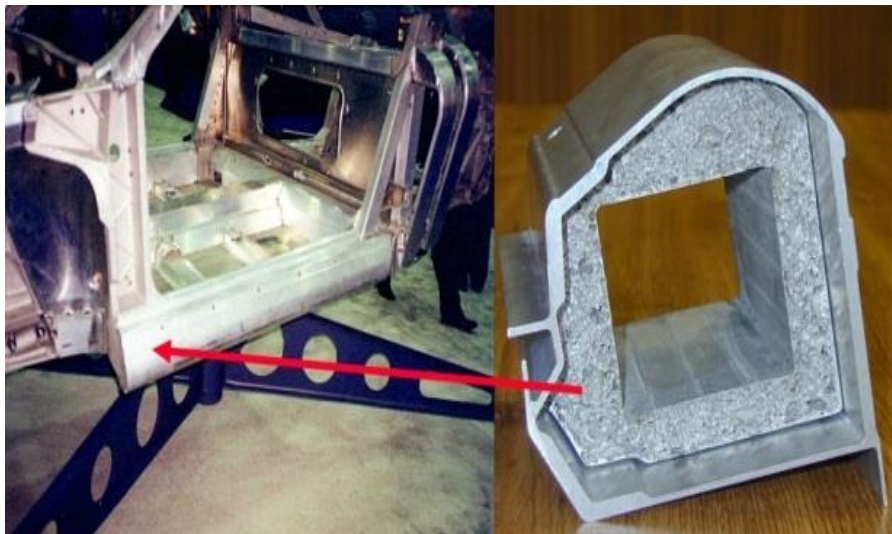
Figure 2.11. Metal foams in the automotive industry (Fraunhofer, 2008).
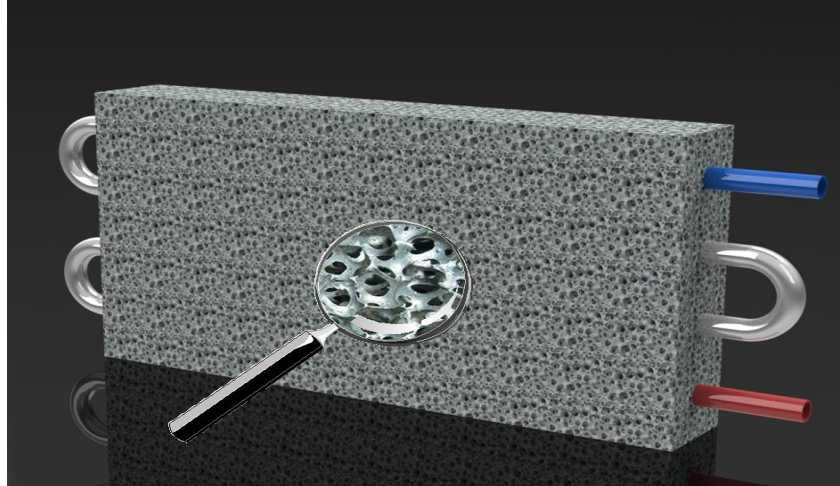
Figure 2.12. Metal foams in heat exchanger applications (Fraunhofer, 2008).

2.2 Metal matrix syntactic foams

Metal matrix syntactic foams are composite materials that consist of a matrix that incorporates porous or hollow ceramic particles (Zhao, 2011). This type of foam is a new classification of material that can be produced using several metals matrices and ceramic micro-spheres.

Matrix syntactic foam is a light material, which has a high energy absorption capacity (Castro and Nutt, 2012). Researchers who have studied metal matrix syntactic foams have focused particularly on the compressive behaviour and fabrication of these materials (Orbulove and Majlinger, 2012). The most frequently used method for manufacturing metal matrix syntactic foams is melt infiltration (Zhao, 2013). With this method, molten metal is pressure-infiltrated into ceramic micro-spheres. However metal matrix syntactic foams tend to deform under compression in a brittle mode, failing either by cracking or by shear, due to the high volume fraction of ceramic micro-spheres (Balch et al., 2006).

The brittle deformation can lead to a significant reduction in plateau strength and energy absorption.

In comparison with fully-dense alloys and metals, metal matrix foams show a high specific stiffness, a low density, a mechanical damping capacity and a high energy absorption capacity. Additionally, their closed-cell geometry is appealing due to the insulating and mechanical properties it conveys to the foam (Balch et al., 2005).

2.2.1 Fabrication process

Most metal matrices in these matrix syntactic foams will be comprised of low density materials, such as aluminium, magnesium and titanium. Three types of ceramic micro-spheres have been used to fabricate metal matrix syntactic foams. These are amorphous silica, Al_2O_3 spheres, ceramic spheres of crystalline mullite and steel spheres (Zhao et al., 2008). There are three main methods for fabricating metal matrix syntactic foams via a liquid state infiltration process, which are as follows:

- Stir casting and spray process

- Solid state processes

- Deposition processes

In stir casting, metal matrix syntactic foams are fabricated by mixing a liquid metal matrix with the ceramic particles, followed by casting (Rohatgi et al., 2011). This method is extremely simple and less costly, but can lead to an inhomogeneous structure. The technique of stir casting is commonly used for the manufacturing of metal matrix composites (Sable and Deshmukh, 2012). In the stir casting method, the ceramic particle volume fraction can be adjusted in an easy manner. However, this method also has a few disadvantages associated with it; for example, the molten metal does not wet the ceramic

29

particles in a proper manner and consequently these particles start clustering (Sharma et.al., 2011). As a result of this, the particles float to the top of the molten metals, as they are lighter. These two disadvantages cause the ceramic particles to have poor dispersion in the liquid metal and a resulting inhomogeneous structure (Zhao & Tao, 2009). In infiltration casting, the metal matrix is placed above the ceramic spheres and is pressed in order to infiltrate the ceramic sphere, where it is solidified to yield a metal matrix syntactic foam (Orbulov, 2013). This is shown in Figure 2.13. Infiltration casting can be carried out using gas pressure or die casting. This method offers the advantage that the matrix and the ceramic micro-spheres are well bonded and the micro-spheres are usually distributed uniformly.

| Introduction of powder into crucible | Powder packing by vibration | Addition of aluminium | Placement in pressure infiltration chamber and evacuation |

| Heating to 750°c under vacuum | Pressurization | Directional solidification |
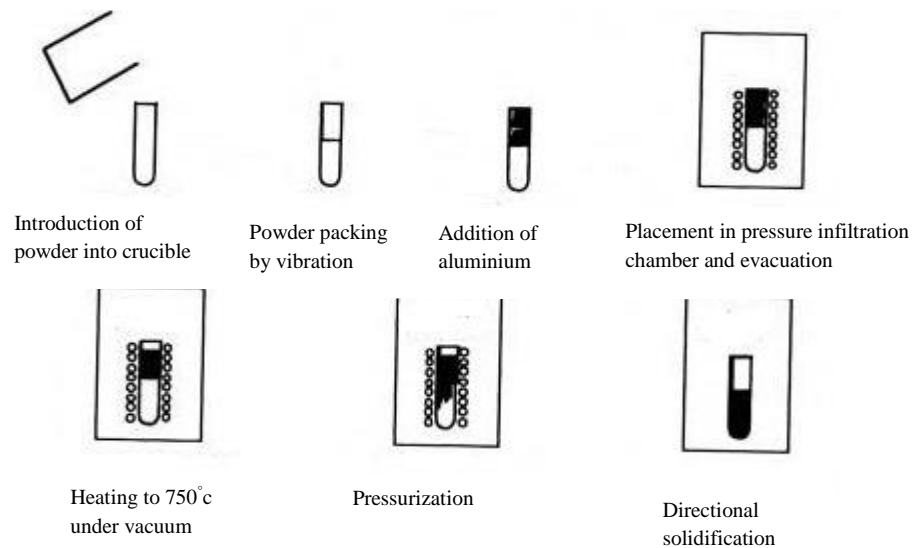
Figure 2.13. Various steps in the infiltration casting method (Evans et al., 2003).

With the spray deposition method, there are only two ways to fabricate the metal matrix syntactic foam. Either cold metal is continuously fed into a fast heat injection zone, or a droplet stream is used, which is yielded from a molten bath (Clyne, 2001).

2.2.2 Porosity

There are two classifications of porosity, namely, open or closed. Classification as open or closed porosity depends on the ratio of void space volume to bulk volume (Cebon et al., 2001). The porosity of foam depends on the shape and size of the pores. The strength of the micro-spheres in a syntactic foam can be altered by varying the radius or the wall thickness of the micro-spheres (Kiser et al., 1999).

The parameter that has the most significant effect on the porosity of a metal matrix syntactic foam is the porosity of the ceramic micro-spheres. Ceramic sphere porosity can be calculated using the following equation:

$$\theta_s = (1 - \frac{\rho_s}{\rho_o}) \tag{2.1}$$

The term θ_s indicates the porosity of the ceramic micro-sphere, ρ_s is the effective density and ρ_o is the micro-sphere solid part density. Therefore, the porosity of a metal matrix syntactic foam can be calculated using the following formula:

$$\theta_f = (1 - f_{al})\theta_s \tag{2.2}$$

where θ_f is the potential porosity of the syntactic foam and f_{al} is the volume fraction of the metal matrix. Zhang and Zhao (2007) developed a general formula that has been used to calculate the porosity of metallic syntactic foam for all types of spheres. The formula is as follows:

$$\theta_s = \frac{\rho_m - \rho_f}{\rho_m - \rho_s}(1 - \frac{\rho_s}{\rho_o}) \tag{2.3}$$

where ρ_m is the density of metal matrix present and ρ_f is the density of the syntactic foam. Kiser et al. (1999) reported that the thickness and radius of the shells of the hollow spheres control the composite porosity of a metal matrix syntactic foam.

It has been reported that compressive failure in a metal matrix syntactic foam is affected by the volume fraction of ceramic micro-spheres. High volumes of metal matrix cause ductile failure in the form of collapse of the material (Tao and Zhao, 2009). In contrast, low volumes of metal matrix tend to lead to brittle failure, in the form of shear. The failure behaviour of metal matrix syntactic foams is different from an ordinary foam, due to its composition (Neville and Rabiei, 2008).

There are conflicting reports in the literature on the relationship between failure type and cell size in metallic syntactic foams. For example, Kiser et al. (1999) found that syntactic foam metal matrices with low values of the wall thickness to the radius ratio (t/r) failed due to brittle behaviour, while those with higher ratio values experienced ductile failure in the form of crushing or collapse. Multiple studies have reported that metal matrix syntactic foams with low t/r ratio values failed due to their ductile properties and were crushed or collapsed, while those with higher values failed due to brittle behaviour leading to shearing (Gupta and Woldesenbet, 2004; Wu et al., 2007). Therefore, in general, it may be concluded from the present literature review that the ratio of (t/r) is a factor that affects the compressive failure of metal matrix syntactic foams.

2.2.3 Density

Rohatgi et al. (2011) was found that the higher density of syntactic foams have a higher modulus, peak stress, plateau stress. In addition, it was reported that the low density of

syntactic foams could be used to replace their matrix alloys in load bearing applications, which could result in weight saving.

Moreover, it was revealed that the foams with monomodal ceramic microspheres have a similar density and porosity due to the volume fraction of ceramic microspheres in the foams while, the foams with bimodal ceramic microspheres have lower densities and higher porosities due to the increases of the volume fraction of ceramic microspheres in the foams (Tao et al., 2009).

Furthermore, it was found that the plateau stress increases with the increasing density of the aluminium matrix syntactic foams, as shown in Figure 2.14
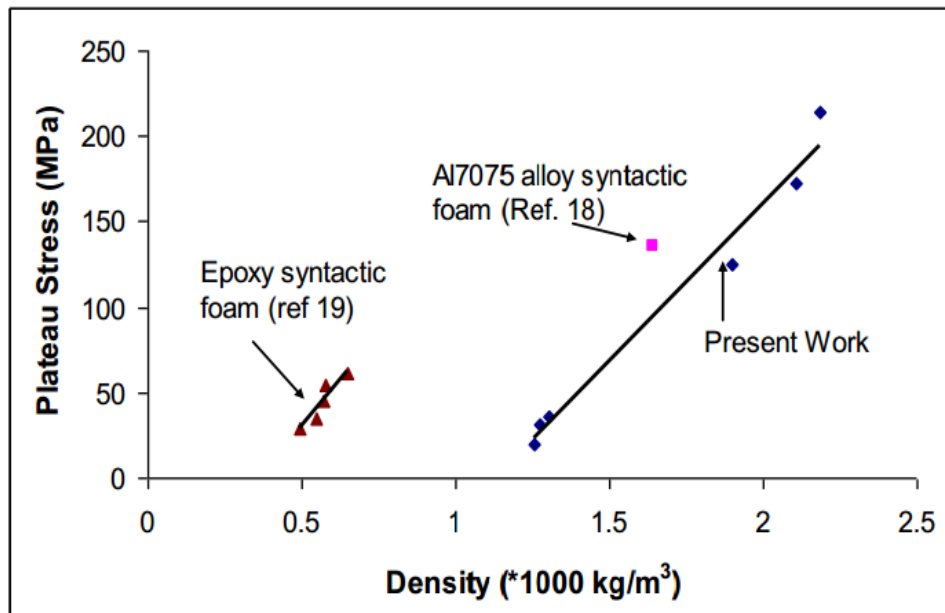
Figure 2.14. Variation in plateau stress with density of the syntactic foams (Rohatgi et al., 2006).

2.2.4   Dynamic compressive testing of matrix syntactic foams

Previous studies have investigated the behaviour of metal matrix syntactic foams under dynamic compression loads (Luong et al., 2013; Tao et al., 2009). Low and high velocity impact tests have been carried out to characterise metal matrix syntactic foams and their behaviour has been studied using drop-weight and split pressure Hopkinson bar tests (Hopkinson, 1914; Tao et al., 2009). It was found that the yield strength of metal matrix syntactic foams under dynamic loading is approximately ten to thirty percent higher, as compared with quasi-static compression (Gupta et al., 2010). Additionally, samples of aluminium matrix syntactic foams were investigated under impact and it was reported that many oscillations appeared at the beginning of the stress–strain curve, where the strain was low due to the high vibration of the drop hammer (Zhang and Zhao, 2007). Tao and Zhao (2009) evaluated the behaviour of aluminium matrix syntactic foams under drop weight impact loading. The split pressure Hopkinson bar was used in order to characterise the behaviour of the material under dynamic loading. It was concluded that aluminium matrix syntactic foams at high strain-rates had 10-30% higher plateau stress and higher peak strengths compared to those measured during a quasi-static test.

2.2.5   Low velocity dynamic loading

The drop-weight impact test method has been used to study the dynamic response of aluminium syntactic foams at different strain-rates. A heavy weight is guided by two smooth steel rails and falls from a height to strike the specimen (Hsiao and Daniel, 1998). The behaviour of the foam is affected by the size of the ceramic micro-spheres and the

type of aluminium matrix, which has an effect on the level of energy absorbed during impact loading (Castro et al., 2013).

2.2.6 High velocity dynamic loading

High velocity dynamic loading have been conducted using Hopkinson bar and blast tests. With the Hopkinson bar technique, the induced wave, propagated in a long elastic metallic bar, has been used to measure the pressure produced during dynamic events. The Hopkinson bar test is used for measuring the dynamic stress–strain response of materials. It is used for studying the constitutive laws of materials at a high strain-rate (Deshpande and Fleck, 2000). High precision strain gauges, signal conditioners and high speed digital oscilloscopes are used in the Hopkinson bar test with high sensitivity and accuracy. The sensitivity of the pressure bar is determined by the properties of the bar material, such as the elastic wave impedance and the density (Li and Lambros, 1999).

The Hopkinson bar technique is used to determine the properties of the material under dynamic loading (Song and Chen, 2004). Additionally, it has been used to characterise metal foams and soft materials that possess low values of mechanical impedance required for increasing the sensitivity of the testing device (Dung et al., 2011).

The stress in the output bar is found by converting the strain gauge data (volts) to stress using the following relationships (Lopatnikov et al., 2003):

$$\sigma(t) = \frac{E_b.2.\varepsilon_v(t)}{G_g.K_g.v_i(1+v_b)} \tag{2.4}$$

or

$$\sigma(t) = \frac{A.E_b.\varepsilon_t(t)}{A_o} \tag{2.5}$$

where k_g is the strain gauge factor, $\varepsilon_v(t)$ is the strain gauge voltage as a function of time, G_g is the amplification factor, $\sigma(t)$ is the stress of the transmitter bar as a function of time, E_b is the elastic modulus of the bar, A is the cross-sectional area of the bar, υ_b is Poisson's ratio of the bar material, A_o is the cross-sectional area of the sample, v_i is bridge input voltage and $\varepsilon_t(t)$ is the transmitted axial strain pulses. In addition, the time-dependent strain-rate and specimen strain are calculated using the following equations:

$$\dot{\varepsilon}(t) = \frac{2.c_b \varepsilon_r(t)}{l_o} \tag{2.6}$$

$$\varepsilon(t) = \int_0^t \dot{\varepsilon}(t)dt \tag{2.7}$$

where c_b is the sound wave velocity, l_0 is the initial length of the sample and $\varepsilon_r(t)$ is the reflected axial strain pulses.

2.2.6.1   Source of sensitivity

Several studies have investigated the deformation behaviour of cellular materials at different strain-rates. reported that A honeycomb material was affected by strain-rate (Goldsmith and Sackman, 1992). Additionally, aluminium foams were studied at varying strain-rates and it was concluded that the compressive strength increases with an increase in strain-rate (Edwin et al., 2009). It was found that the energy dissipation capacity of an aluminium foam increases with strain-rate. However, the densification strain decreases with an increase in strain-rate until a certain limit and then it remains constant with a further increase in strain-rate (Shen et al., 2010). The source of such sensitivity in metal foam materials could not be clearly identified, because of the differences in

manufacturing processes and the compositions of the foams discussed in the literature (Banhart, 2001).

There are four parameters that are known to cause sensitivity in cellular materials. They are (Zhao et al., 2005):

- Solid material rate-sensitivity;
- Pressure of the trapped air in the cells;
- Micro-inertia effects;
- Shock enhancement.

The effect of air pressure trapped inside the cells due to the existence of gas has been studied (Zhao et al., 2005). During static loading, there is sufficient time for the gas to escape, whereas during dynamic loading, the time period during which the gas can escape is extremely short. It was concluded that the internal pressure of closed-cells has no effect on the rate-sensitivity of the foam (Zhao et al., 2005). However, it was reported that the strain-rate sensitivity of Alporas foam has a relationship with sequential buckling of the wall cells that control gas from the structure (Mukai et al., 2005; Dannemann and Lankford, 2000).

The stress behind the shock front has been reported to be larger than the stress in front of the shock at a fixed velocity. Meanwhile, it has been shown that cell wall buckling under dynamic loading is delayed due to micro-inertia effects under impact loading (Calladine and English, 1984).

2.2.6.2   Terminal ballistics

Ballistics is the science of bullet mechanics, or the art of designing a projectile to acquire aspired performance. Ballistics science is divided into three approaches. Internal ballistics

deals with the behaviour of the projectile within the gun barrel (Merlen and Dyment, 1991). External ballistics deals with the motion of the projectile in the air after leaving the gun. Terminal ballistics is concerned with the effect of the projectile on a target (Borvik et al., 2002). The interaction between the projectile and a target is very important to increase the performance of the projectile. In contrast, the performance of the target can be improved (Walley, 2009).

A gun is considered as a combustion chamber, where heat is produced, which is converted into kinetic energy, and its function is to raise the projectile toward specified targets. There are a wide variety of firearms to be found today, but they have a similar concept from a ballistic stand-point (Al Bakri, 2001).

2.2.6.3   Blast testing

Following a blast, a high pressure shock wave is formed within the explosive filling. Consequently, the heated gas expands and forces out the volume it occupies. As a result, the shock wave that is formed within this volume contains the majority of the energy released by the explosion (Ngo et al., 2007). Therefore, the blast wave raises the value of the pressure above the ambient value. Over time, the pressure drops down below the ambient value, resulting in a negative phase (Igra et al., 2013). This is illustrated in Figure 2.15.
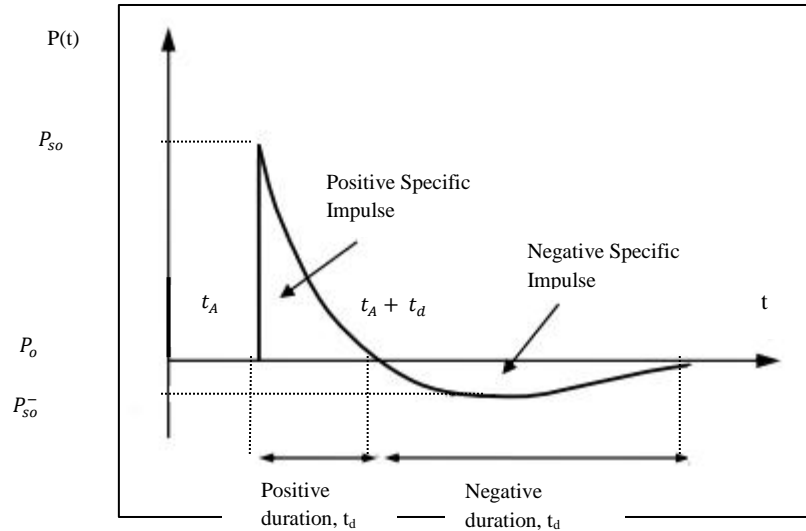
Figure 2.15. Shock wave pressure (Ngo et al., 2007).

The physical properties of the source of an explosion are known to have a considerable effect on the characteristics of the air blast (Rajendran and Lee, 2009). As shown in Figure 2.15, for t_A, a short period of time, where the pressure at that position is suddenly raised to a peak value of overpressure P_{so}, amplified by a reflection factor, a pressure wave encounters a structure in its path. Over t_d, a further short period of time, the pressure decays to the ambient condition at $(t_A + t_d)$ and then further decays to pressure point P_{so}^-, building a negative phase region.

The shock wave pressure curve shows two main phases. These are the positive and the negative phases. In the positive phase, the pressure is higher than the ambient value, and in the negative phase, the pressure drops below the ambient pressure. The negative phase has a lower intensity and a longer duration compared with the positive phase. The stand-off distance of the charge to the target controls the amplitude and the duration of the pulse (De Carli and Meyers, 1981). When the stand-off increases, the duration of the

positive phase blast wave increases. This result in lower amplitudes and a shock pulse of a longer duration (Ngo et al., 2007). The blast impulse depends on the blast pressure (p), blast duration (T_{blast}) and the explosive radius (R) (Mays and Smith, 1995). The blast magnitude impulse was calculated using the following equation:

$$I = \pi R^2 p T_{blast} \qquad (2.8)$$

where T_{blast} is calculated by the following equation:

$$T_{blast} = \frac{L_{explosive}}{v} \qquad (2.9)$$

where $L_{explosive}$ is the distance travelled by the explosive from the central detonation to the outer ring of the explosive and v is the explosive burn front velocity.

The blast impulse is usually measured by the swing of the ballistic pendulum. The ballistic pendulum is levelled using spring steel wires. The test specimen is located at either end of the pendulum. The balancing material is used to balance the pendulum to ensure that the impulse acts through the centroid of the pendulum as shown in Figure 2.16.
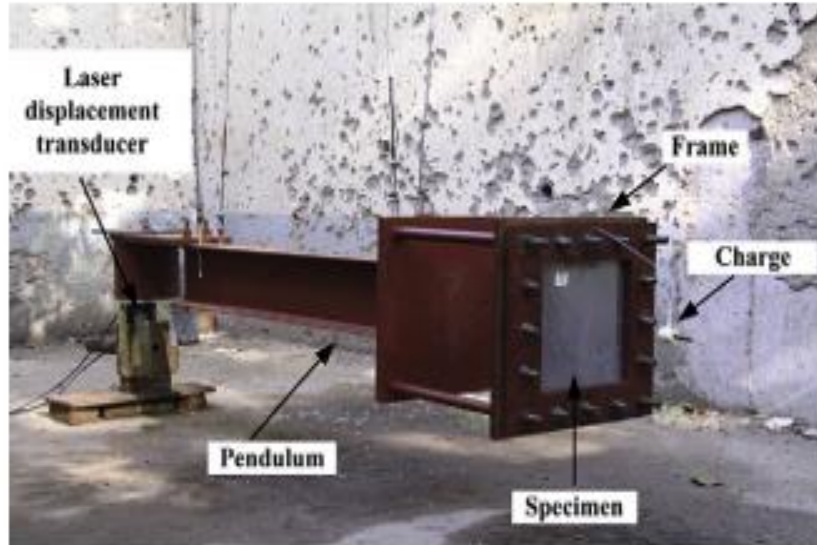
Figure 2.16. Conventional ballistic pendulum.

Aluminium foam has been investigated under blast loading using a ballistic pendulum (Hanssen et al., 2002). Radford et al. (2006) made a comparison between the behaviour of a monolithic plate of aluminium foam sandwiched between plates with aluminium alloy metal foam cores and AISI 304 stainless steel face sheets. Additionally, Langdon et al. (2010) studied the effect of the density of a core of aluminium foam and the thickness of the cover plate on the blast response of sacrificial cladding panels.

2.3 The finite element modelling

This section describes the background of the finite element method, the modelling of foams and other issues related to static and dynamic numerical loading.

In structural mechanics, the FE method is an important discretisation technique. It is a method to determine estimated solutions for numerical problems of boundary value conditions. There are several FE methods, each with its own corresponding advantages.

2.3.1 Abaqus/Standard

The Abaqus/Standard package makes technology that is suitable for solving static problems in which finding an accurate stress value is crucially significant. It can be used to solve a wide range of linear and non-linear problems that involve the static responses of components. Abaqus/Standard can solve a wide range of steady-state transport and static transport analyses using an implicit solution technique. It solves a system of equations implicitly at each step 'increment'. Abaqus/Standard can use the results found by Abaqus/Explicit as starting conditions (Hibbit et al., 2012).

2.3.2 Abaqus/Explicit

Abaqus/Explicit employs a solution technology that is suitable for transient events, such as ballistic impact, automotive crash worthiness, drop-weight testing and blast problems. It is very useful for tackling many types of non-linear behaviour, for example that found in energy-absorbing activities, such as slow crushing and forging. As mentioned before, Abaqus/Explicit results can be used as the initial conditions in Abaqus/Standard. The flexibility offered by this integration enables Abaqus/Explicit to be implemented in transient dynamic problems (Hibbit et al., 2012).

2.3.3 Modelling of foams

Ming et al. (2013) used FE analysis to predict the effect of particle clustering on the tensile properties and failure mechanisms of hollow spheres infiltrated by syntactic foams. It was found that the elastic behaviour of syntactic foams is insensitive to the degree of the particle clustering.

Tao et al. (2008) developed FE analysis to study the performance and failure mechanisms of the polymeric foam sandwich structures subjected to flexural loading. It was found that the weaker the foam is, the more optimal the pin-reinforced foam core becomes, and that sandwich beams with pin-reinforced polymers foam cores are structurally more efficient than foam cored sandwich beams.

Ozturk and Anlas (2011) used commercial codes Abaqus and Ls-Dyna to carry out FE analysis to predict response of foams under multiple compressive loadings. The predicted results were compared with each other.

2.4   Summary

This literature review has provided a review of different types of cellular materials. These include metal foams, syntactic foams, honeycombs, trusses and textiles. The compressive behaviour of cellular materials and their compressive stress–strain curves are studied in detail. Cellular metallic materials have found applications in various types of industries. A brief overview of the applications of cellular materials is provided. In the final part of this literature review, the background to blast testing, the sacrificial cladding structures and the process of testing cellular materials are discussed in detail.

CHAPTER 3: MATERIALS AND EXPERIMENTAL METHODS

Initially, this chapter will present details of the manufacturing processes for the production of aluminium matrix synthetic foams. Subsequently, there will be a discussion on the experimental procedures for the mechanical tests used for characterising the properties of the foams, which cover both static and dynamic loading conditions.

3.1   Materials

The raw materials that were used to fabricate the synthetic foams were aluminium and a ceramic micro-sphere powder. Two types of aluminium, i.e. Al6082-T6 and Al 7075-T6, were used to examine the influence of changing the grade of aluminium on the foam mechanical properties. Envirospheres Ltd. of Australia supplied the ceramic micro-spheres that were used in the manufacture of the foams. These micro-spheres were divided into three groups with size distributions between 25-100 µm, 100-250 µm and 250-500 µm. These three grades of micro-spheres were designated as ceramic micro-spheres (CM) I, II and III respectively, which were used for the evaluation of the effect of the size of micro-spheres on the mechanical behaviour of the foams.

3.1.1   Aluminium matrix (6082-T6) syntactic foam

Aluminium 6082-T6 is an aluminium alloy that has a medium strength with an excellent resistance to corrosion. It is widely known as a structural alloy. It is used in the form of a block in the fabrication of aluminium matrix syntactic foam, which is manufactured by the infiltration of molten aluminium into the CM by using an infiltration casting method. Due to its exceedingly high strength, it has replaced alloy 6061 in the majority of applications. Alloy 6082-T6 has an extremely good weld-ability, however it has a

reduced strength in the weld zone (Aalco, 2013). This alloy was used in the form of a block in the fabrication of aluminium matrix syntactic foam by the infiltration of molten aluminium into the CM using the method of infiltration casting. The 6082-T6 alloy has the highest strength among the 6000 series alloys as a result of its high magnesium content. The chemical compositions of aluminium 6082-T6 are as follows (Aalco, 2013):

- (0.7-1.3) wt % Si
- 0.1wt % Cu
- (0.4-1) wt % Mn
- 0.5 wt % Fe
- 1.2 wt % Mg with the balance being aluminium

Alloy 6082 is generally used in bridges, trusses, highly stressed applications, milk churns, beer barrels, skips, transport applications, cranes and so forth (Aalco, 2013).

The physical and mechanical properties of the aluminium 6082-T6 alloy are presented in Table 3.1.

Table 3.1. Physical and mechanical properties of Al 6082-T6.

Density (kg/m^3)	2700
Melting point (˚ C)	555
Modulus of elasticity (GPa)	70
Shear strength (MPa)	210
Proof stress 2% (MPa)	310
Tensile strength (MPa)	180

Clearly, the percentage of ceramic spheres that are used in the production of a foam will have an effect on the mechanical properties of the resulting foam. These particles are commonly known as ceramic micro-spheres, ceno-spheres or nano-spheres due to their

extremely small size. Ceramic micro-spheres have two different inner structures, either porous or hollow. Both types have the same effective density and porosity. The shape of each ceramic micro-sphere is different. Hollow ceramic micro-spheres have a perfect spherical shape, while porous ceramic micro-spheres have a spherical shape, with a rough surface (Tao, 2010). Ceramic micro-spheres are semi-transparent having a fine particle size and a high strength. It is an ideal material for improving both the hardness and filler loading, whilst at the same time providing gloss control. The ceno-sphere family of ceramics offer extremely high value of hardness. The chemical compositions and technical specifications of ceramic micro-spheres are presented in Tables 3.2 and 3.3 respectively.

Table 3.2. Chemical composition and technical specification of the micro-spheres.

Chemical Properties	Typical composition (by weight):
Silica SiO_2	55 - 60%
Alumina Al_2O_3	36 - 40%
Iron Oxide Fe_2O_3	0.4 - 0.5%
Titanium Dioxide TiO_2	1.4 - 1.6%

Table 3.3. Technical specifications of the micro-spheres.

Technical Details SL Series	Typical Physical Properties
Form	Free flowing powder
Particle Size	12 - 500 microns
Colour	White
Relative density	0.6 - 0.8
Bulk density	0.3 - 0.4g/cc
Shell thickness	approx. 10% of diameter
Melting point	1600 - 1800 ^{o}C
Compressive strength	~6,500 psi (45 MPa)

The ceramic micro-spheres (CM) were divided into three groups, in accordance to their varying sizes. For the purpose of this study, three different grades of ceramic micro-spheres were used in order to examine the effect of the size of micro-spheres on the behaviour of the foam. The three grades of ceramic micro-spheres that were used include: the finest grade (25-100 µm), a general-purpose range grade (100-250 µm) and a coarse grade (250-500 µm).

3.1.2   Aluminium matrix (7075-T6) syntactic foam

Aluminium 7075-T6 consists of zinc as a primary alloying element. It is a strong metal that offers strength, which is comparable to the strength of steel. Additionally, this has an average level of machinability and a good fatigue strength. One of its main disadvantages is that it possesses a poorer resistance to corrosion than many other aluminium alloys. This category of aluminium alloy is typically found in automotive, aviation, marine and other transport applications because of its extremely high ratio of strength to density. An application of this alloy is found in the manufacturing of American military M16 rifles (Udomphol, 2007). Additionally, this alloy is also commonly used in shafts for lacrosse sticks, fork sets, and camping knives. As this alloy possesses the ability to be finely polished, and due to its thermal properties, high density and strength, it also has applications in mould tool manufacture. Furthermore; it is regarded as being more expensive than many of its counterparts. The chemical composition of Al7075-T6 is as follows (Aalco, 2013):

- (5.1-6.1)% Zn (the source of its strength)
- 0.3 wt % Mn
- 0.4 wt % of Si

- 0.5 wt % Fe

- (2.1-2.9) wt % Mg with the balance being aluminium

The physical and mechanical properties of the aluminium 7075-T6 matrix are given in Table 3.4.

Table 3.4. Physical and mechanical properties of Al7075-T6 (Matweb, 2006).

Properties	Values
Density (kg/m^3)	2800
Poisson's ratio	0.33
Elastic modulus (GPa)	71.7
Yield strength (MPa)	503
Elongation (%)	11
Hardness (HB500)	87
Shear strength (MPa)	331

3.2   Manufacturing methods (Fabrication of the metal matrix syntactic foams**)**

Metal matrix syntactic foams consist of a combination of ceramic micro-spheres and a metal matrix. Most metal matrices should be light, such as aluminium, magnesium, or titanium. In this study, the melt technique that was used is shown schematically in Figure 3.1.
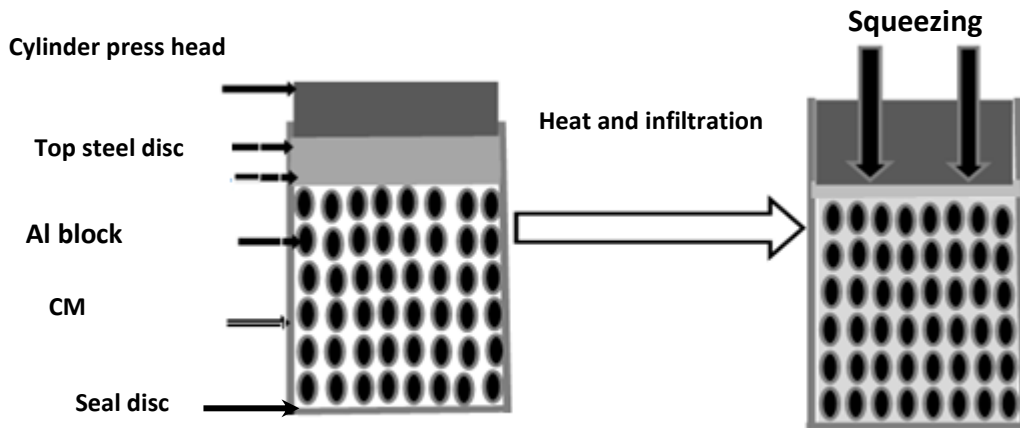
Figure 3.1. Schematic of melt infiltration casting.

In the infiltration casting technique, the metal matrix is positioned over the ceramic spheres. The metal matrix is then pressed so that it infiltrates in the ceramic spheres where it solidifies to produce a metal matrix syntactic foam (Altenaiji et.al., 2012). This technique can be carried out by die-casting or gas pressure. It is very advantageous in that the ceramic spheres and metal matrix bond well together. Additionally, the micro-spheres are distributed in a uniform manner in this technique.

In this thesis, the process of pressure infiltration casting was used to create aluminium matrix syntactic foams that contain micro-spheres with diameters size distribution between 25-100, 100-250 and 250-500 µm. The volume fraction of micro-spheres in the finished samples was approximately 67%. A circular steel disc was used to seal a steel tube at the bottom, which was 44 mm in diameter and 55 mm in length. This steel tube was used as a mould. It was partly filled with the ceramic micro-sphere powder. An aluminium alloy block was positioned on the CM powder and the height of CM powder in the tube was maintained at approximately 25 mm. This was equivalent to 16 g, whereas the height of the aluminium block was 12 mm, weighing approximately 46 g.

The volume ratio of ceramic micro-spheres to aluminium was 2:1. Furthermore, a circular steel disc that had a slightly smaller diameter than the steel tube's internal diameter was positioned on the top of the aluminium block. The assembled apparatus was subsequently positioned in a furnace and the temperature of the furnace was raised to 740 $^{\circ}$C (i.e. above the melting point of aluminium). This temperature was maintained for a period of 40 minutes in order to ensure complete melting of the aluminium matrix. The assembled apparatus was then removed from the furnace and the molten aluminium was immediately pressed to infiltrate into the ceramic micro-spheres. This was achieved with the help of a hydraulic press at a pressure of 4 MPa. The assembly was then left to cool and the syntactic foam was consequently removed from the steel tube. The compositions of the various foams investigated in this dissertation are summarised in the following table.

Table 3.5. Composition of the aluminium syntactic foams.

Sample ID No.	Al alloy	Size of ceramic micro-spheres
CM (I)	7075-T6	250-500μm
CM (II)	7075-T6	100-250μm
CM(III)	7075-T6	25-75μm
CM (IV)	6082-T6	250-500μm
CM (V)	6082-T6	100-250μm
CM (VI)	6082-T6	25-75μm

3.3 Mechanical properties of the aluminium matrix syntactic foams

Characterisation of the mechanical properties of the syntactic foams was carried out at dynamic and quasi-static rates of strain. The compression, shear and three point bending tests were undertaken at quasi-static loadings rates. Dynamic tests were conducted through a series of drop-weight, split Hopkinson pressure bar, terminal ballistics and blast tests. In order to successfully analyse these tests, the micro-structural observation facilities available at the University of Liverpool were used. Scanning Electron Microscope (SEM) and optical microscopes were used to investigate the distribution of ceramic micro-spheres in the aluminium matrix along with the examination of bonding conditions between the two. An Instron 4045 machine was used to conduct the quasi-static tests, whilst a drop-weight impact tower was used to conduct the low velocity impact tests. In addition, high-speed impact tests were performed at the Defence Academy, RMCS (Cranfield University, UK) using a split Hopkinson pressure bar facility, a short firing range and a blast facility. For all these tests, three samples were used to assess the repeatability of the experimental data.

3.3.1 Preparation of the surface and size of sample

Specimens of aluminium matrix syntactic foam can be machined with the help of several standard techniques. An initial study showed that the cutting procedure had an effect on the material properties. For example, the procedure of cutting using a band saw can destroy the ceramic micro-sphere cells. This leads to a reduction in the Young's modulus and compressive strength of the material. In contrast, electric discharge machining or cutting using a diamond saw can minimise damage to the cells in the foam.

51

3.3.2 Micro-structural observations

The samples were cut to the desired size and polished for examination under an optical microscope. The distribution of the ceramic micro-spheres in the aluminium matrix along with the overall degree of bonding between them was investigated in depth. This investigation was carried out using optical microscopy as well as SEM procedures. These techniques were also used to investigate the fracture behaviour of the aluminium matrix syntactic foams following mechanical testing.

3.3.3 Quasi-static testing

3.3.3.1 Compression Testing

Uniaxial quasi-static compression tests were conducted on cube-shaped specimens having dimensions of approximately 20x20x20 mm^3, i.e. with a height to width ratio that is equal to one. The thickness of each specimen was therefore more than seven times the size of the cells. Stress-strain curves were recorded at a crosshead speed of 1 mm/min. The displacement was measured from the crosshead position using an extensometer. The strain was calculated by dividing the displacement by the original sample length; while the stress was computed by dividing the load applied by the initial cross sectional area. Typically, stress-strain curves for an aluminium matrix syntactic foam exhibit localised plasticity at stress levels below the compressive strength of the foam. As a consequence of this plasticity, the shape of the loading curve reduces. Therefore, the material Young's modulus should be measured from an unloading curve. The unloading curve is typically measured at 75% of the compressive strength. The intersection of the elastic and the plateau region is taken as the compressive strength of the material. Additionally, the test

sample's surface, which is in contact with the loading platens, should be greased in order to minimise friction.

3.3.3.2   Three point bending tests

The three-point bending test, as shown in Figure 3.2, is a flexural test, which measures the force required to deform beams in bending. The flexural modulus is an indication of the stiffness of the material under bending. In this case, 10 mm thick aluminium matrix syntactic foam plates were cut into samples with length and width dimensions of 80 mm and 10 mm. The sample was supported by two 10 mm cylindrical supports and loaded centrally by a 10 mm diameter cylindrical bar, as presented in the diagram.
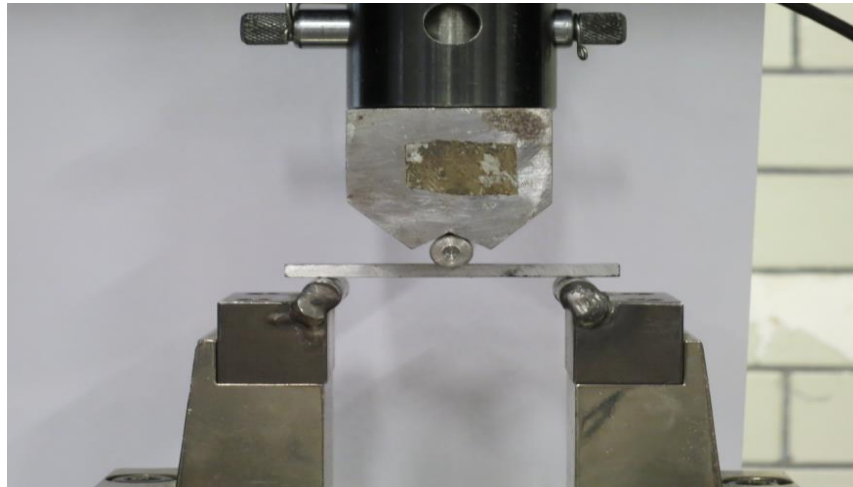
Figure 3.2. Three point bending test.

The flexural strength was calculated at the maximum load using the following equation:

$$\sigma_F = \frac{3PL}{2Bh^2}$$ (3.1)

where σ_f is the stress at mid-span, P is the load at a given point on load-displacement curve, L is the support span, w is the width of the test sample, h is the thickness of the sample, d is the deflection of the centreline of the sample at the middle of the support span and m is the initial straight line portion of the load deflection. The flexural modulus was determined by drawing a tangent to the slope of the stress-strain curve. The flexural modulus was calculated using the following equation:

$$E = \frac{L^3 m}{4Bd^3}$$ (3.2)

The flexural strain can be calculated using Equation 4.1 (BS EN 2746, 1998).

$$\varepsilon_f = \frac{6dw}{L^2}$$ (3.3)

where L, w and d are span length, width and maximum deflection, respectively.

3.3.3.3 Shear testing

A shear test differs from a tensile or compression test in that a load is applied parallel to the upper and lower faces of the sample under test. Two halves of occlusive cylinders were used to conduct the shear test on the aluminium matrix syntactic foam, as shown in the Figure 3.3.
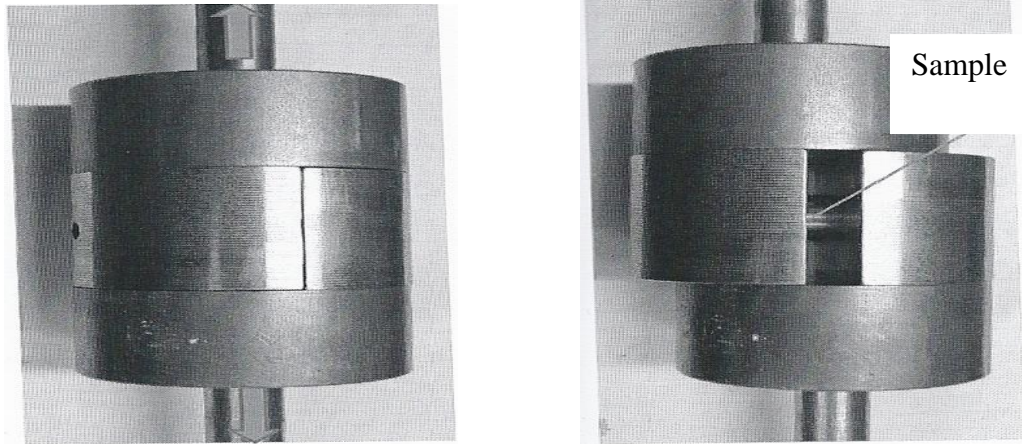
Figure 3.3. Fixture of the shear test.

The diameter and the height of the foam sample were 19 mm and 24 mm respectively. The specimen was placed through the occlusive cylinder and a screw balance was used in order to ensure that shear fracture occurs in the middle of the sample. A tensile force was applied to the two halves of the occlusive cylinder, leading to the generation of a shear force in the metal syntactic foam sample.

3.3.4   Dynamic Testing

3.3.4.1   Low Velocity Impact Testing (Drop-weight)

The dynamic properties of the foams ($20 \times 20 \times 20$ mm^3) were investigated by performing low velocity impact tests on an instrumented drop-weight tower. This is shown in Figure 3.4.
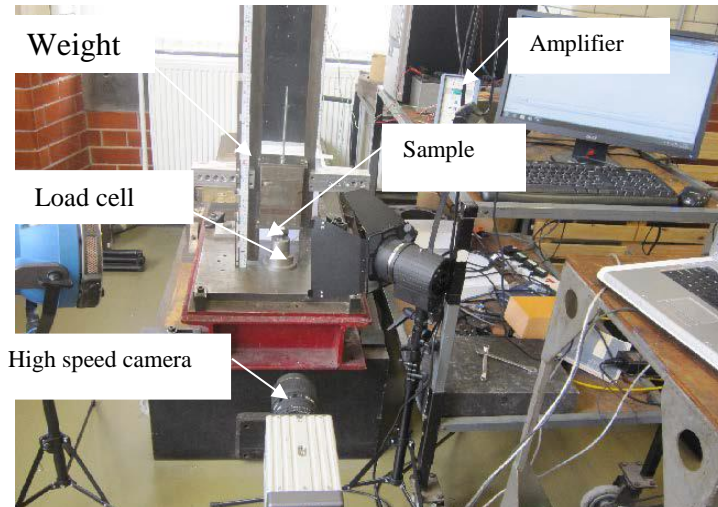
Figure 3.4. The drop-weight test facility at the University of Liverpool.

In these tests, a carriage with a mass of 12 kg was guided by two vertical steel bars to impact the top surface of the sample. The sample was supported by a solid steel base. Varying the release height of the carriage changes the impact velocity. The maximum impact velocity that can be achieved using this facility is 6.5 m/s. The maximum height used was 1.5 m, which leads to a maximum velocity of 5.42 m/s. In addition, the kinetic energy of the striker can be altered by varying the mass of the carriage between 0.4 kg and 35 kg. A Kistler 9061A piezo-electric load-cell was used to measure the force-time history. The maximum capacity of the load-cell was 200 kN. The load-cell was located above the 25 mm diameter impact head. The impact force and signal were recorded using a Packard Bell computer using the Data Flow plus software package. The impact calibration factor for converting the voltage to a force was found by conducting a static calibration on the load-cell.

The impactor velocity and the deformation of the sample were measured using a high-speed video camera (MotionPro-X4) located at the front of the drop-weight tower. High

resolution images were captured using a 50 mm lens. The ProAnalyst software package was used to analyse the motion of the striker during impact and the auto-tracking facility was used to obtain the deformation and velocity versus time curves (Cantwell, 2007). Details of the high speed video camera system are given in Table 3.6.

Table 3.6. Details of the high speed video camera (Yang, 2010).

Camera- motionPro X4	Make: integrated design tools, INC. M/N: X4C-U-4 S/N: 24-0507-0875
PROANALYST SOFTWARE	Make: Xcitex Edition: Professional Version: Workstation
Motion Pro software	Make: Redcake Alliance 24-0507-02075

3.3.4.2   Split Hopkinson Pressure Bar (SHPB)

The SHPB test has been widely used for the evaluation of high strain-rate effects on materials. It is used for the measurement of the properties of materials at high rates of strain. Dynamic material properties, strain-rate sensitivity, damage propagation and failure mechanisms can all be measured using the SHPB. Additionally, the SHPB can be used to generate high strain-rate properties under compression, tension, torsion and shear (Weinong and Cheng, 2011). The SHPB apparatus is composed of two long slender bars, a striker, strain gauges, an output system, and a specimen that is located between the two rigid bars, as shown in Figure 3.5. As the striker bar impacts the end of the input bar, an elastic compression pulse is generated which travels through the input bar. At the sample interface of the input bar, a portion of the pulse is transmitted to the output bar whereas

the remainder is reflected. The dynamic material properties can then be found from the superposition of the incident and reflected pulses. There are many factors that have an influence on the accuracy of the results. These factors include the transducer properties, the impedance mismatch between specimen and the bars and longitudinal wave dispersion (Kaiser, 1998).
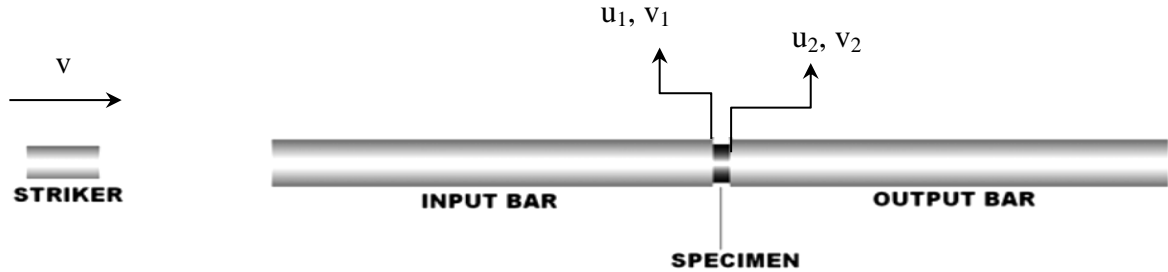
Figure 3.5. Schematic of the SHPB test fixture (Kolsky, 1949).

It was found that plastic deformation was caused by the transmitted waves in the sample. Integration of the strain-rate in the specimen gives strain in specimen. Therefore, the reflected and transmitted pulses need to be identified. The stress in the specimen can be determined using Kolsky's relation (Kolsky, 1949):

$$\sigma_s(t) = E \frac{A_o}{A} \varepsilon_t(t) \tag{3.4}$$

where $\sigma_s(t)$ is the stress in the specimen, E is the output elastic modulus of the pressure bar, A_o is the output bar's cross-sectional area, A is the cross-sectional area of the specimen, and ε_t (t) is the transmitted strain.

During Split Hopkinson Pressure Bar testing, a number of factors can have an effect on the test accuracy. These factors include the dispersion of the longitudinal waves, the mismatch of the impedance between the bars and the specimen, the transducer properties

and other such factors. Impedance is defined as the ratio of the driving force to the velocity in a structure at any given point. Variations in impedance may give rise to wave discontinuities in SHPB tests. Varying the properties of the material and the cross-sectional area of the bars /sample have been found to cause discontinuities in the waves produced in SHPB tests. The mechanical impedance, Z, is defined as:

$$Z = \rho A c_o \qquad (3.5)$$

where ρ is the density of the material, A is the cross-sectional area of the bars, and c_o is the longitudinal wave velocity.

As mentioned previously, wave discontinuities can be attributed to variations in the cross-sectional area of the bars/sample and also to variations in material properties. These are considered in the theory of wave transfer between materials having different properties.
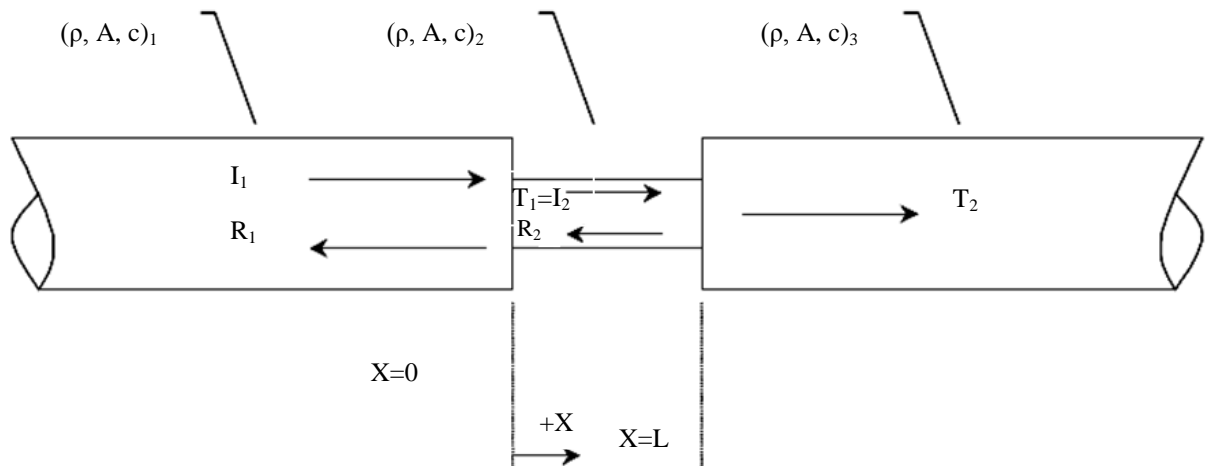
Figure 3.6. Schematic of the changes in material properties and the cross-sectional area of bars/sample SHPB.

In order to compute the variable stress amplitude and the intensity of the wave that is reflected and transmitted at the input and output bar interfaces within the sample, there is a need for an understanding of the dynamic characteristics of the interface between the bars and the sample at each face. Equilibrium of the velocities at the interfaces of the specimen and the bar also has to be achieved. In addition, the forces at each interface must balance with each other to achieve equilibrium. The theory governing the aforementioned requirements, i.e. the equilibrium of velocity and force at the interfaces of two bar specimens, is presented below:

At x=0

$$\frac{I_1 - R_1}{(\rho c)_1} = \frac{T_1}{(\rho c)_2} \tag{3.6}$$

$$A_1(I_1 + R_1) = A_2(T_1)$$

At x=L

$$\frac{I_2 - R_2}{(\rho c)_2} = \frac{T_2}{(\rho c)_3} \tag{3.7}$$

$$A_2(T_1 + R_2) = A_3(T_2)$$

where I, R and T are incident, reflected and transmitted waves.

In addition, the transmitted and reflected coefficients should be defined to solve Equations 3.5 and 3.6 explicitly. The transmission coefficient is the average amplitude of the transmitted stress wave that has passed through the boundary. In contrast, the reflection coefficient is the average of the waves that are reflected at the boundary. The

transmission coefficient has values in the range of zero to one. A value of zero represents complete reflection of the wave, while 1 represents complete transmission of the wave. The reflection and transmission coefficients are defined as:

$$\beta = 1 - \alpha \qquad (3.8)$$

where

$$\alpha = \frac{A_T}{A_I}$$

where A_T, A_I are the area of the transmitted and the area of incident bars. Typically, longitudinal waves develop due to changes as a result of material properties in the cross-sectional area at the bar-specimen interface. At the free end of the bar, it was found that the displacement value had doubled. As a consequence, any measurement of the pressure bar strain has to be conducted at some distance from the free end. Graff reported that the sign of the incident wave was opposite to that of the reflected wave (Graff, 1991). Therefore, the tensile wave can be calculated from initial reflected wave in the pressure bar. During incident bar impact on the specimen, an average stress in the specimen can be found in terms of force on each face of the specimen, as shown in Figure 3.7.
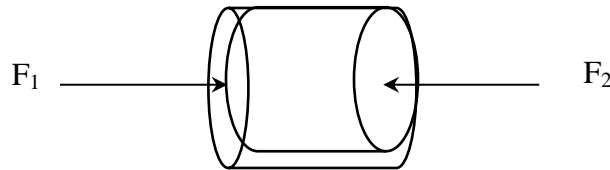
Figure 3.7. Schematic of forces on the SHPB specimen.

The average stress that is on specimen face can be calculated by:

$$\sigma_{av} = \frac{F_1 - F_2}{\frac{\pi}{4}d_s^2} \tag{3.9}$$

where:

$$F_1 = E\big(\varepsilon_i + \varepsilon_r(t)\big)\frac{\pi}{4}\,d_{bar}^2 \tag{3.10}$$

$$F_2 = E\big(\varepsilon_t(t)\big)\frac{\pi}{4}\,d_{bar}^2 \tag{3.11}$$

where F_1, F_2, d_s, ε_i, ε_r, ε_t, d_{bar} correspond to the force applied on Face 1, the force applied on Face 2, the specimen diameter, the incident strain, the reflected strain, the transmitted strain and the diameter of the bar, respectively.

The expression for the average stress on specimen, in terms of the pressure bar strain, can be found by substituting Equations 3.11 and 3.10 into Equation 3.9 as follows:

$$\sigma_{av} = E\frac{d_{bar}^2}{2d_s^2}(\varepsilon_i + \varepsilon_t + \varepsilon_r(t)) \tag{3.12}$$

When the incident pressure bar strain is equal to the pressure in the transmitter bar, the specimen will deform uniformly according to:

$$\varepsilon_t = \varepsilon_i + \varepsilon_r(t) \tag{3.13}$$

Therefore, Equation 3.12 can be expressed as follows:

$$\sigma_{av} = E\frac{d_{bar}^2}{d_s^2}(\varepsilon_t(t)) \tag{3.14}$$

The strain-rate is described as strain divided by time. In this expression, velocity is defined by displacement divided by time. As a result, the strain-rate in the specimen can

be found by recording the interface velocities. Using wave theory, the wave equation can be shown as (Jacob et al., 2004):

$$\frac{d^2u}{dx^2} = \frac{1}{c_0^2}\frac{d^2u}{dt^2}$$

(3.15)

where

$$c_o = \sqrt{\frac{E}{\rho}}$$

(3.16)

where c_o is the longitudinal wave velocity; E is the Young's modulus, and u is the displacement, respectively. The average strain rate at a given time can be found using Equation 3.17.

$$\frac{d\varepsilon}{dt} = \frac{v_{interface\ 2} - v_{interface\ 1}}{L}$$

(3.17)

where

$$V_{interface\ 1} = c_o(\varepsilon_i - \varepsilon_r)$$

(3.18)

$$V_{interface\ 2} = c_o(\varepsilon_t)$$

(3.19)

By substituting equations (3.18) and (3.19) in to Equation (3.20), the expression of strain-rate in terms of the pressure bar strain can be calculated as follows:

$$\frac{d\varepsilon}{dt} = \frac{c_o(\varepsilon_t - \varepsilon_i + \varepsilon_r)}{L}$$

(3.20)

where

$$\varepsilon_t = \varepsilon_i + \varepsilon_r(t)$$

$$\frac{d\varepsilon}{dt} = \frac{2c_o(\varepsilon_r)}{L} \qquad\qquad (3.21)$$

By integrating Equation 3.21, the specimen strain can be found as follows:

$$\varepsilon_s = \frac{2c_o}{L} \int \varepsilon_r(t)dt \qquad\qquad (3.22)$$

3.3.4.3   Terminal ballistic tests

These tests were conducted using the shooting range at RMCS (Cranfield University). The length of the indoor range is 20 metres. The range is equipped with an MS instruments ballistic computer that is located in a monitoring room, which is protected using bullet proof windows. The computer is connected to sensors that measure the velocity of the bullets, which are mounted at 6 and 10 metres down the range. Figures 3.8 to 3.10 provide views of the small arms experimental range and equipment used for ballistic trials at Cranfield University. The aluminium matrix syntactic foam target discs were bonded to the plate of aluminium matrix which was fixed to the stand using a panel clamp.
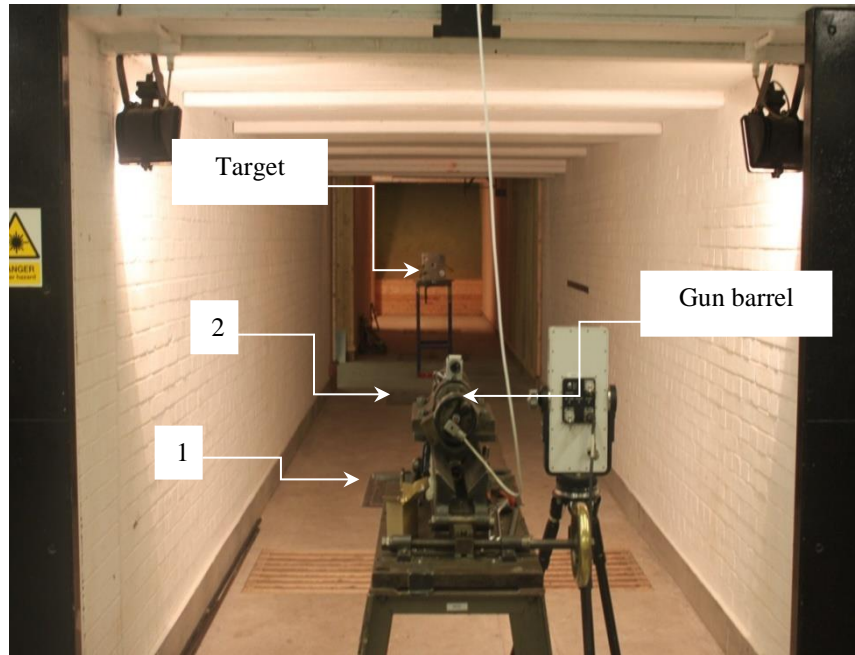
Figure 3.8. Small ballistic experimental range, Cranfield University.
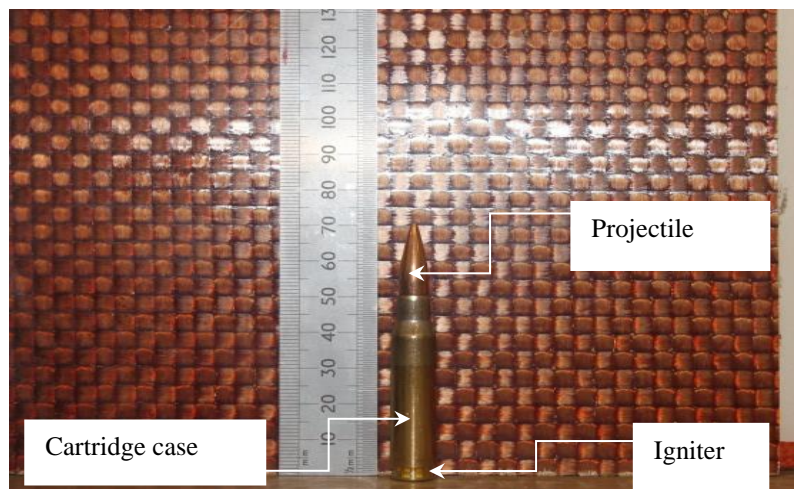
Figure 3.9.The projectile that was used 7.62 x 39 mm AK47.
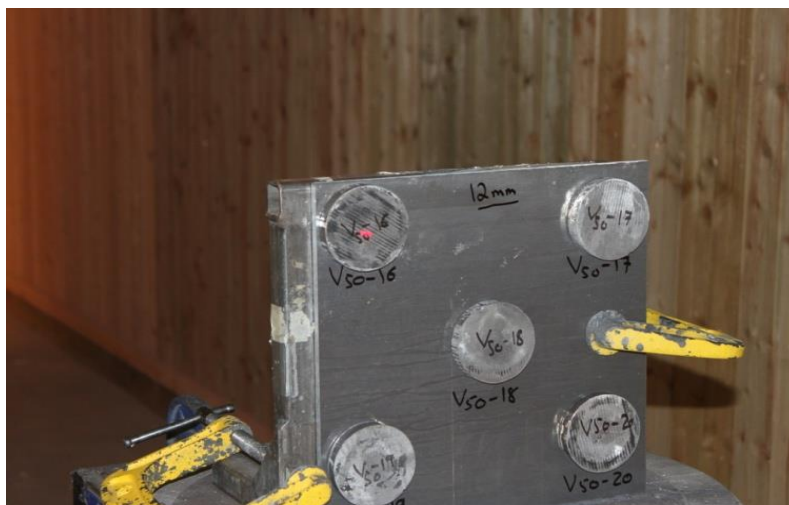
Figure 3.10. Target clamped to the stand.

The labels marked 1 and 2 in Figure 3.8 are the two sensors that measure the projectile velocity. The bullets used in these tests were the Russian AK47 7.62 x 39 mm Kalashnikov. The bullet consists of four main components: the projectile, the propellant, the jacket or cartridge case, and the primer or igniter. After positioning the target, the bullet was loaded in the gun and all personnel were required to move to the control room.

3.3.4.4 Blast Tests

Blast impulses applied were generated using a ballistic pendulum. This experimental method was used previously by Jacob et al. (2004).

Blast testing was conducted as follows:

- Plastic explosive PE4 used for imparting the impulse;

- A ballistic pendulum was used to measure the impulse;

- A steel tube with a 90 mm internal diameter and a 180 mm length for the stand-off distance;

- Steel clamps with a circular aperture.

The ballistic pendulum is made up of an I-beam that is suspended on 4 spring steel cables, which are attached by 4 screws that are adjustable in order to level the pendulum. Counter balancing masses are added to the pendulum end in order to ensure that each spring steel cable carries on equal load. The explosive charge generates an impulse through the centroid of the pendulum. The oscillation amplitude was recorded using a soft tip recording pen and sheet that were located at the end of the pendulum, as shown in Figure 3.11.

Figure 3.11. Photograph of the ballistic pendulum at the University of Cape Town.

Several measurements were taken to calculate the impulse from the tracing paper. These are reported in Table 3.7.

Table 3.7. Mass of the ballistic pendulum and its components.

Mass of I-Beam	25.22 kg
Mass of Clamping Rig	18.22 kg
Mass of Counter Balance	18.20 kg
Total Pendulum Mass (M)	61.64 kg

The test rig is made up of two clamping frames that are made from 20 mm thick steel. The steel is screwed onto one of the clamping plates. The sample was located between two the clamping plates. The test rig is connected to the I-beam with the help of 4 connecting rods which allow the plate to deform without contact with the I-beam. Plastic explosive PE4 was used in these tests. The blast load (20 mm) is fixed on a polystyrene disc that has an equivalent diameter to the specimen, as shown in Figure 3.12. The diameter of the polystyrene pad was 90 mm and its thickness was 13 mm.
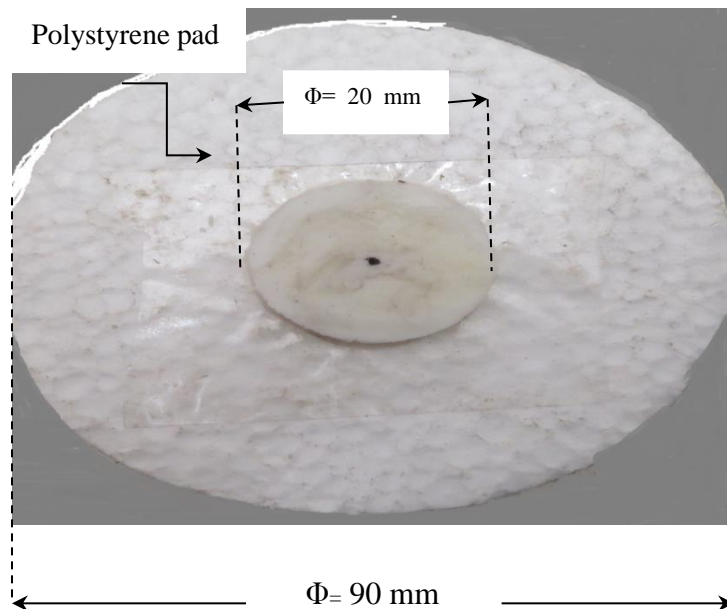
Figure 3.12. Photograph of a disc-shaped PE4 explosive.

The composition and characterisation of PE4 is given in Table 3.8.

Table 3.8. Composition of PE4 (Wharton et al., 2000).

Density	1.6 (g/cm^3)
Lithium and RDX grease	12 % lithium and 88% RDX and
TNT equivalent	130% (by ballistic mortar tests)
Detonation velocity	8200 (m/s)

The mass of the charge was varied while the leader of explosive mass was fixed at 0.5g as shown in Figure 3.13. The charge masses used in the investigation were 3, 2.5, 2.0, 1.5 and 1 grams.

Disc shaped PE4 main charge of diameter 20 mm

0.5 g PE4 leader charge
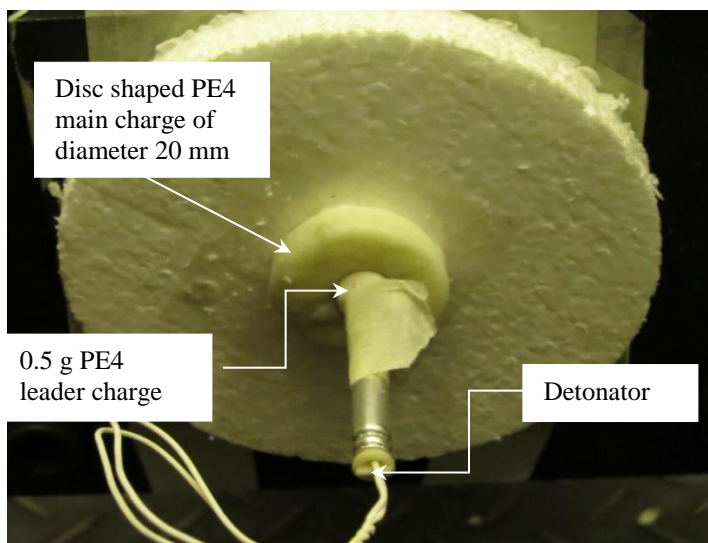
Detonator

Figure 3.13.Photograph of disc-shaped PE4 explosive with a 0.5 g leader attached to the detonator.

A summary of the experimental details is given in Table 3.9.

Table 3.9. Summary of the experimental details.

Test parameters	Detail
Plate thickness	3.10, 5.80, 9.12, 12.8, 14, 16 and 20 mm
Plate diameter	90 mm
Stand-off distance	180 mm
Charge mass	1,1.5, 2, 2.5, 3 grams

In this investigation, PE4 explosive was fixed onto the polystyrene disc where the stand-off distance is 180 mm. The responses of the aluminium syntactic foams will be studieded at different charge mass and plate thickness at a fixed stand-off distance of 180 mm.

3.4   Summary

This chapter presents details of the fabrication of the aluminium matrix syntactic foams and the testing procedure for both quasi-static and dynamic loading. In this chapter, the aluminium syntactic foams were fabricated from two different aluminium grades (Al 6082-T6 and Al 7075-T6) and three different sizes of ceramic micro-sphere (25-75, 150-250 and 250-500 µm). The fabrication process and the specimen geometries were explained in detail. The mechanical properties of the material were tested in compression, three point bending and shear. In addition, the mechanical properties of a number of foams were investigated under drop-weight impact and using a Split Hopkinson Pressure Bar. One type of foam was also tested under terminal ballistic and blast loading.

CHAPTER 4: EXPERIMENTAL RESULTS AND DISCUSSION

In this chapter the experimental results will be presented and discussed. Firstly, the general results from the manufacturing process of the metal syntactic foam and its effects on the material microstructure will be presented. Secondly, the results from compression, three-point bending and shear tests on the aluminium matrix syntactic foam with different configurations will be shown. Thirdly, there will be a discussion on the findings of the drop-weight impact and the Split Pressure Hopkinson Bar studies. Here, that special attention is given to the mechanical properties and fracture characteristics of aluminium matrix syntactic foam. Finally, the results of the terminal ballistic and blast tests on the aluminium matrix syntactic foam will be analysed and evaluated.

4.1 Morphology and Microstructure of the Aluminium Syntactic foam

The microstructures of the three types of aluminium syntactic foam are shown in Figures 4.1 to 4.3. The difference between each type of foam is in the grade of the ceramic micro-spheres and aluminium. The diameter of the coarse grade of the ceramic micro-spheres is between 250 and 500 µm (CM (I) and CM (IV)), the general-purpose grade range is 100–250 µm (CM (II) and CM (V)), and the fine grade is 25–75 µm (CM (III) and CM (VI)). The metal matrix for CM (I), CM (II) and CM (III) is Al7075-T6, while Al 6082-T6 is the metal matrix for CM (IV), CM (V) and CM (VI).
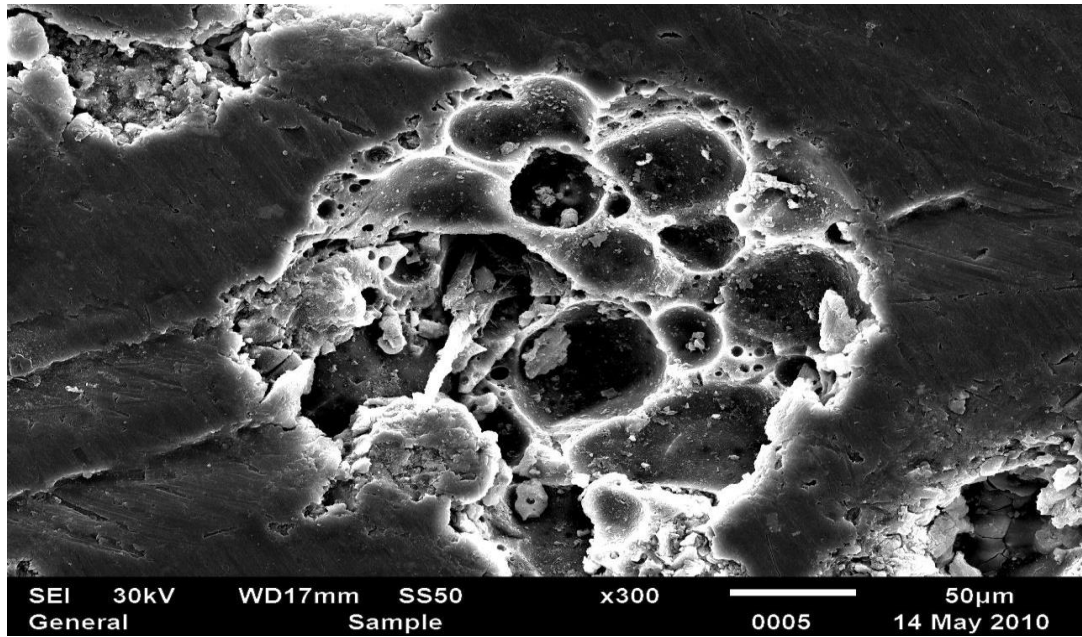
Figure 4.1. Optical micrograph of the aluminium matrix syntactic foam CM (I).
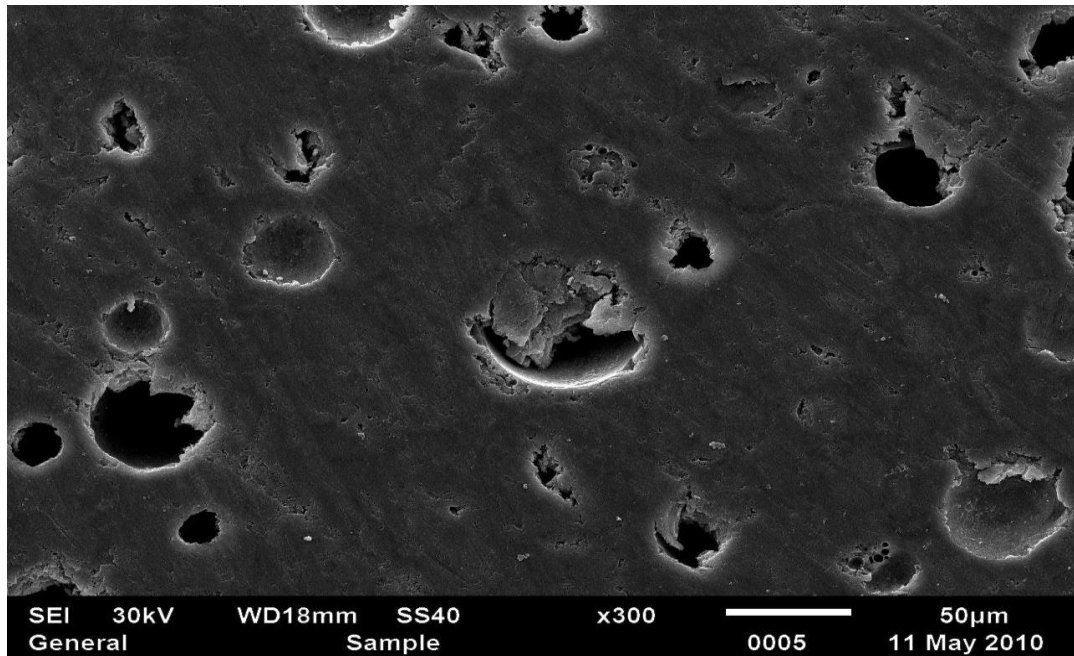
Figure 4.2. Optical micrograph of the aluminium matrix syntactic foam CM (II).
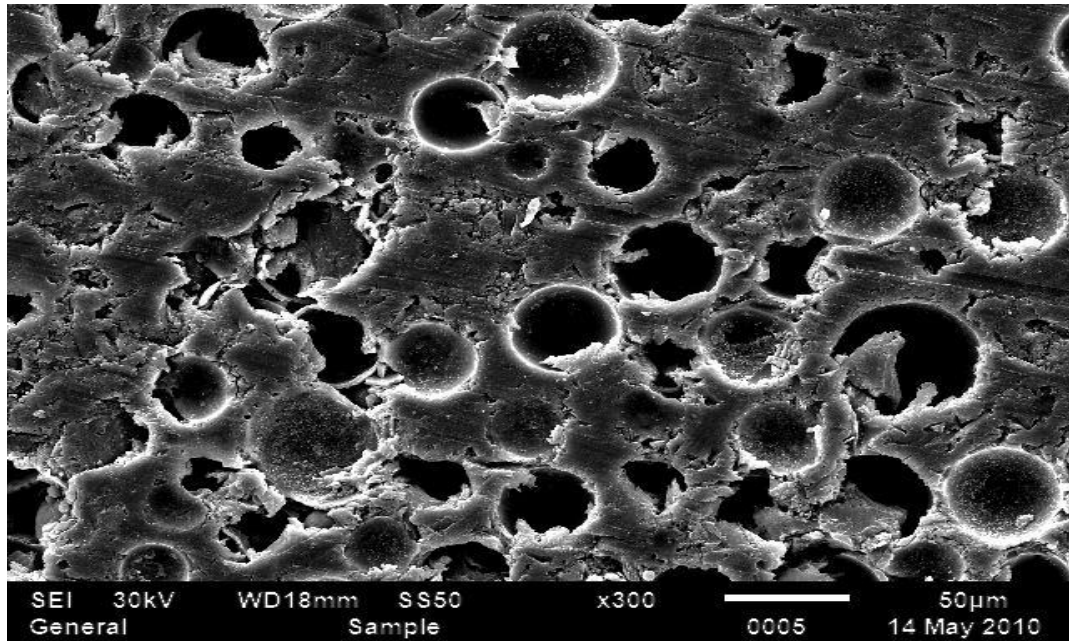
Figure 4.3. Optical micrograph of the aluminium matrix syntactic foam CM (III).

The densities of the six types of syntactic foam (I, II, III, IV, V, VI) were calculated using the average of three sample densities of each type. The density is different in each type of syntactic foam, due to the difference in the size of the ceramic micro-spheres, the possibility of differences in full infiltration and the number of voids between the ceramic micro-spheres and the aluminium matrix. Typically, syntactic foams types I and IV are more likely to have an increased percentage of infiltrated ceramic micro-spheres and fewer voids between the ceramic micro-spheres.

In most cases, the densities of the aluminium matrix syntactic foams were within a range of 1500–2390 kg/m^3, as shown in Figure 4.4. The calculated density was obtained using a rule of mixtures with a volume fraction of ceramic micro-spheres of 63% and sphere density in the range of 600–900 kg/m^3. The calculated density is higher than experimental density as shown in Figure 4.5, due to the assumption that the aluminium matrix is fully

infiltrated into the ceramic micro-spheres and there are no voids between the ceramic micro-spheres and no porosity inside the micro-spheres.
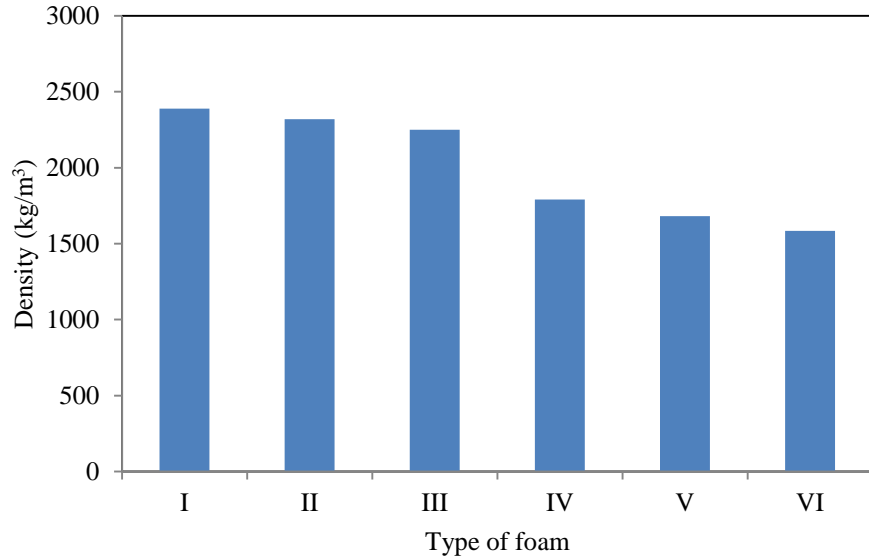
Figure 4.4. Density of aluminium syntactic foam for different sizes of ceramic micro-spheres and different aluminium matrix grades.
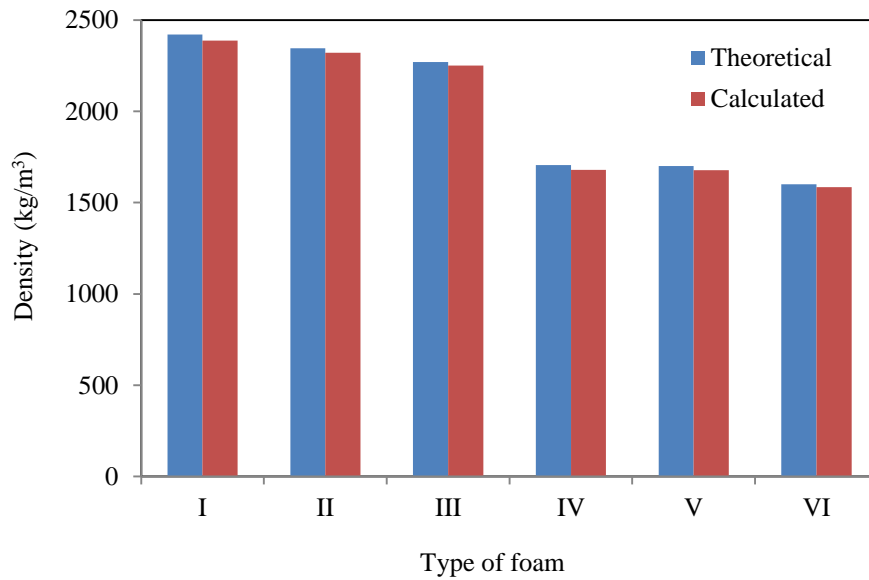
Figure 4.5. The calculated and measured densities of the aluminium syntactic foam for different sizes of ceramic micro-spheres.

4.2 Characterising the Behaviour of the Aluminium Syntactic Foam under Quasi-static Loading

4.2.1 Compression response of the aluminium matrix syntactic foam

Figure 4.6 shows a typical stress–strain curve for an aluminium matrix syntactic foam. There are three typical phases observed in the compression of cellular solids. Initially, it starts with a linear elastic phase, where the strain is less than 3% and the stress–strain relationship follows Hooke's law. The slope of the first part is defined as the Young's modulus. This is followed by a section where the peak stress is reached, plastic deformation of the matrix starts and the load transfer between the matrix and ceramic micro-spheres reaches its maximum. This is where the compressive strength is measured. Next, there is a small reduction in stress due to the reduced load-bearing capacity caused by the crushing of the ceramic micro-spheres, which results in the movement of the specimen. The second phase occurs between strains of 10% and 43%, characterised by a relatively constant plateau stress, where the micro-porosity in ceramic micro-spheres densifies plastically and where the fracture band expands. The energy absorption capacity can be found in this region, where the stress remains constant with the increasing strain. The final phase is densification, which starts when the stress increases to a high value very quickly, while the strain increases slowly. The densification strain is located at the intersection of the tangents to the densification stage phase and the plateau phase. The mechanical properties of the syntactic foams are listed in Table 4.1. Figure 4.7 shows the compressive stress–strain curves of the syntactic foams CM (I), CM (II), CM (III), CM (IV), CM (V) and CM (VI). The difference between each type of foam is the grade of the aluminium matrix or the size of the ceramic micro-spheres. The larger ceramic micro-

spheres offer a higher strength under compression than the smaller ones. The results show that the peak stress of CM (I) reaches 179 MPa, which is higher than those of CM (II) and CM (III) based on the same grade of aluminium (7075-T6), which have peak stress values of 167 MPa and 160 MPa, respectively. This is due to the lower void volume fraction and the higher volume fraction of ceramic micro-spheres. In addition, the thinner walls ensure lower deflections.
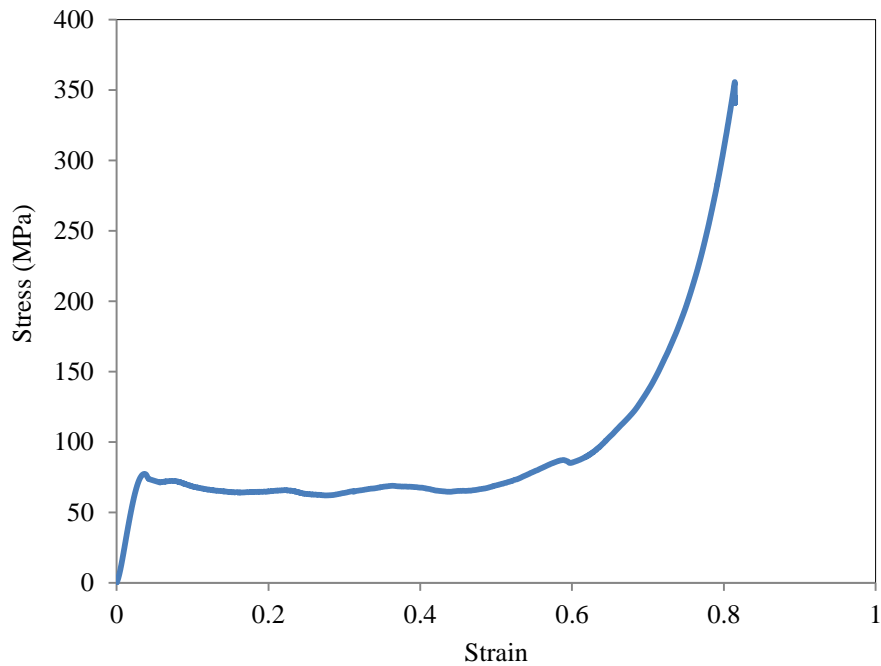
Figure 4.6. A typical stress–strain trace following quasi-static testing on the aluminium matrix syntactic foam sample CM (VI).

Table 4.1. Average mechanical properties of the aluminium matrix syntactic foam.

Foam	Density (kg/m^3)	Plastic collapse stress, σ_{pl} (MPa)	Compressive modulus, E_c (GPa)	Steady state stress, σ_{ss} (MPa)	Densification strain, ε_D %
CM(I)	2388	179	3.22	175	36
CM(II)	2321	167	2.83	150	41
CM(III)	2250	160	2.45	148	43
CM(IV)	1790	130	2.40	128	43
CM(V)	1680	101	2.25	78	44
CM(VI)	1585	75	2.10	65	50
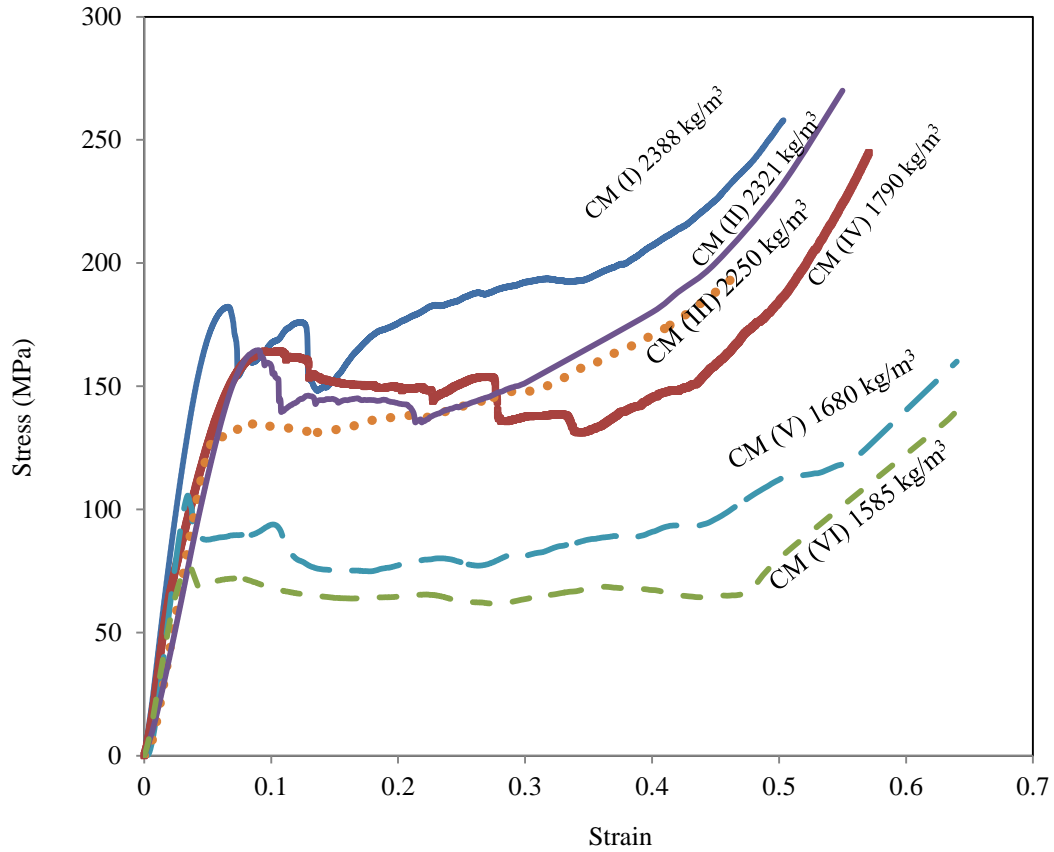
Figure 4.7. Typical average stress–strain curves following quasi-static tests on the aluminium matrix syntactic foams.

The effects of varying the density of the aluminium matrix syntactic foam on its mechanical response are also shown in Figure 4.7. The figure shows that an increase in density results in an increase in the plastic collapse strength, the modulus of the elasticity and the steady-state stress as well as a decrease in the densification strain. It has been shown that the plastic collapse strength and Young's modulus increase steadily with increasing cell size (Zhang and Zhao, 2007).

From Figure 4.7, it is clear that an increase in density leads to an increase in the plateau stress before the aluminium matrix syntactic foam begins to densify. The nominal densification strain was 36% for the 2388 kg/m^3 foam, 41% for the 2321 kg/m^3 foam, 43% for the 2250 kg/m^3 foam, 42% for the 1790 kg/m^3 foam, 44% for the 1681 kg/m^3 foam and 50% for the 1585 kg/m^3 foam. Therefore, the densification strain increases with a decrease in foam density.

It was also found that the grade of aluminium matrix also affects the compressive strength of the associated syntactic foam. When the Al7075-T6 matrix was used, the average compressive strength of syntactic foam increased by approximately 40% compared to that containing Al6082-T6, due to the grade of the aluminium matrix. The results show that a stronger metal matrix leads to a higher compressive strength (Rohatgi, 2011).

An increase in the aluminium volume fraction has an effect on the behaviour of the composite. It was observed that the strength of the syntactic foams increases with aluminium volume fraction. In spite of the increase in the volume fraction of aluminium, the densification strain stays similar, as shown in Figure 4.8. The volume fraction of aluminium matrix affects the behaviour of the foam under quasi-static compression

loading. It has been found that increasing the percentage of aluminium matrix changes the failure mode in the syntactic foam (Kiser et al., 1999). The results show that the foam matrix becomes more ductile with an increase in the volume fraction of aluminium matrix. The mode of fracture changes to x-shaped cracks, which appear in the middle of the sample, instead of the shear failure, as shown in Figure 4.9.
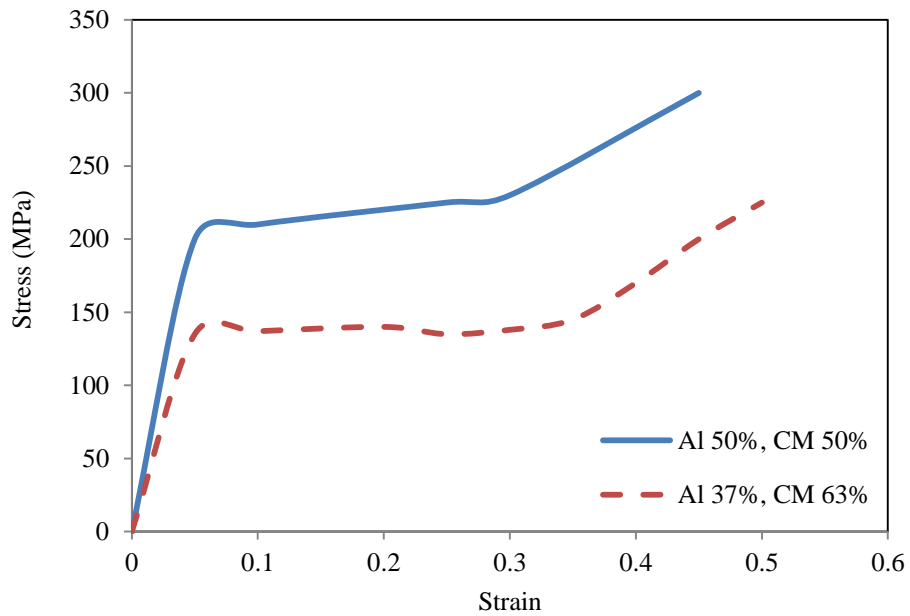
Figure 4.8. Comparison of the compressive response of the aluminium matrix syntactic foam for two volume fractions of aluminium matrix.

<center>(a)   (b)</center>
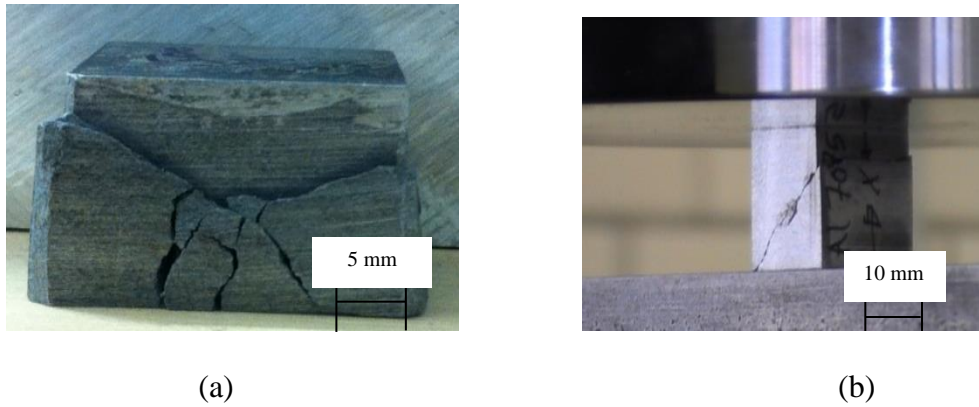
Figure 4.9. Photograph of the failure of the aluminium matrix syntactic foam; (a) aluminium matrix percentage of 50%; (b) aluminium matrix percentage of 33%.

Figure 4.10 summarises the variation of the average value of plastic collapse stress (σ_{pl}) with density for six syntactic foams at quasi-static rates of loading. It is clear that the value of σ_{pl} for all types of syntactic foam increases with changing aluminium grade, however the increase for the 7075-T6 system is small. Recent work by Tao (2010) showed that as the syntactic foam density increases, the compressive collapse strength increases according to a power law relationship. From Figure 4.10, it is evident that the syntactic foam based on a 7075-T6 matrix is superior to the syntactic foam based on the 6082-T6 matrix. Balch et al. (2005) found that 7075-T6 has a higher yield stress than other types of aluminium matrix. The results show that the average value of σ_{pl} for a syntactic foam based on aluminium 7075-T6 is approximately 40% higher than that for a syntactic foam based on aluminium 6082-T6.
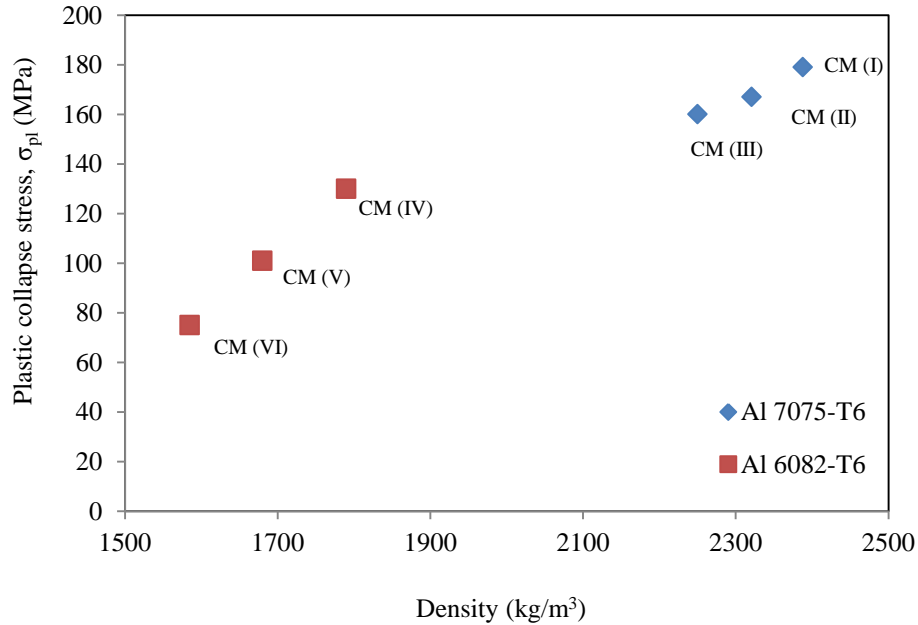
Figure 4.10. The variation of the plastic collapse stress with density for different syntactic foams.

Figure 4.11 shows that the Young's modulus is sensitive to the density of the syntactic foam. All of the foam materials exhibit an increasing compressive modulus with increasing foam density. When the ceramic micro-sphere size is fixed (CM (I) and CM (IV)) with different aluminium matrix grade, the density increases by 25% and the Young's modulus value of the syntactic foam increases by 25.5%.

Figure 4.12 shows that the plateau stress rises with increasing foam density, since increasing the density resulted in a greater resistance to cracking of the ceramic micro-spheres.
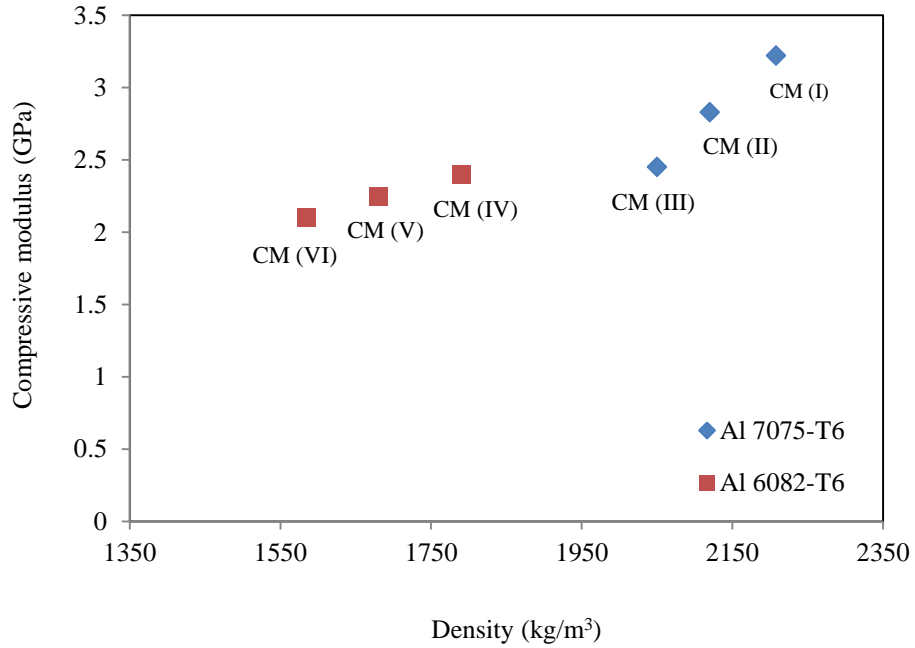
Figure 4.11. The variation in compressive modulus with density for different syntactic foams.
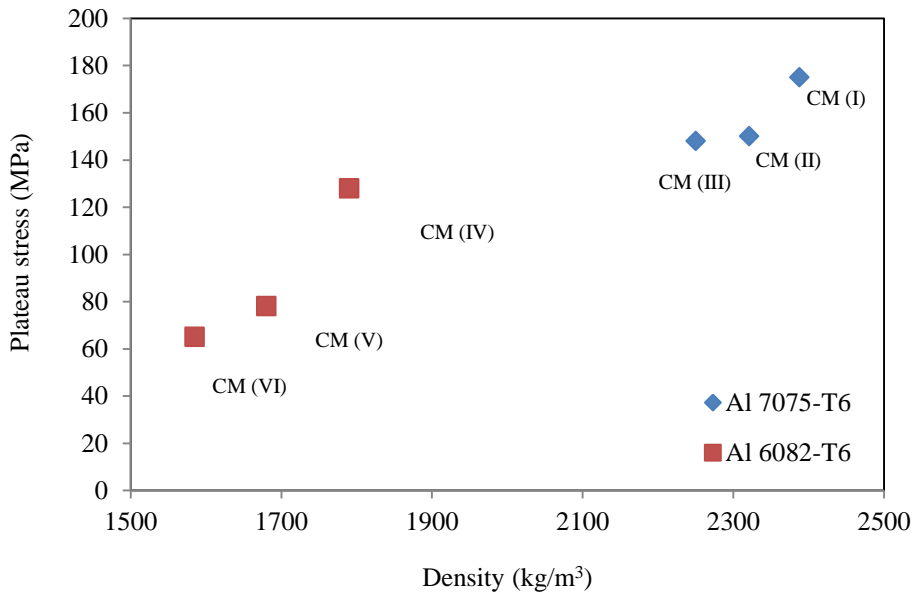
Figure 4.12. The variation in plateau stress with density for different syntactic foams.
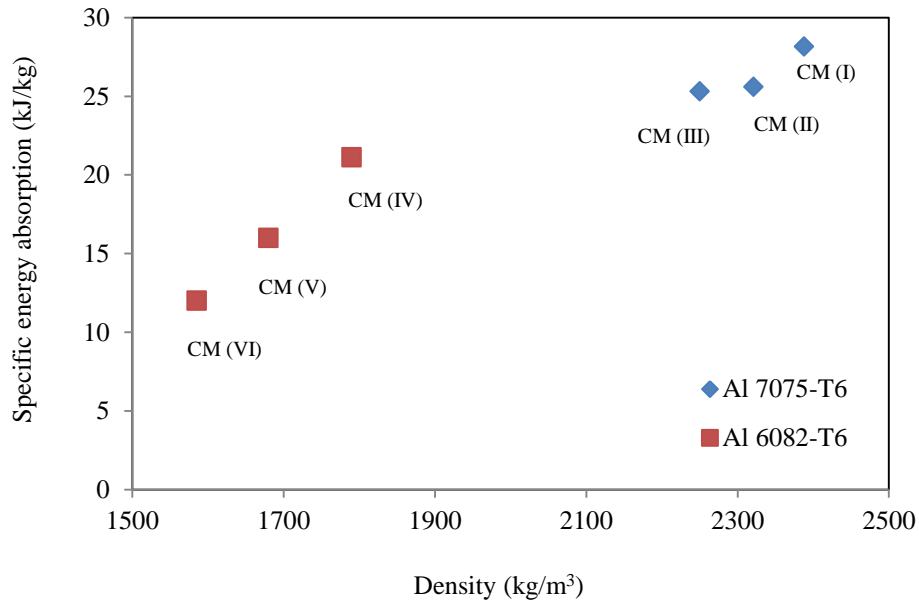
Figure 4.13. Plot of the specific energy absorption vs. density for different syntactic foams.

The area under the load-displacement curve was used to calculate the energy absorbed by the syntactic foam during the test. Figure 4.13 shows that the absorbed energy increases when increasing the foam density. Increasing the density resulted in an increase in the steady state stress (plateau stress) and densification strain. The higher compressive strength led to a higher plateau strength and, due to this, a larger area under the compressive curve and therefore a higher consumed specific energy (Orbulov, 2012). The energy absorbed by the syntactic foam depends on the plateau strength and the densification strain. The plateau strength depends on the strength of the matrix and the ceramic particles, as well as the volume ratio between the metal matrix and ceramic micro-spheres, whereas the densification strain is mainly dependent on the level of porosity in the syntactic foam. In addition to this, an increase in the aluminium ratio in the composite can lead to an increase in the compressive strength and the steady-state

stress (plateau stress), resulting in an increase in energy absorption capability, as shown in Figure 4.8.

Figure 4.14 shows stress–strain curves following quasi-static compression tests on the aluminium (Al7075-T6) system at different strain-rates. The graph shows the effect of strain-rate on the material response, which indicates that aluminium matrix syntactic foam is sensitive to strain-rate. As the strain-rate is increased, the compressive strength and steady-state stress of the aluminium syntactic foam increase.
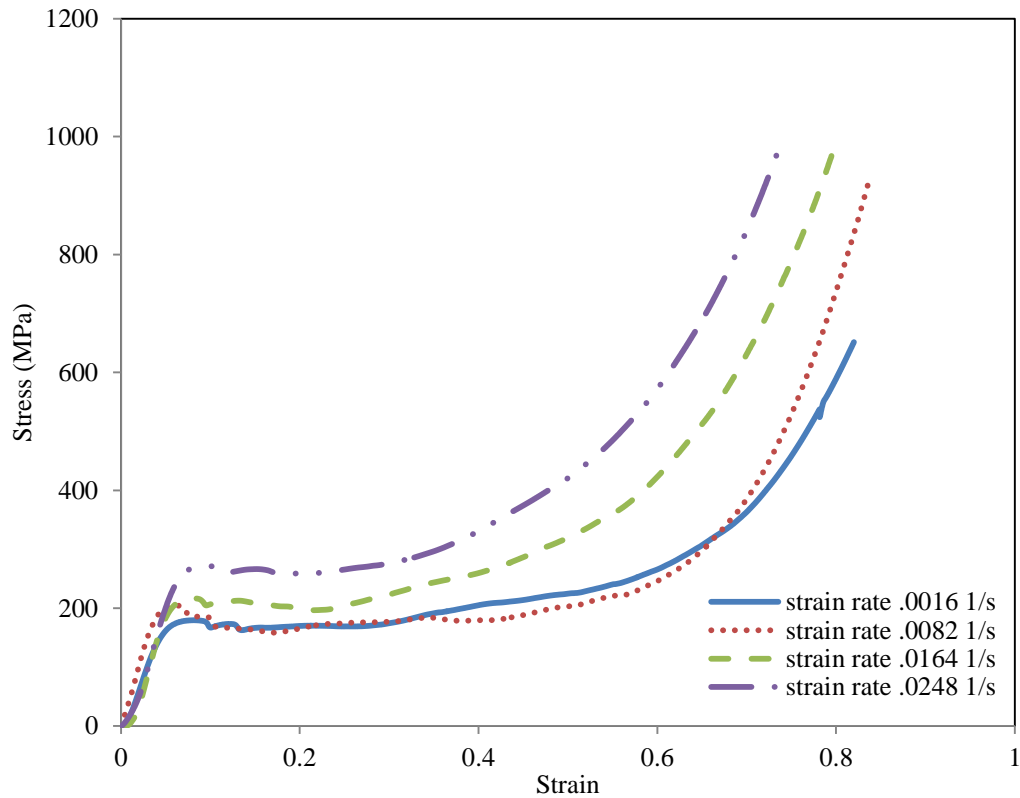
Figure 4.14. Stress–strain traces for aluminium (7075-T6) syntactic foam at different strain-rates.

4.2.2 Flexural response of the aluminium matrix syntactic foam

The flexural properties of syntactic foams are listed in Table 4.2, and Figure 4.15 shows the quasi-static three-point bending load-deflection curves for the aluminium matrix syntactic foams with different sizes of ceramic micro-sphere.
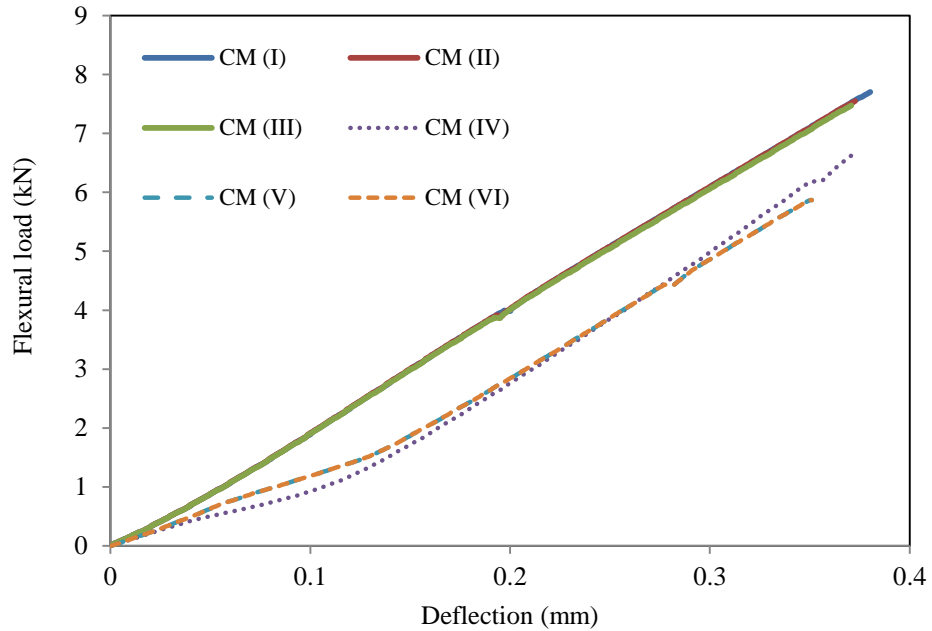
Figure 4.15. Three-point bending response of the aluminium matrix syntactic foams.

Table 4.2. Average flexural properties of the aluminium matrix syntactic foams.

Foam	Density (kg/m^3)	Maximum deflection (mm)	Peak load (kN)	Stiffness (kN/mm)	Flexural modulus (GPa)	Flexural strength (MPa)	Flexural strain (bottom)	Specific energy (kJ/kg)
CM(I)	2388	0.385	7.70	21.91	2.07	462.23	0.00641	1.469
CM(II)	2321	0.377	7.55	20.46	2.06	452.98	0.00628	1.412
CM(III)	2250	0.375	7.47	19.77	2.03	448.40	0.00625	1.390
CM(IV)	1790	0.373	6.66	19.43	2.02	399.50	0.00621	1.033
CM(V)	1630	0.359	6.16	17.10	2.00	369.75	0.00598	0.982
CM(VI)	1616	0.352	5.87	16.05	1.98	352.15	0.00586	0.920

The results show that the elastic region of the load-deflection traces and the responses of specimens to the applied load are quite similar. This is apparent from the constant slope in this region for the different types of aluminium syntactic foam. All of the syntactic foams failed in a brittle fracture mode. As observed from the results, the curves are smooth until they reach the maximum load, except for the CM (VI) system, which deviates slightly from linearity before reaching the maximum load. It was observed that failure starts in the form of cracks on the tensile side of the specimen as the deflection increases. The effect of varying the density of the aluminium matrix syntactic foam on the flexural response of the foam is also shown in Table 4.2. The table shows that an increase in density results in an increase in stiffness, the specific energy absorption and the flexural strain. The load-deflection data are used to calculate the strength, the energy absorbed and the flexural modulus. All these properties are discussed below.

Table 4.2 gives a comparison of the fracture strain values for aluminium syntactic foams of varying densities. The results show that there is a 6% increase in the failure strain of the CM (III) foam based on Al7075-T6 compared to CM (VI) foam based on Al6082-T6. The grade of aluminium plays an important role in increasing the failure strain. Furthermore, on increase in the size of the ceramic micro-spheres enhances the failure strain. For example, Al 6082-T6, with 250–500 μm ceramic micro-spheres (CM IV), with a density of 1790 kg/m^3, offered a failure strain value of 0.00621, compared to the values of 0.00586 for a density of 1616 kg/m^3 in Al 6082-T6 with 25–75 μm ceramic micro-spheres (CM VI).

Figure 4.16 shows a comparison of the maximum deflection values versus density for various aluminium syntactic foams. The results show that the syntactic foam with an Al

7075-T6 matrix exhibits a 3% increase in maximum deflection (CM I) compared to CM (IV), which based on Al 6082-T6. In addition, the size of the ceramic micro-spheres has an effect on the maximum deflection. It was found that the maximum deflection increases with an increase in foam density. The results show that among the six syntactic foams tested, the aluminium syntactic foam based on Al 6082-T6 with ceramic micro-spheres in the range of 25–75 µm in diameter offers the lowest value of maximum deflection for a given density. It should also be noted that, due to the density of the aluminium matrix, the aluminium syntactic foam based on Al 7075-T6 and ceramic micro-spheres with diameters 250–500 µm offers a greater deflection than that exhibited by the five other foams. For example, the aluminium syntactic foam based on Al 7075-T6 and ceramic micro-spheres of 250–500 µm in diameter, with a density of 2388 kg/m^3, offered a value of 0.385 mm, compared to 0.373 mm for the 1790 kg/m^3 Al 6082-T6 system containing 250–500 µm ceramic micro-spheres (CM IV). Here, it is clear that the strength of the aluminium plays an important role in determining the maximum deflection.

Figure 4.17 shows a comparison of the peak load versus density for various aluminium syntactic foams. The results show that syntactic foams based on the Al 7075-T6 matrix exhibit an average 13.5% increase in peak load. In addition, the size of the ceramic micro-spheres has an effect on the peak load. The results also show that of the six syntactic foams tested, the aluminium syntactic foam containing Al 6082-T6 and 25–75 µm ceramic micro-spheres (CM VI) has the lowest value of peak load for a given density. In addition, due to the density of the aluminium matrix, the aluminium syntactic foam with Al 7075-T6 and 250–500 µm ceramic micro-spheres (CM I) offers a higher peak load than those offered by the five other foams. For example, the aluminium syntactic

foam with Al 7075-T6 and 250–500 µm ceramic micro-spheres, with a density of 2388 kg/m^3, offered a value of 7.70 kN, compared to the values of 6.66 kN for the 1790 kg/m^3 Al 6082-T6 and 250–500 µm system (CM IV).

Figures 4.18 and 4.19 show the flexural stiffness and flexural modulus, respectively, for the various syntactic foam densities, the figures highlight an increase with an increase in foam density. The increases in the stiffness and flexural modulus can be related to the increases in the strength of the metal matrix and the size of the ceramic micro-spheres.
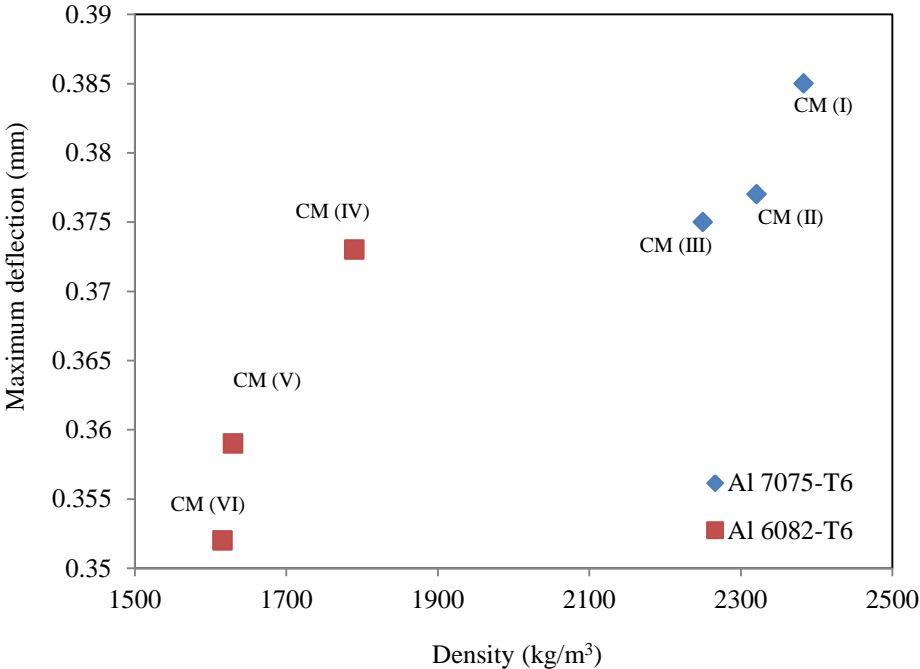
Figure 4.16.   Plot of the maximum deflection vs. density for different syntactic foams.
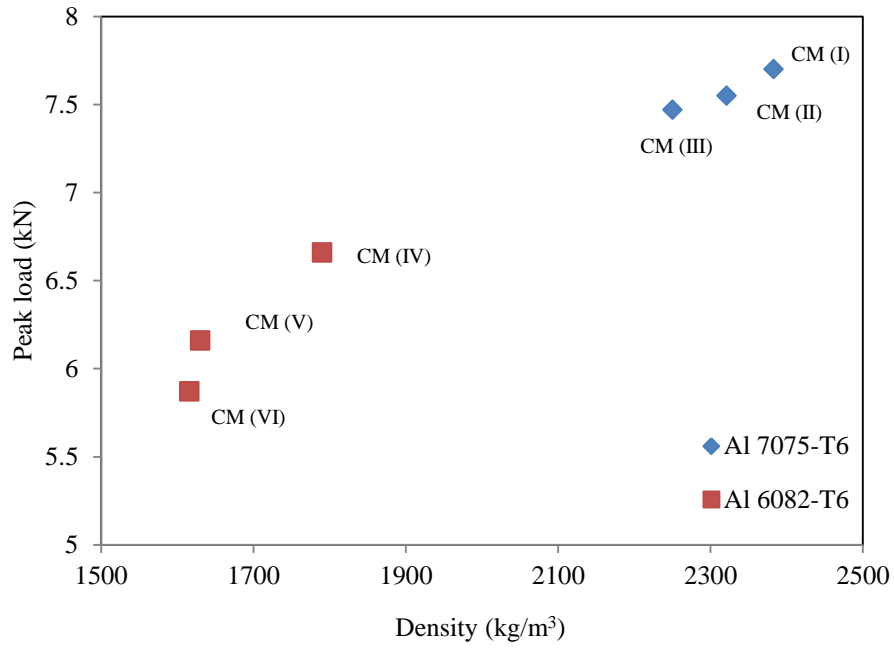
Figure 4.17. Plot of peak load vs. density for different syntactic foams.
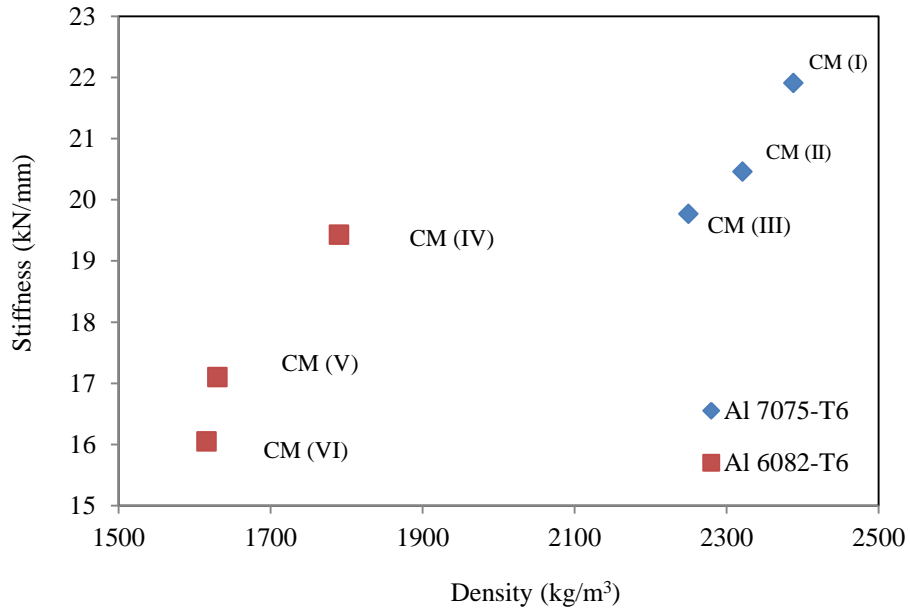
Figure 4.18. Plot of the stiffness vs. density for different syntactic foams.

Figure 4.19. Plot of the tangent modulus vs. density for different syntactic foams.

Figure 4.20 shows a comparison of the flexural strength of several aluminium syntactic foams. It can be seen that the flexural strength increases with increasing foam density. Cracks appeared at small deflections in the aluminium matrix with Al6082-T6 and 25–75 μm ceramic micro-spheres, due to the inherent weakness of the ceramic micro-spheres (Maharsia et al., 2006).
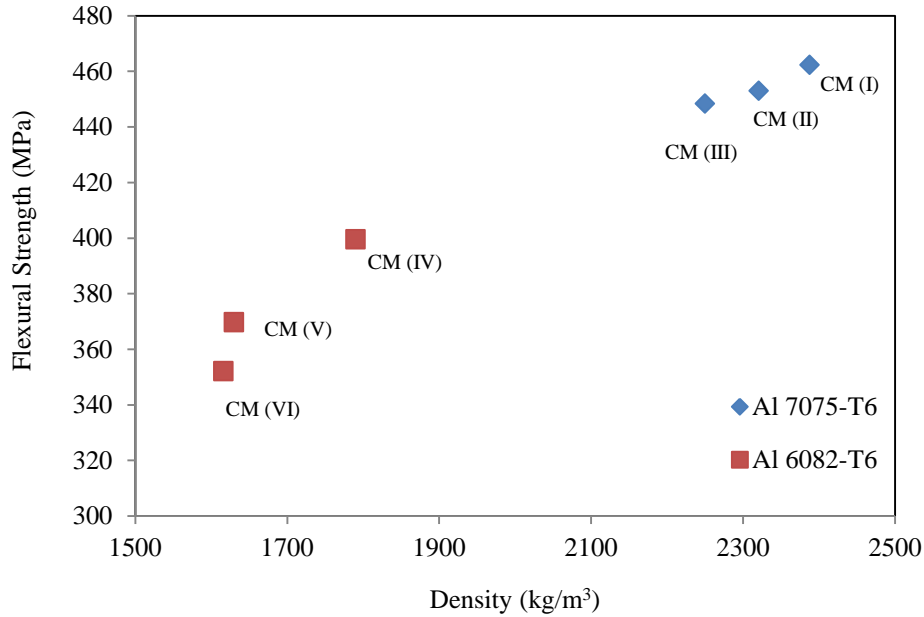
Figure 4.20. Plot of the flexural strength vs. density for different syntactic foams.

The influence of the size of the ceramic micro-spheres on the load-deflection response of aluminium syntactic foam was also studied. An increase in the size of the ceramic microspheres resulted in an increase in the peak load, as well as the maximum deflection. The area under the load-deflection curve could be used to characterise the energy absorption in the specimens. Figure 4.21 shows the influence of the density of the syntactic foams on energy absorption. An increase in matrix strength leads to an increase in energy absorption. The results show that energy absorption depends on the flexural strength and deflection. For example, Al 7075-T6 with 250–500 μm ceramic micro-spheres (CM I), with a density of 2388 kg/m^3, offered a value of 1.47 kJ/kg, compared to a value of 1.03 kJ/kg for a density of 1790 kg/m^3 in Al 6082-T6 with 250–500 μm ceramic micro-spheres (CM IV).
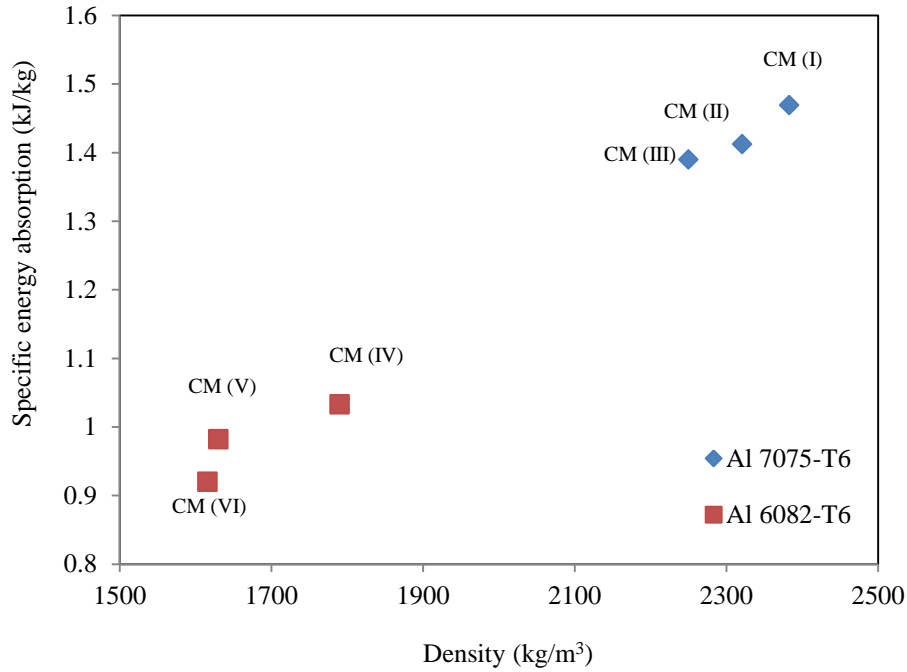
Figure 4.21. Plot of the specific energy absorption vs. density for different syntactic foams.

4.2.3 Shear response of the aluminium matrix syntactic foam

Shear tests were conducted on six types of aluminium matrix syntactic foam cylinder at a crosshead displacement rate of 1 mm/min to investigate their shear properties. The result for each type of aluminium matrix syntactic foam was obtained by averaging the values of three repeat tests. The shear properties of the syntactic foams are listed in Table 4.3. Figure 4.22 shows the shear load-displacement curves for the syntactic foams CM (I), CM(II), CM(III), CM (IV), CM (V) and CM (VI), where brittle behaviour is observed.
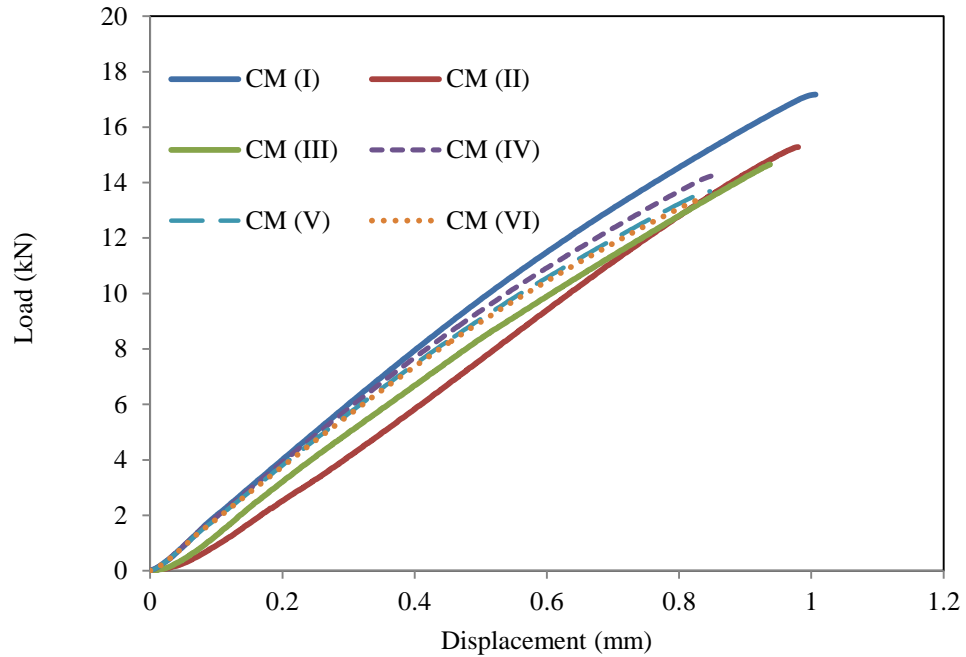
Figure 4.22. Shear response of the aluminium matrix syntactic foam.

Table 4.3. Average shear properties of the aluminium matrix syntactic foam.

Foam	Density (kg/m^3)	Maximum displacement (mm)	Peak load (kN)	Stiffness (kN/mm)	Shear modulus (MPa)	Shear strength (MPa)	Shear strain	Energy absorption (kJ/kg)
CM (I)	2381	1.027	17.18	17.11	448	60.60	0.054	0.596
CM (II)	2323	0.995	15.30	16.91	440	53.89	0.052	0.474
CM (III)	2205	0.937	14.66	16.18	415	51.69	0.049	0.449
CM (IV)	2182	0.873	14.26	16.15	414	50.28	0.046	0.446
CM (V)	2147	0.864	13.69	15.93	410	48.27	0.045	0.440
CM (VI)	2029	0.855	13.41	15.81	408	47.31	0.045	0.439

The results show that the load-displacement curves and the mechanical responses of specimens are quite similar. This is apparent from the similar slope in elastic region for

93

different types of aluminium syntactic foam. These syntactic foams failed in a relatively brittle fracture manner. The curves are smooth until the maximum load is reached. Because of the cylindrical shape of the specimens, shear loading results in a non-uniform deformation from the centre to the outer surface. A crack initiates from the centre before propagations to the outer surface causing failure. Once a ceramic micro-sphere wall cracks, the local stress distribution causes an increase in stress on the neighbouring cell walls.

The influence of foam density on shear response is shown in Table 4.3. The table shows that an increase in density results in an increase in the stiffness, the absorbed energy and the shear strain. The results show that all the foams fail in a brittle fracture mode at the end of the elastic region. The load-displacement data were used to calculate the stiffness, strength, energy absorbed and shear modulus. All these properties are discussed below.

Figure 4.23 shows that the maximum shear displacement values of foams based on the 7075-T6 aluminium matrix are greater than those of produced using the 6082-T6 aluminium matrix. It was found that maximum displacement increases with increasing syntactic foam density. However, the results show that of the six syntactic foams tested, Al 6082-T6 with 25–75 μm ceramic micro-spheres (CM VI) exhibits the lowest value of maximum displacement for a given density. It is also important to note that, due to the density of the aluminium matrix, Al 7075-T6 with 250–500 μm ceramic micro-spheres offers a greater displacement than those exhibited by the five others syntactic foams. For example, Al 7075-T6 with 250–500 μm ceramic micro-spheres CM(I), with a density of 2381 kg/m^3, offered a value of 1.03 mm, compared to a value of 0.873 mm for CM (IV) with a density of 2182 kg/m^3 (Al 6082-T6 with 250–500 μm ceramic micro-spheres). The

results show the influence of the density of the aluminium matrix on the maximum displacement of the aluminium foam. They confirm the dependency of the foam behaviour on the metal matrix strength and show that the syntactic foam with the highest density exhibits an average 12% increase in maximum displacement compared to the other types of syntactic foam with lower densities. However, the size of the ceramic micro-spheres has an effect on the maximum displacement. For example, the 6082-T6 system with larger ceramic micro-spheres (CM IV) has a higher maximum displacement (0.873 mm) than CM VI.
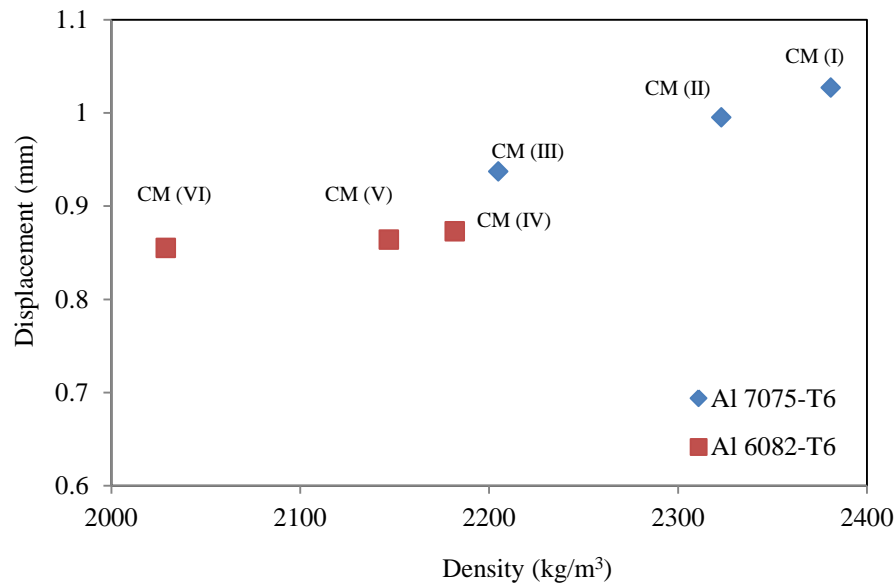
Figure 4.23. Plot of the maximum displacement vs. density for different syntactic foams.

Figure 4.24 shows that the peak load values for the 7075-T6 syntactic foams are, in general, greater than the values for 6082-T6 syntactic foams. The results show that syntactic foams with the Al 7075-T6 matrix offer higher peak load by 12.6 %. However, 6082-T6 syntactic foam with 25–75 μm ceramic micro-spheres (CM VI) has a slightly lower peak load value than other type of aluminium (6082-T6) with larger ceramic micro-

spheres (CM IV). The lower peak load in this material can be attributed to the lower strength of the syntactic foam. In addition, due to the density of the aluminium matrix, Al 7075-T6 with 250–500 μm ceramic micro-spheres (CM I) has a higher peak load value than those exhibited by the five other syntactic foams. For example, Al 7075-T6 with 250–500 μm ceramic micro-spheres (CM I) and a density of 2381 kg/m^3, offered a value of 17.18 kN, compared to a values of 14.26 kN mm for CM (IV) (density of 2182 kg/m^3 for Al 6082-T6 with 250–500 μm ceramic micro-spheres).
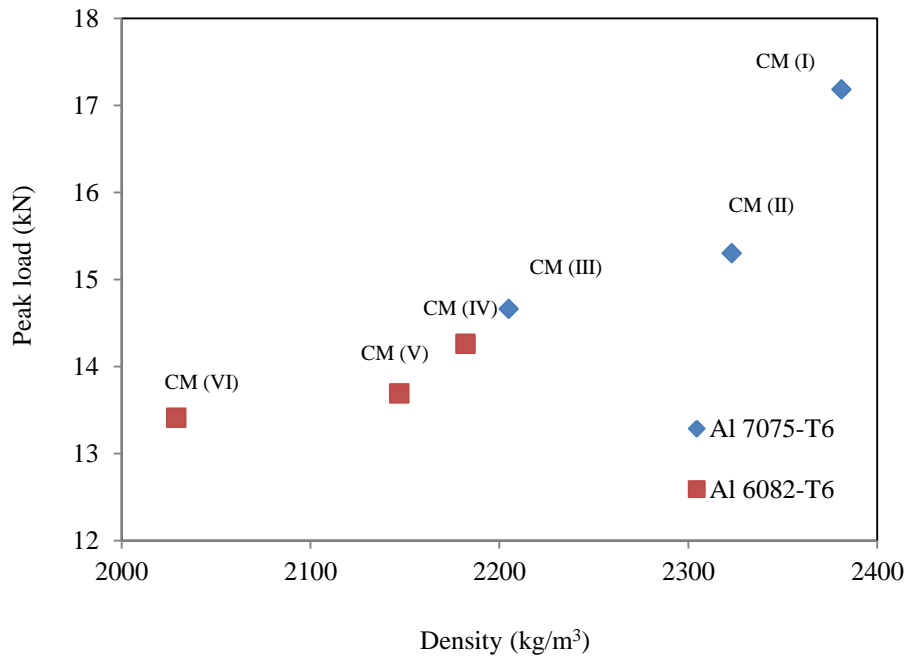
Figure 4.24. Plot of the peak load vs. density for different syntactic foams.
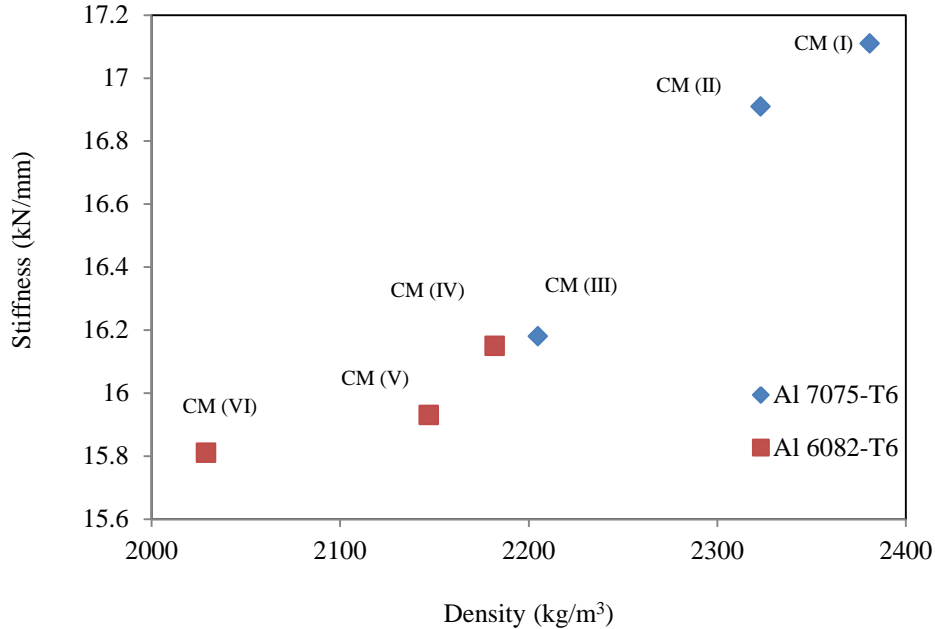
Figure 4.25. Plot of the stiffness vs. density for different syntactic foams.

Figures 4.25 and 4.26 show that the stiffness and shear modulus values of 7075-T6 syntactic foams are, in general, greater than the values for 6082-T6 syntactic foams. The results show that Al 7075-T6 syntactic foam has an average 5.3% and 6.8% increase in stiffness and shear modulus, respectively. However, the 6082-T6 syntactic foam with 250–500 µm ceramic micro-spheres (CM IV) offers slightly higher stiffness and shear modulus values than the other types of 6082-T6 syntactic foam with smaller ceramic micro-spheres. The reduced stiffness and shear modulus in this material can be attributed to the strength of the syntactic foam. In addition, due to the higher strength of the aluminium matrix, the Al 7075-T6 foam with 250–500 µm ceramic micro-spheres (CM I) offers a higher stiffness and shear modulus than those exhibited by the five other syntactic foams. For example, Al 7075-T6 with 250-500 µm ceramic micro-spheres (CM I) and a density of 2381 kg/m^3, offers value of 17.11 kN/mm and 448 MPa, for the stiffness and shear modulus, respectively. On other hand, Al 6082-T6 foam with 250–500

µm ceramic micro-spheres (CM IV) and a density of 2182 kg/m^3, offers values of 16.15 kN/mm and 414 MPa, for the stiffness and shear modulus, respectively.
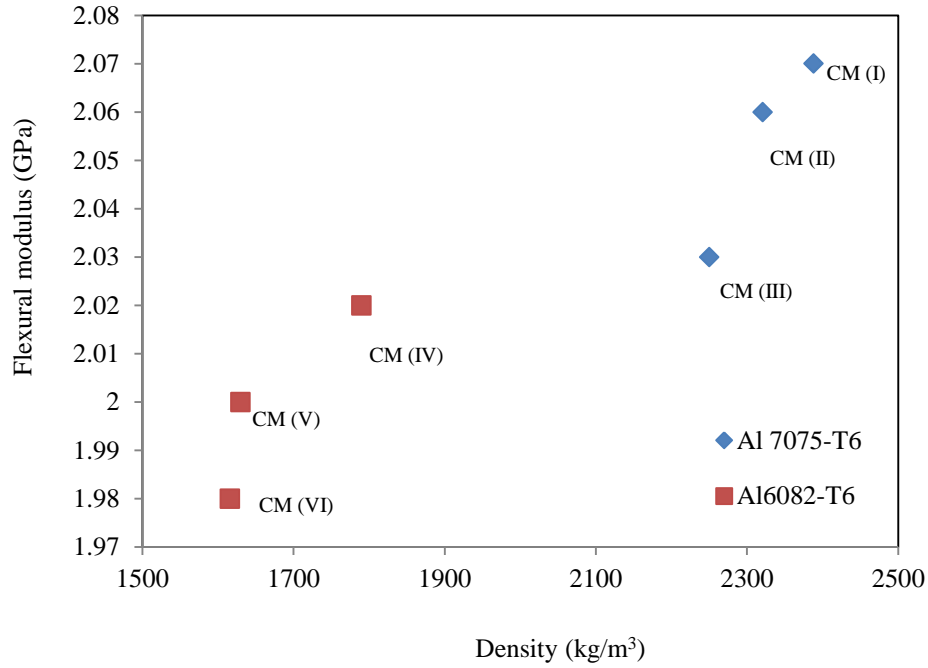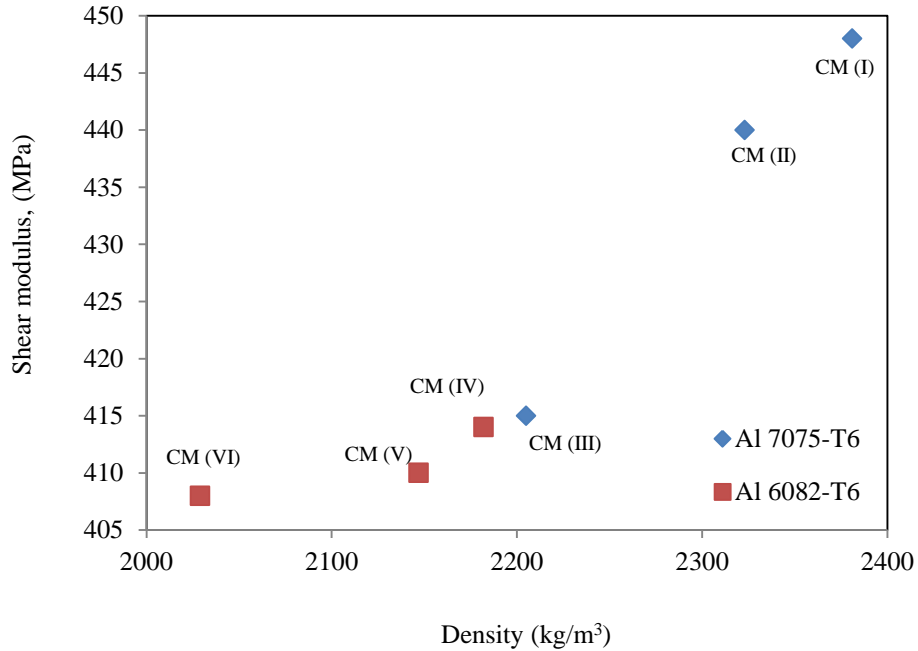

Figure 4.26. Plot of the shear modulus vs. density for different syntactic foams.

Figure 4.27 shows a comparison of the shear fracture strength for several aluminium syntactic foams. It can be seen that the shear strength also increases with foam strength. Cracks appeared in the core of the sample due to cracks in the walls of the ceramic micro-spheres that observation is in agreement with (Alonso et al., 2006) and propagated to the surface of the aluminium syntactic foams.
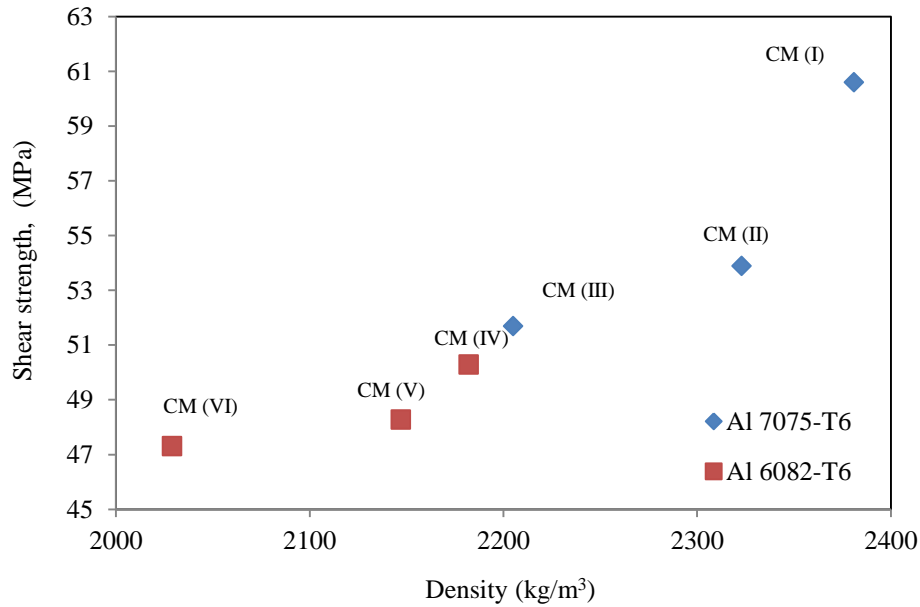
Figure 4.27. Plot of the shear strength vs. density for different syntactic foams.

Figure 4.28 shows a comparison of the shear fracture strain values for different foam densities. The results indicate an average 12% increase in the failure strain of the Al7075-T6 system compared to the corresponding Al6082-T6 syntactic foams. The results also reveal the influence of the grade of aluminium matrix on the failure strain of the foam. Moreover, increasing the size of the ceramic microspheres increases the failure strain. For example, Al 6082-T6 with 250–500 µm ceramic micro-spheres (CM IV) and a density of 2182 kg/m^3, offered a failure strain of 0.046, compared to values of 0.045 for a density of 2029 kg/m^3 in the Al 6082-T6/ 25–75 µm (CM VI). The shear strain values obtained here are in line with those reported by Tao (2010).
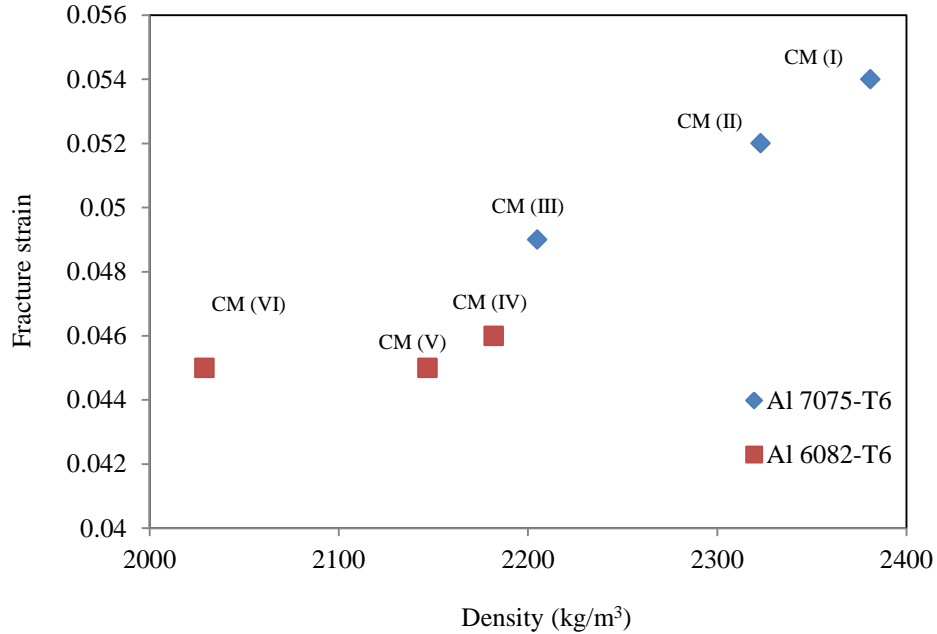
Figure 4.28. Plot of the fracture strain vs. density for different syntactic foams.

The absorbed energy for the 6082-T6 syntactic foams shows a linear dependence on density that tends to increase with increasing density. In Figure 4.22 the load-displacement curves show that the failure in the aluminium syntactic foam under shear is brittle for all densities. The data indicate that of the six syntactic foams tested, the 6082-T6 foam with 25–75 μm ceramic micro-spheres (CM VI) exhibited the lowest values of absorbed energy for a given density.

As far as the absorbed energy is concerned, the 7075-T6 syntactic foams appear to be the toughest system, offering values of absorbed energy above those exhibited by the other foams.

4.3   Characterising the Behaviour of the Aluminium Syntactic Foam at Higher Strain Rates

Higher strain rate tests were achieved using a drop-weight impact tower, a split Hopkinson pressure bar, and terminal ballistic and blast tests. It was found that aluminium (7075-T6) syntactic foams offer a higher plastic collapse stress, modulus of elasticity, steady-state stress and absorbed energy, in comparison to the aluminium (6082-T6) syntactic foams.

4.3.1   The compression behaviour of the syntactic foams under low velocity impact

Higher strain rate tests were conducted using a drop-weight impact tower. Details of the samples used in the drop-weight impact tests are summarised in Table 4.4. The low velocity impact properties of the syntactic foams are listed in Table 4.5. Figure 4.29 shows load-displacement traces for the aluminium matrix syntactic foam CM (III) following testing at various impact velocities. All three curves exhibit similar responses, i.e. the load increases to a maximum value followed by a subsequent drop due to cracking in the ceramic micro-spheres, before tending to plateau to an approximately constant force, This is similar to published results on aluminium foams (Goldsmith and Sackman, 1992; Lopatnikov et al., 2002; Radford et al., 2005; Tan et al., 2005). The force-displacement traces can be divided into three regions: a linear elastic region, a significant softening zone and an oscillating plateau region. The impact peak force, which is the maximum force before plastic deformation, is found to increase with increasing impact velocity. When the impact velocity was increased from 4.4 m/s to 5.14 m/s, the average

maximum increased by 24%. When the impact velocity was increased from 5.14 m/s to 5.42 m/s, the average maximum force increased by 33%.

Table 4.4. Summary of the aluminium matrix syntactic foam samples used in the low velocity impact tests.

ID	Mass (g)	Height (mm)	Width (mm)	Depth (mm)	Initial velocity (m/s)	Relative density ρ/ρ_s	Strain rate (1/s)
$CM(I)_1$	2.32	10.22	10.20	10.10	3.97	0.79	100
$CM(I)_2$	2.38	10.25	10.20	10.15	4.40	0.81	136
$CM(I)_3$	2.40	10.15	10.10	10.20	5.24	0.82	204
$CM(II)_1$	2.35	10.25	10.20	10.05	3.97	0.79	96
$CM(II)_2$	2.33	10.30	10.20	10.15	4.40	0.78	130
$CM(II)_3$	2.45	10.30	10.25	10.10	5.24	0.82	202
$CM(III)_1$	2.30	10.20	10.30	10.05	3.97	0.78	91
$CM(III)_2$	2.32	10.30	10.25	10.10	4.40	0.77	120
$CM(III)_3$	2.25	10.20	10.35	10.02	5.24	0.76	199

$\rho_s = 2800$ kg/m^3

Table 4.5. Results following low velocity impact tests on the aluminium matrix syntactic foams CM (I), CM (II) and CM (III).

Foam ID	Peak load (kN)	Yield strength (MPa)	Plateau strength (MPa)	Specific energy absorption (kJ/kg)	Impact energy (J)
CM (I)$_1$	22.5	215.8	206.2	33.40	94.8
CM (I)$_2$	34.2	327.1	267.8	47.40	115.8
CM (I)$_3$	57.5	560.9	347.1	55.30	176.6
CM(II)$_1$	22.3	213.3	191.2	31.90	94.8
CM(II)$_2$	29.5	280.7	276.0	43.85	115.8
CM(II)$_3$	53.0	502.0	338.8	48.04	176.6
CM(III)$_1$	20.1	191.3	152.3	29.09	94.8
CM(III)$_2$	21.2	200.8	189.4	42.50	115.8
CM(III)$_3$	39.4	373.2	334.0	45.60	176.6
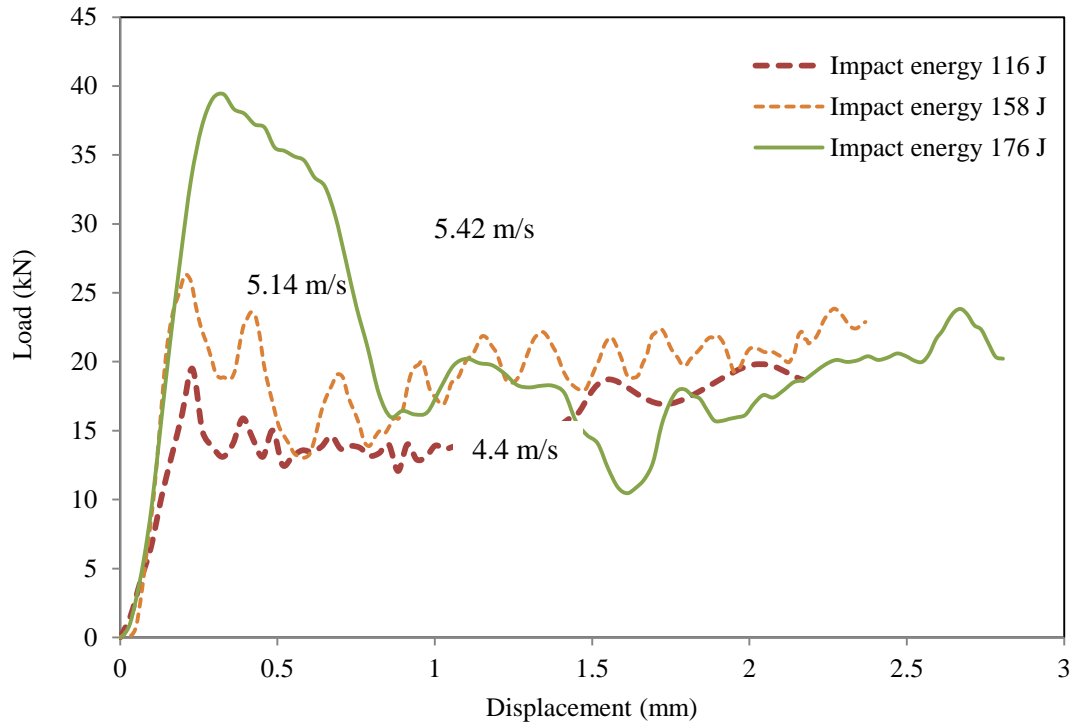
Figure 4.29. Low velocity impact response of aluminium matrix syntactic foam CM (III) at different impact velocities.

Typical stress–strain curves for one of the aluminium matrix syntactic foam CM (III), at both quasi-static and dynamic rates of strain are shown in Figure 4.29. A significant increase in plateau stress and compressive Young's modulus is observed at higher strain-rates. The results show that the peak stress during low velocity impact is 40% higher than that at quasi-static rates. Zhang and Zhao (2007) found that the compressive strength of an aluminium syntactic foam is doubled under low velocity impact relative to quasi-static compression. The higher maximum stress during low velocity impact is due to micro-inertial hardening of the rapidly-displacing ceramic micro-sphere cell walls within and ahead of the localised deformation band. The effect of the inertia becomes evident and

the resistance of the ceramic micro-spheres to collapse is increased with strain-rates, which leads to an increased plateau stress and peak stress, as shown in Figure 4.31.
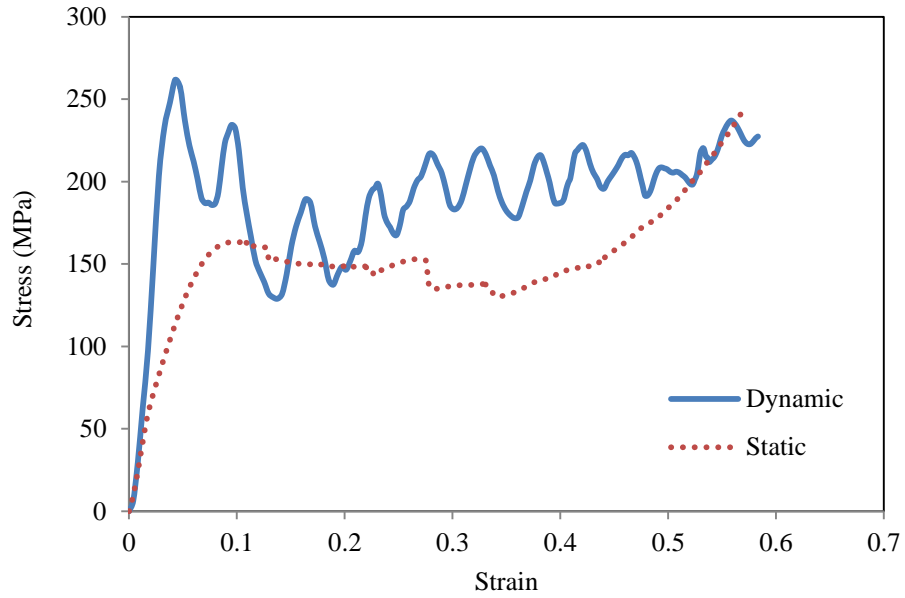
Figure4.30. Dynamic and quasi-static stress–strain curves for the aluminium syntactic foam CM (III).
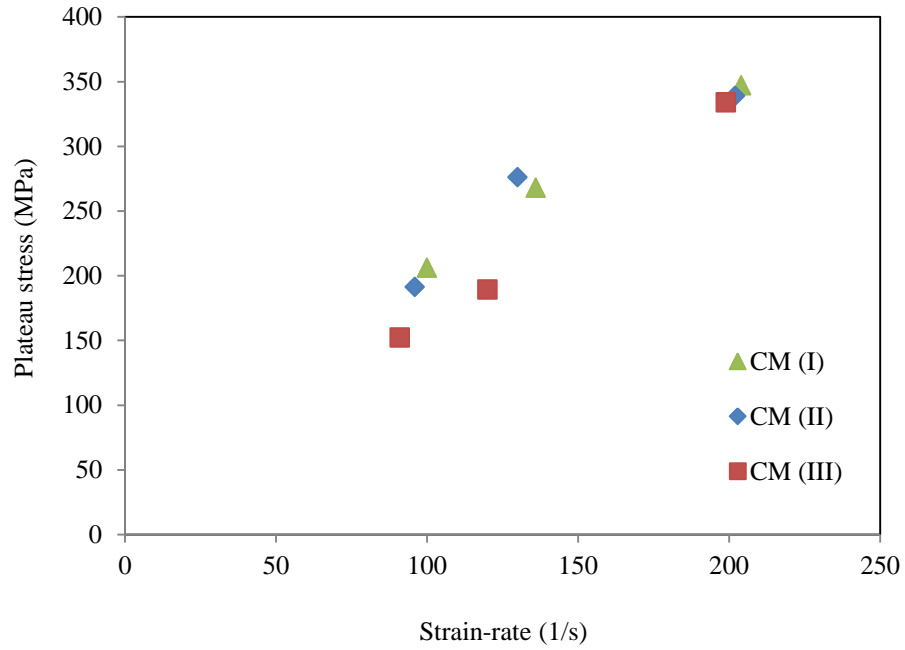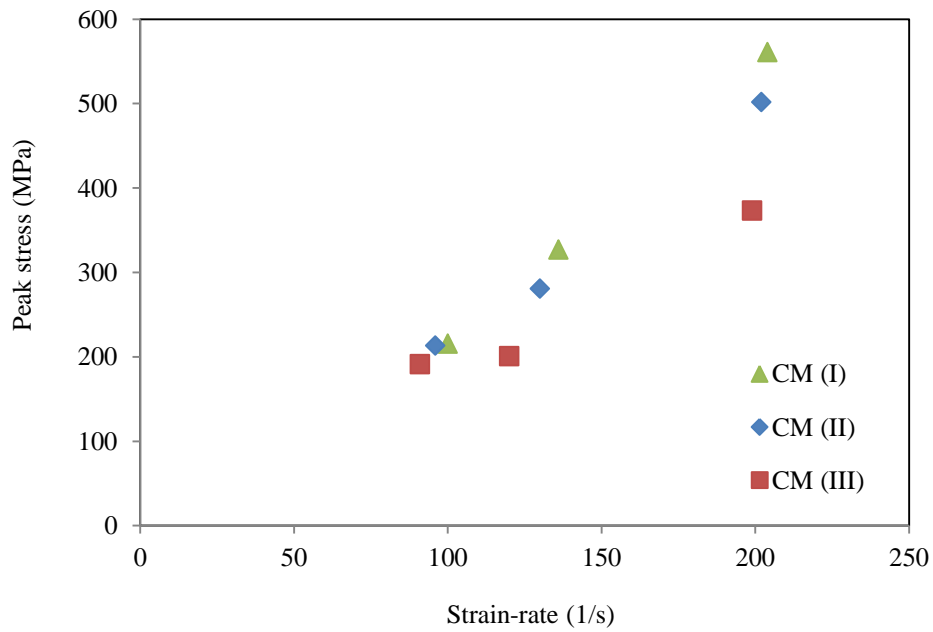
Figure 4.31. Plots of (a) peak stress and (b) plateau stress vs. strain rate for the aluminium syntactic foam.

The capability of the aluminium syntactic foams to absorb impact energy was determined by calculating the area under the load-displacement traces. Figure 4.32 shows that the specific energy absorption increases with increasing strain-rate. The specific energy absorption is more sensitive to high strain-rates. For example, the specific energy absorption is 55.30 kJ/kg when the strain-rate is 204 1/s, while the specific energy absorption is just 33.40 kJ/kg at a strain-rate of 94.8 1/s. The increase in energy absorption depends on the high plateau stress and the densification strain. Obviously, the results in Figure 4.32 show that the sample loaded at a strain-rate of 204 1/s has a higher peak stress. Consequently, it has the capability to absorb greater energy than a sample at a lower plateau stress and densification strain.
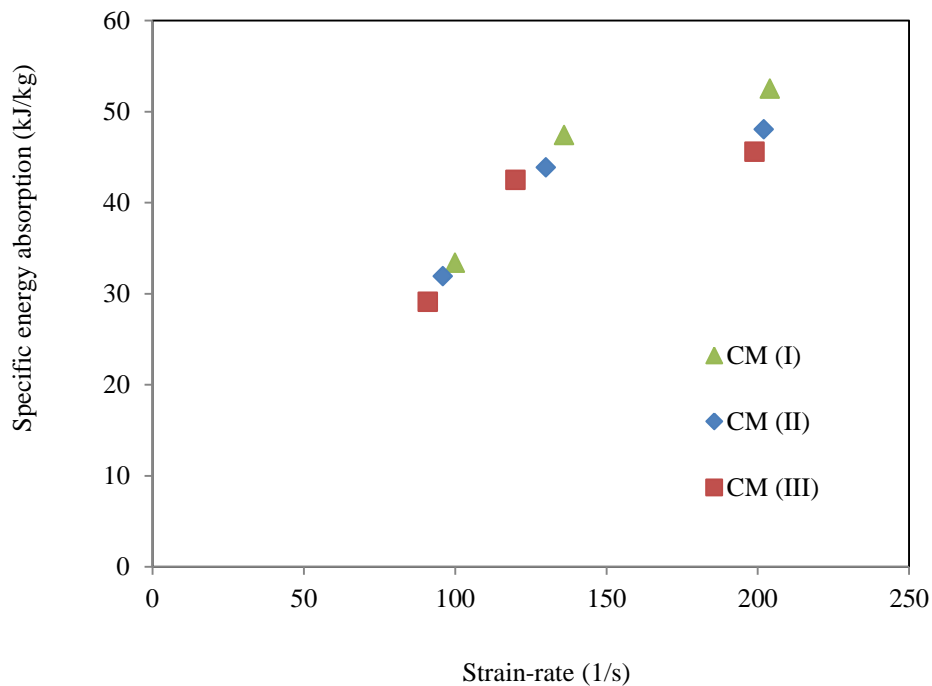
Figure 4.32. Plots of the specific energy absorption by the aluminium syntactic foams CM (I), CM (II) and CM (III) at different strain rates.

4.3.2 The compression behaviour of the syntactic foams under high velocity impact

Split Hopkinson pressure bar (SHPB) tests were conducted on the syntactic foams at different strain-rates to investigate their dynamic properties and failure behaviour. The results of the tests were obtained by averaging the values of three samples. The dynamic properties of the aluminium syntactic foams are listed in Table 4.6. Figure 4.33 depicts a typical set of incident, reflected and transmitted signals that were obtained from a SHPB test (for an aluminium matrix (Al7075-T6) syntactic foam).
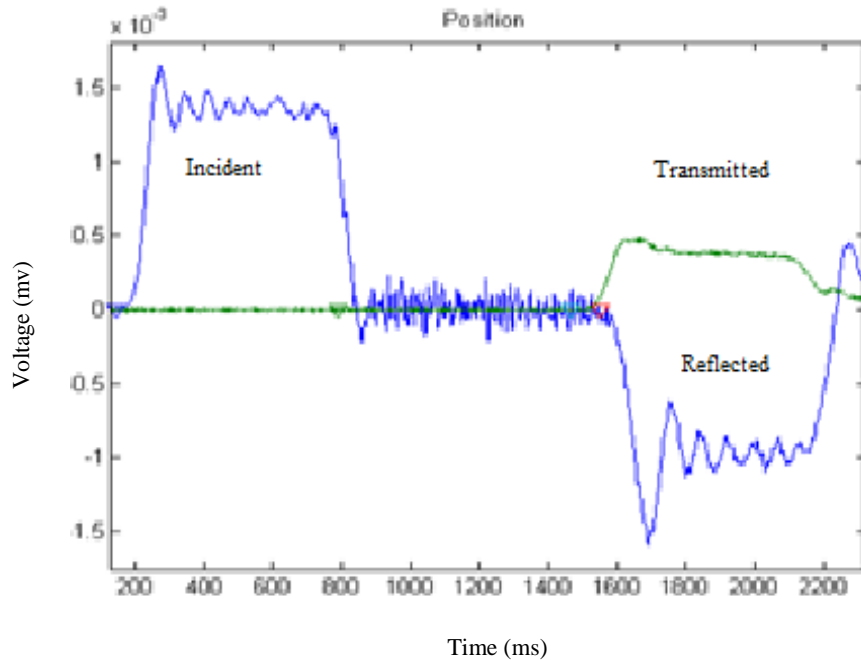
Figure 4.33. Voltage pulses acquired from the incident and transmitted bars.

Table 4.6. Average high-velocity impact properties of aluminium matrix syntactic foams (CM (I), CM (II) and CM (III)).

ID	Young's Modulus (GPa)	Dynamic compressive strength (MPa)	Dynamic strain rate (1/s)	Relative density, (ρ/ρ_s)	Relative yield strength, (σ/σ_s)	Relative Young's modulus, (E/E_s)	Sensitivity parameter $\sum$
CM(I)$_1$	14.22	601.4	1578	0.891	0.752	0.151	0.204
CM(I)$_2$	13.95	574.9	1547	0.890	0.719	0.148	0.192
CM(II)$_1$	13.16	487.9	1517	0.889	0.609	0.139	0.151
CM(II)$_2$	12.87	461.0	1273	0.880	0.922	0.184	0.140
CM (III)$_1$	11.93	265.0	1263	0.797	0.650	0.099	0.043
CM(III)$_2$	9.04	203.0	882	0.755	0.490	0.057	0.018

[*] E_S, σ_s and ρ_s of aluminium 7075-T6 are 94.4 GPa, 646 MPa and 2810 kg/m^3, respectively (Mocko, 2012).

These signals were converted to a stress–strain graph as shown in Figure 4.34, which shows the dynamic compressive stress–strain curves of CM (I), CM (II) and CM (III). The results indicate the dynamic dependence of the aluminium matrix syntactic foam. For example, the yield strength for CM (III)$_2$ increased from 203 MPa at 882 s^{-1} to 601.4 MPa at 1578 s^{-1} CM (I)$_1$ as shown in Table 4.6. Also, it was found that the dynamic compressive strength of the aluminium syntactic foam was about 30–45% higher than that of the static compressive strength. The peak stress is shifted slightly to lower strains for all samples, which can be seen as a result of the strain-rate sensitivity of the foam matrices leading to higher yield strengths and lower strain. The results show that the peak stress at a lower strain-rate is occurs at a strain of 0.05. This indicates that the volume fraction of metal matrix within a foam has an effect on the strain-rate sensitivity. It was found that syntactic foams with a higher percentage of metal matrix were more rate-sensitive.

The results in Figures 4.35, 4.36 and 4.37 show the influence of strain-rate on specific energy absorption, plateau stress and peak stress, respectively. The results confirm the dependency of the aluminium syntactic foam behaviour on strain-rate. An increase in the strain-rate leads to an increase in the specific energy absorption, plateau and peak stresses.

The failure mode observed in the aluminium syntactic foam under high-velocity impact loading was compressive failure rather than shear failure, as the high strain-rate can hinder the rearrangement of the ceramic micro-spheres required for shear deformation. A strain-rate sensitivity parameter was used to evaluate the effect of strain-rate on the material under dynamic loading. The strain-rate sensitivity parameter, ($\sum$) is calculated using the following equation (Balch, 2005):

$$\sum = \frac{\sigma_d - \sigma_q}{\sigma^*} \left[\frac{1}{\ln\frac{\dot{\varepsilon}_d}{\dot{\varepsilon}_q}} \right] \tag{4.1}$$

where σ is the stress, σ^* is the static stress at 5% strain at a strain-rate of 10^{-3} s^{-1}, $\dot{\varepsilon}$ is the strain-rate and d and q are subscripts that refer to dynamic and quasi-static testing, respectively. Table 4.6 shows that the sensitivity parameter is in the range of 0.018–0.204. This reveals that aluminium syntactic foam is sensitive to strain-rate. In contrast, Luong et al. (2013) reported that A356/SiC syntactic foam is insensitive to strain-rate. Balch reported that the rate-sensitivity of the aluminium matrix induces rate-sensitivity in the aluminium syntactic foam. However, micro-inertia has an effect on the rate-sensitivity of syntactic foams. In addition, Goel et al. (2012) inferred that the size of the ceramic micro-spheres as well as the fabrication method used have an effect on the rate-sensitivity of a syntactic foam.
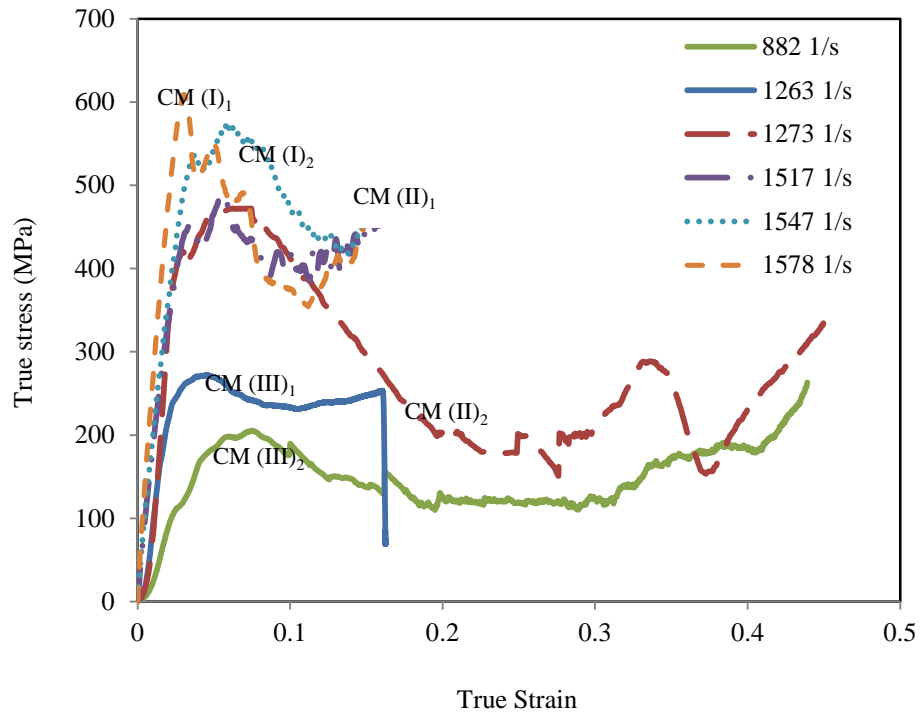
Figure 4.34. Compressive stress–strain curves for the aluminium matrix syntactic foam at high strain-rates.
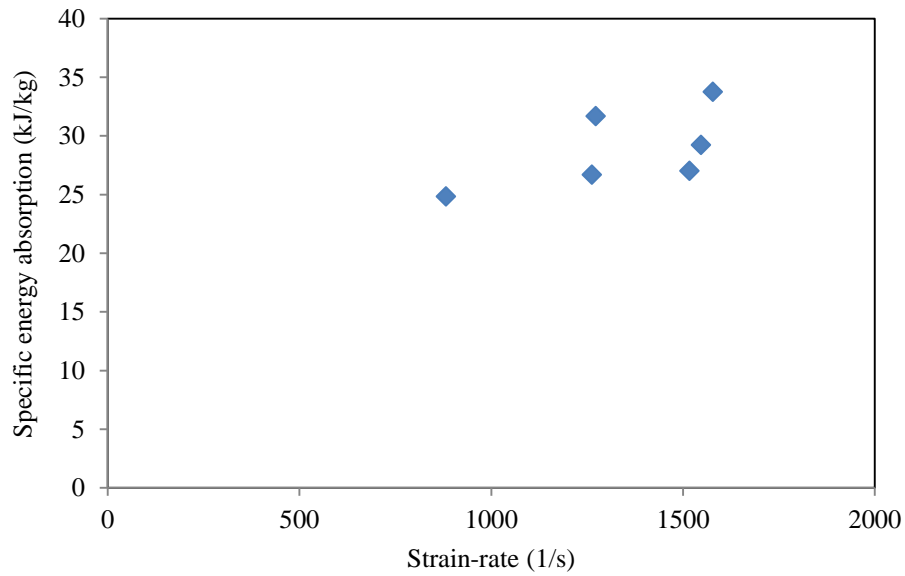
Figure 4.35. Plot of the variation of specific energy absorption with strain-rates.

110
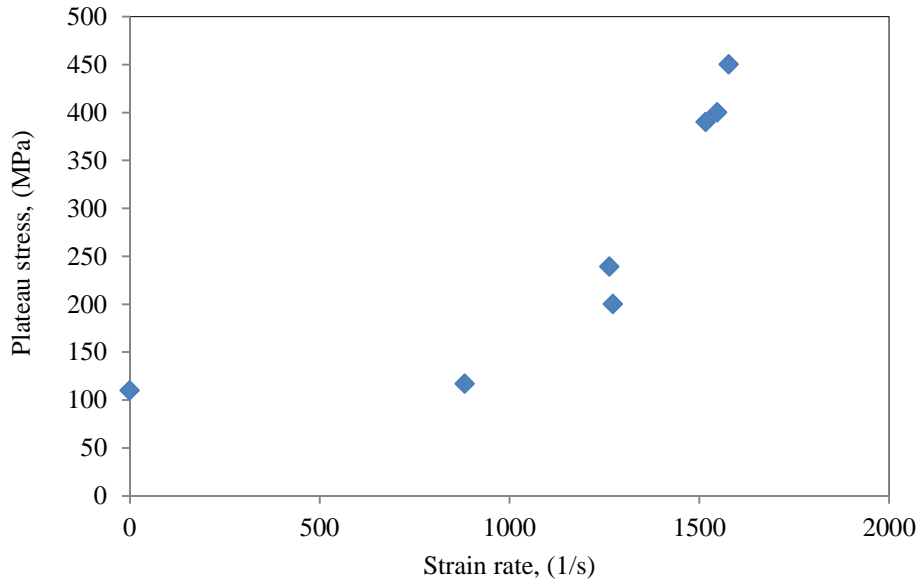
Figure 4.36. Plot of the variation of plateau stress with strain rates.
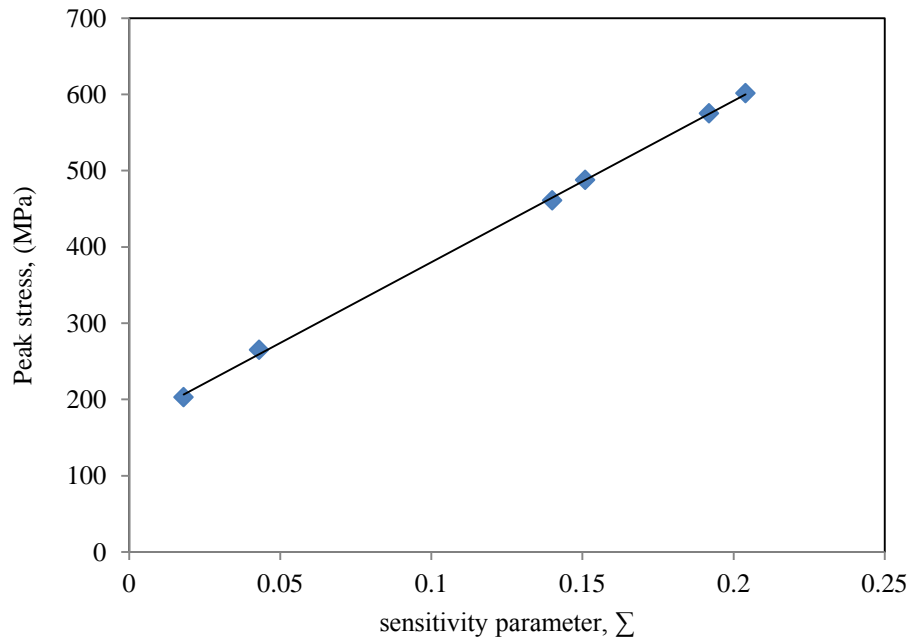
Figure 4.37. Plots of the peak stress for different sensitivity parameter values.

4.3.3 Behaviour of the syntactic foams under terminal ballistic impact

The ballistic response of different thicknesses of aluminium matrix syntactic foams was investigated using a ballistic impact test. A summary of the results from the ballistic tests is shown in Tables 4.7 and 4.8. Ten tests were conducted for each target to determine the ballistic limit velocity. Figure 4.38 shows the penetration depends in the aluminium matrix syntactic foam CM (I). Here, the data have been curve fitted with a linear function. The results show that the depth of penetration increases with strike velocity according to:

$$P_{Al7075\text{-}T6\ (75\ \mu m)} = .5627 + .4187\ v_s \qquad (4.2)$$

where $P_{Al7075\text{-}T6\ (75\ \mu m)}$ is the DOP (depth of penetration) into foam and v_s is the strike velocity (in metres per second).

Table 4.7. Average terminal ballistic properties of the aluminium matrix syntactic foam up to 20 m/s impact velocity.

Id	Thickness (mm)	Impact velocity (m/s)	Depth of penetration (mm)	Areal density (kg/m^2)
G1	13.2	20	8.94	18.35
G2	14	17	7.60	19.46
G3	15	14	6.50	20.85
G4	15.6	11	5.24	21.68
G5	15.6	8	3.27	21.68

Table 4.8. Average terminal ballistic properties of the aluminium matrix syntactic foam.

ID	Thickness of the sample (mm)	Impact velocity (m/s)	Residual velocity (m/s)
T1	6	812	740
T2	6	815	742
T3	6	845	760
T4	8	850	830
T5	8	750	727
T6	8	650	625
T7	10	550	520
T8	10	450	415
T9	10	350	310
T10	12	250	203
T11	12	150	81
T12	12	120	33
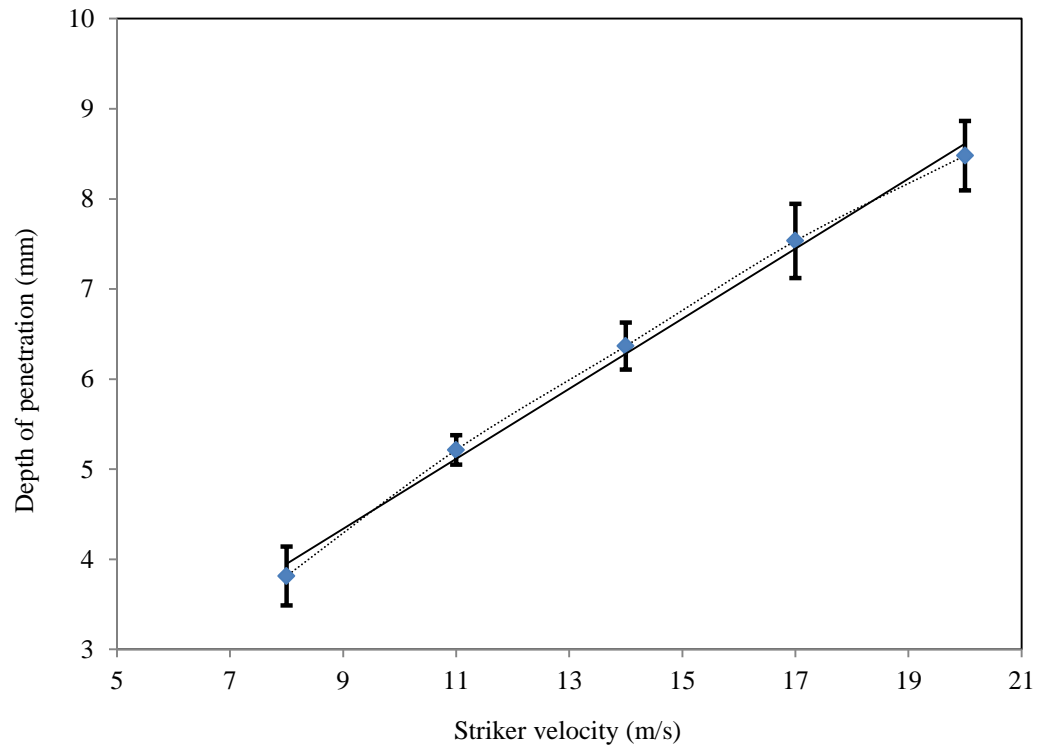
Figure 4.38. Penetration into aluminium syntactic foam vs. strike velocity.

Mohotti et al. (2013) reported that kinetic energy has an inverse relationship with the thickness of an aluminium matrix syntactic foam sample. Figure 4.39 shows the mean bullet residual velocities corresponding to ten different impact velocities. The results show that the syntactic foam can stop a projectile with a velocity of up to 116 m/s, but that for higher velocities the armour was perforated. These results are reasonable, since at 116 m/s, the depth of penetration was 10.90 mm for a total thickness of 13.2 mm. When the impact velocity was increased up to 120 m/s, the depth of penetration was 12.7 mm and the sample started to perforate, as shown in Figure 4.40.

Penetration of a target by a projectile depends on several variables, such as material properties, impact velocity, projectile shape and target position (Wilkins, 1978). In addition, identification of the target and projectile failure is required in order to design a target with the minimum areal density required to defeat the projectile. The thickness of the target, the radius of the projectile and impact velocity are all parameters that control perforation. If the ratio of the target thickness to the radius of the projectile is greater than one, the target plate is considered thick, whereas if the ratio is less than one, it is considered to be thin.
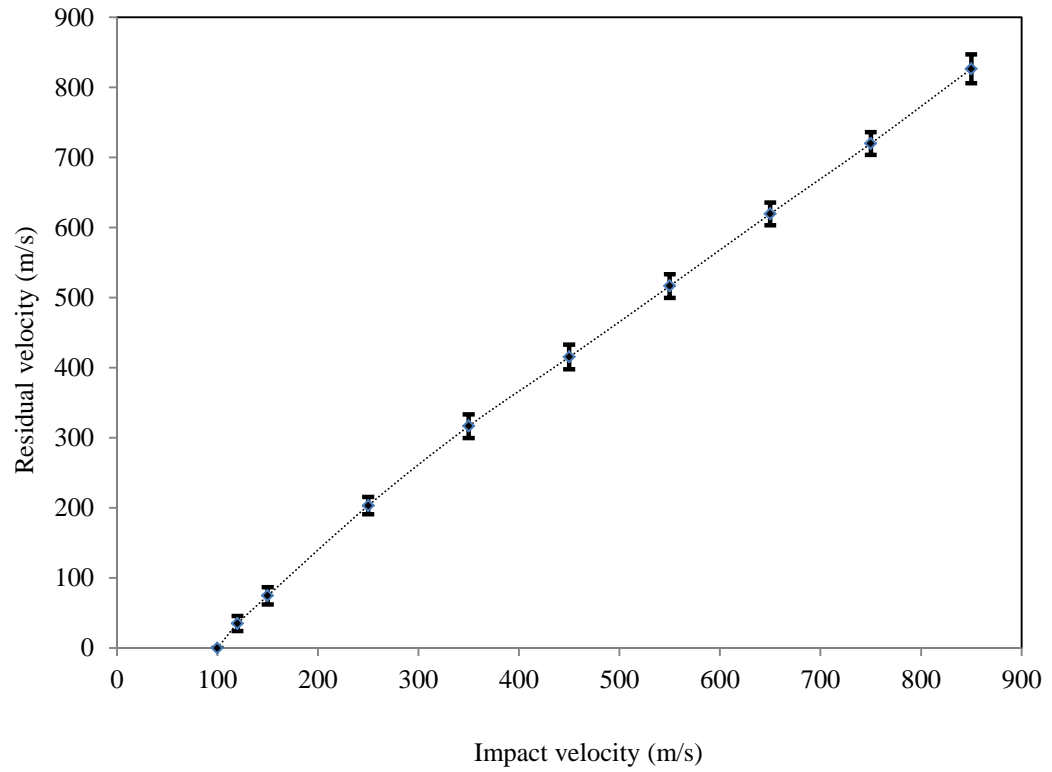
Figure 4.39. Initial versus residual velocity for samples impacted by 7.62 mm spheres for different plate thickness.

a) 100 m/s

b) 550 m/s
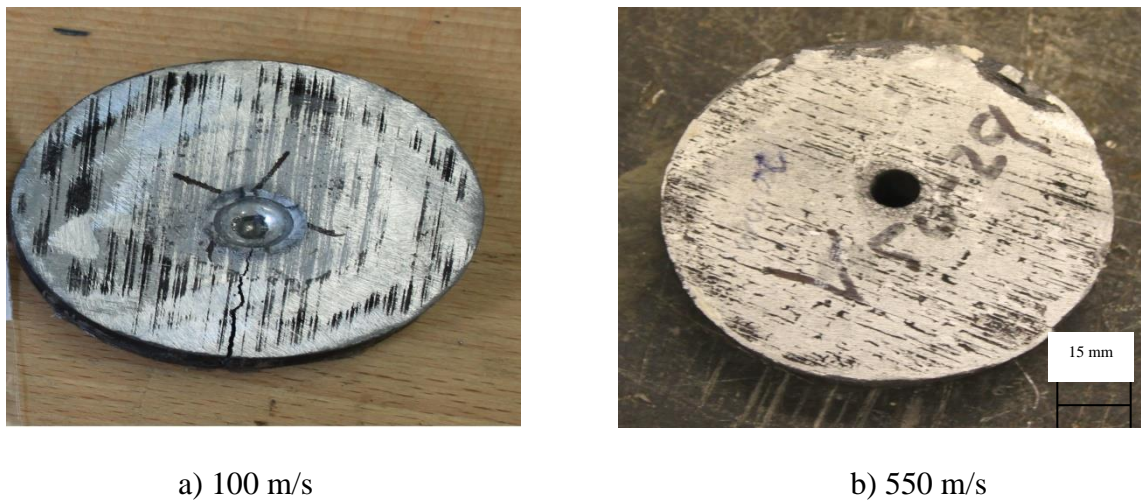
Figure.4.40 Photographs of penetrated and perforated plates of aluminium syntactic foam.

Figure 4.41 shows the results of the relationship between the residual velocities for different target thicknesses and the initial velocities. As expected the results indicate that residual velocity decreases with increasing target thickness. An increase in target thickness increases the areal density of the target, which reduces the residual velocity of the projectile. In addition, the results show that as expected increasing the impact velocity increases the residual velocity for the same target thickness.
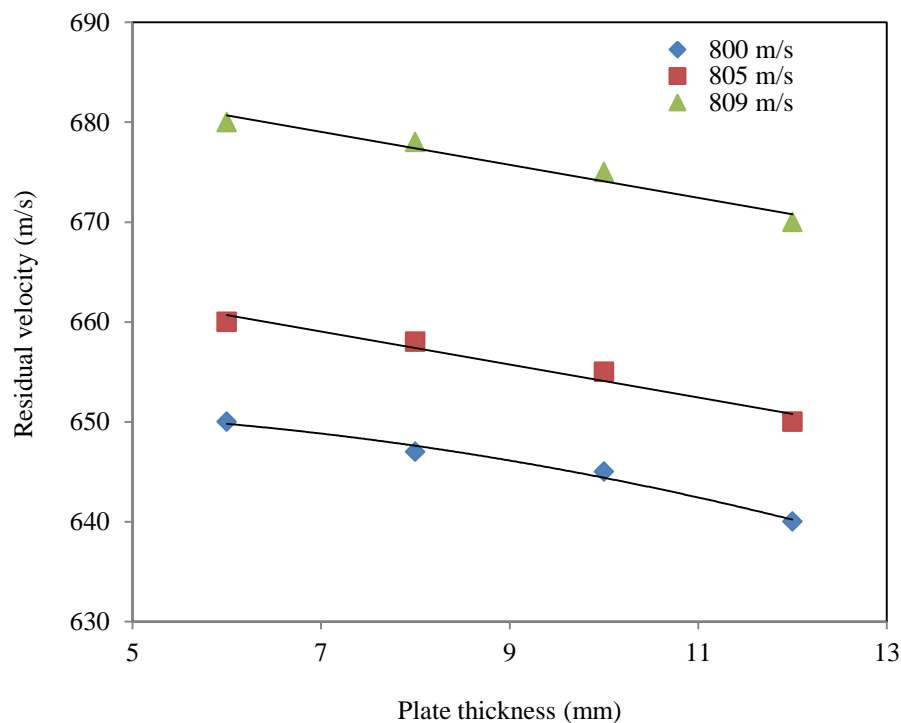
Figure 4.41. Residual velocity vs. plate thickness at different initial velocities.

4.3.4 Behaviour of the syntactic foams during blast loading

The blast response of different thicknesses of foam (CM I) was investigated using a ballistic pendulum. A summary of the tests on the foams is given in Tables 4.9 and 4.10,

covering the mass of explosive used, the impulse measured and the resulting permanent displacement. The results show that the measured impulses lie between 3.07 Ns and 29.8 Ns. These results are lower than those reported by Teeling-Smith (1991) for steel, which reflects the brittle nature of aluminium syntactic foams. Here, the impulse increases with increasing charge mass, as shown in Figure 4.42. Also, the permanent displacement increased with increasing impulse, as shown in Figure 4.43.

Table 4.9. Summary of the mass of explosive used during testing when the stand-off distance was 180 mm.

ID	Sample thickness (mm)	Mass of PE4 (g)	Impulse (Ns)	Mid-point deflection (mm)
B1	3.07	1.5	3.82	*
B2	5.8	1.5	3.36	*
B3	9.12	1.5	3.09	0.45
B4	9.18	2.0	4.50	*
B5	10.0	1.0	4.20	0.50
B6	10.2	2.0	4.30	0.35
B7	10.5	2.0	4.32	*
B8	12.5	2.0	3.72	0.48
B9	12.8	2.5	5.4	*
B10	14.0	2.5	4.82	0.50
B11	16.0	2.5	4.79	0.45
B12	20.0	3.0	6.12	0.60

* Sample completely failed
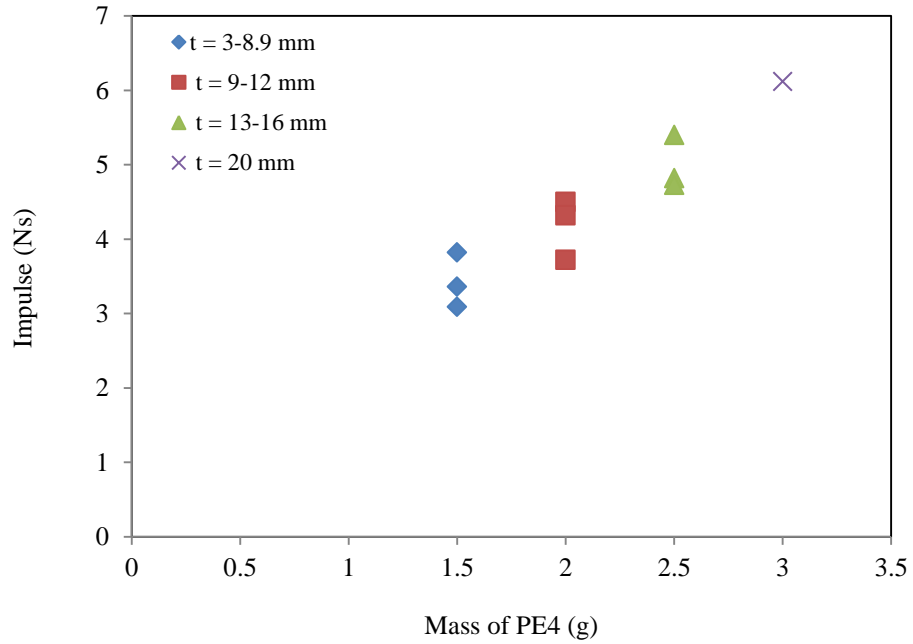
Figure 4.42. The variation of impulse with mass of PE4 for a constant stand-off distance 180 mm at different sample thickness.
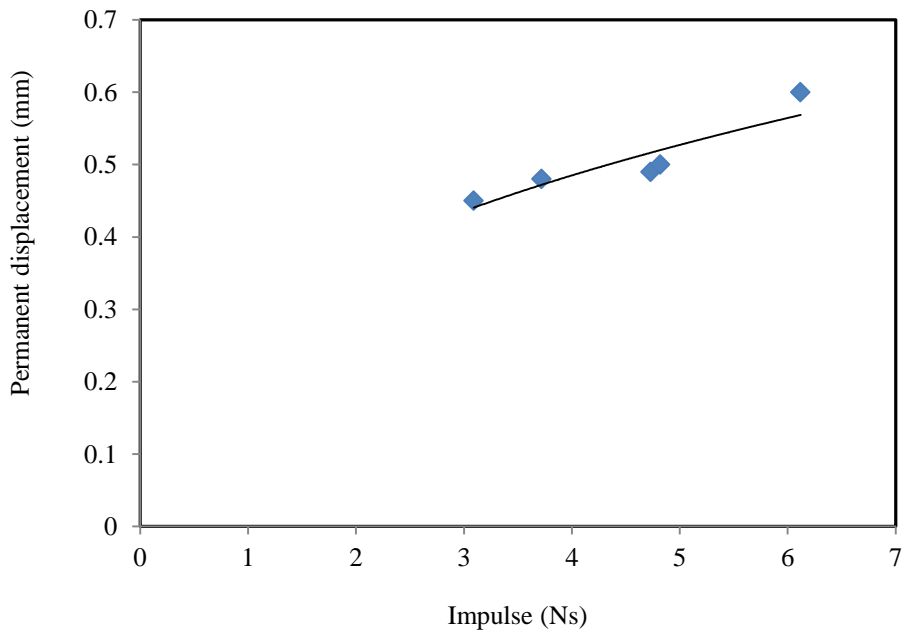
Figure 4.43. The permanent displacement vs. impulse for a constant stand-off distance of 180 mm.

Table 4.10. Summary of the mass of explosive used during tests with a steel front plate.

ID	Sample thickness (mm)	Mass of PE4 (g)	Impulse (Ns)	Permanent displacement (mm)
B1D	16	10	26.9	0.5
B2D	16	11	27.3	0.65
B3D	16	12	29.4	0.82
B4D	16	12.5	29.8	*

* Sample completed failed.

Yahya (2008) reported that the applied impulse increases with increasing charge mass and the permanent displacement increases with increasing impulse. Here, the sample was fixed with a steel front plate (5 mm thick) and the charge was fixed directly to the front plate. The results show that the charge mass has an influence on the impulse and the permanent displacement of the target: the higher the charge mass, the greater the impulse and permanent displacement. The permanent displacement at the midpoint increases with increasing impulse, which leads to tearing along the plate boundary. In addition, experimental observations reveal that the load distribution is localised to the centre of the plate, as shown in Figure 4.44. This concurs with the conclusions of a previous study (Nurick et al. and Teeling-Smith et al.,1991).
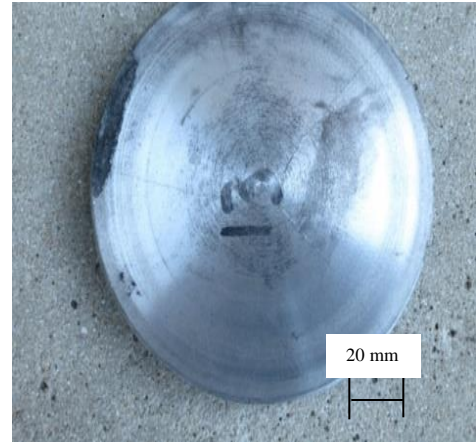
| a) 4.82 Ns | b) 26.9 Ns |

Figure 4.44. Photographs of plate profiles showing the permanent deflection at the centre of the plate due to localised loading.

4.4 Summary

In this chapter, the experimental results from static and dynamic loading tests on aluminium matrix syntactic foams have been presented. The results show that aluminium matrix syntactic foam is a good energy absorption material during compressive loading, while it is a very weak material during flexural and shear loading. The specific energy absorption of aluminium matrix syntactic foam CM (I) during quasi-static compression is 28.16 kJ/kg, while 1.469 and 0.596 kJ/kg during flexural and shear loading, respectively. In addition, the material shows that the specific energy absorption of low velocity impact loading is 55.30 kJ/kg at a strain-rate of 204 1/s. Furthermore, the results show that aluminium syntactic foam has an ability to absorb energy under dynamic loading. It can be used in a sandwich armour structure as an alternative core material, offering a military vehicle protection from harmful blast loads, such as landmine explosions.

Aluminium matrix syntactic foam can be used without front and back plates in some applications, where the strain-rate is less than 1600 1/s. In addition, the results show it has the capability to stop a bullet at a velocity of 120 m/s at thickness of 14 mm and an explosive charge weighing 3g, but in these applications, front and back plates are recommended.

CHAPTER 5: FINITE ELEMENT MODELLING

In this chapter, the finite element (FE) theory and procedures used to model the response of aluminium matrix syntactic foams under quasi-static and dynamic loading are presented. Simulations of the quasi-static compression, shear and three-point bending tests were carried out using the Abaqus/Standard package, whilst the dynamic analyses were conducted using the Abaqus/Explicit package. The numerical output is validated against the corresponding experimental results in the following chapter.

In this study, Abaqus/Standard (Section 2.3.1) and Abaqus/Explicit (Section 2.3.2) were used to create, solve and post-process a number of aluminium matrix syntactic foam models. Simplified 3D simulations were carried out to predict the linear and non-linear structural responses of aluminium matrix syntactic foams in response to compressive, flexure, shear, low and high velocity impact testing, as well as blast testing. The following section presents the constitutive models used in the FE analysis.

5.1 Constitutive Models for Aluminium Matrix Syntactic Foam

A progressive failure analysis of aluminium matrix syntactic foams is required to predict their mechanical behaviour under various loading conditions, and the use of appropriate material constitutive models plays a crucial role.

This section presents the constitutive models for modelling the aluminium matrix syntactic foams. An elasto-plastic model, with and without rate-dependence, was chosen to simulate the behaviour of the aluminium matrix syntactic foams. The elastic, plastic behaviour and failure criteria for the aluminium matrix syntactic foam are described herein.

5.1.1 Isotropic elasticity

A linear elastic model was used to describe the elastic response of the aluminium matrix syntactic foam in the FE model, which is applicable for small elastic strain values (typically less than 5%). It can be either isotropic or orthotropic, and can have temperature-dependent properties (Abaqus Theory Manual, 2011). For materials that display linear elastic behaviour, stress is calculated using Equation (5.1):

$$\sigma = E^{el}\varepsilon^{el} \qquad\qquad (5.1)$$

where σ is stress tensor,

E^{el} is the stiffness matrix, and

ε^{el} is the elastic strain tensor.

The shear modulus, G, can be obtained using $G = E/(2(1 + \upsilon))$, where E is the modulus of elasticity, and υ is Poisson's ratio.

Here, an isotropic and temperature-independent material was used to model the elastic behaviour of aluminium matrix syntactic foam. The experimental elastic property values found in Chapter Four were used in the model.

5.1.2 Plasticity

Plasticity refers to the permanent deformation of a material after the load is released. Isotropic hardening appears when the yield surface changes size in a uniform manner in every direction and the yield stress decreases or increases in every direction of stress as plastic strain is developed. A classical plasticity model was used to model the aluminium matrix syntactic foam. The classic plasticity models are based on a von Mises yield

surface with linked plastic flow that enables isotropic yield. In order to define isotropic hardening, the yield stress, σ_y, is given in a tabular function of plastic strain.

Decomposition of total increment of strain is given by:

$$d\varepsilon = d\varepsilon^{el} + d\varepsilon^{pl} \tag{5.2}$$

For a rate-dependent material, the equivalent plastic strain rate relationship follows the definition of uniaxial flow rate as indicated in Equations (5.3) and (5.4).

$$\dot{\bar{\varepsilon}}^{pl} = h(\bar{\sigma}, \bar{\varepsilon}_{pl}, \theta_T) \tag{5.3}$$

$$\bar{\sigma}(\bar{\varepsilon}_{pl}, \dot{\bar{\varepsilon}}_{pl}) = \sigma_y(\bar{\varepsilon}_{pl})R(\dot{\bar{\varepsilon}}_{pl}) \tag{5.4}$$

where h is the strain-hardening function, $\bar{\varepsilon}^{pl}$ is the equivalent plastic strain, θ_T is the temperature, $\bar{\sigma}$ is the von Mises equivalent stress and R is a stress ratio respectively, which are given as (Hassan et al., 2012):

$$\bar{\varepsilon}_{pl} = \int_0^t \sqrt{\frac{2\dot{\bar{\varepsilon}}_{pl}:\dot{\bar{\varepsilon}}_{pl}}{3}} \, dt \tag{5.5}$$

$$R = \frac{\bar{\sigma}}{\sigma_y} \tag{5.6}$$

In the dynamic models, the rate-dependent yield model is implemented to define the material yield behaviour when the yield strength depends on the strain-rate. The rate-dependent yield model is defined using yield stress ratios (R) for isotropic hardening metal plasticity models. A tabular function method is used to define the yield stress ratio (R) and equivalent plastic strain rate ($\dot{\bar{\varepsilon}}^{pl}$) in the model (Fan, 2010).

5.1.3 Damage evolution

Damage evolution can be used to predict failure of structural members. There are several proposed theories for failure criteria, related to the several types of failure that can occur. Failure may occur when there is a fracture, or due to crack propagation or development. Failure may also occur due to yielding as plastic deformations appear in materials that are ductile in nature. The development of progressive damage and ultimate failure are used to model damage and failure in ductile materials. Quasi-static and dynamic failure can be measured using ductile and shear damage models. The ductile and shear damage models use an equivalent fracture strain as a measure of failure. The initiation of damage due to growth and nucleation of voids in a ductile metal can be predicted using the ductile damage initiation criteria. The equivalent plastic strain at the start of damage, $\bar{\varepsilon}_D^{pl}$, is a function of the stress triaxiality (η) and strain-rate,

$$\eta = -\frac{p}{\sigma} \tag{5.7}$$

where p is the pressure stress which can be expressed as:

$$p = \frac{1}{3}(\sigma_1 + \sigma_2 + \sigma_3) \tag{5.8}$$

Ductile failure will occur when the conditions given below are fulfilled:

$$\omega_D = \int \frac{d\bar{\varepsilon}^{pl}}{\bar{\varepsilon}_D^{pl}(\eta, \dot{\bar{\varepsilon}}^{pl})} = 1 \tag{5.9}$$

where ω_D is a state variable that increases with plastic deformation. During the analysis, every increment, $\Delta\,\omega_D$, which is the incremental damage variable, is calculated by:

$$\Delta\omega_D = \frac{\Delta\bar{\varepsilon}^{pl}}{\bar{\varepsilon}_D^{pl}(\eta,\dot{\bar{\varepsilon}}^{pl})} \geq 0 \qquad (5.10)$$

The shear damage criterion is used to predict the beginning of damage due to localisation of a shear band. The model supposes that at the onset of damage, the corresponding plastic shear strain, $\bar{\varepsilon}_s^{pl}$, is a function of strain-rate and shear stress ratio, $\bar{\varepsilon}_s^{pl}(\theta_s, \dot{\bar{\varepsilon}}_s^{pl})$, where

$$\theta_s = \frac{\bar{\sigma} + K_s P}{\tau_{max}} \qquad (5.11)$$

in which k_s is a material parameter and τ_{max} is the maximum value of shear stress. A typical value of k_s for aluminium is taken as $k_s = 0.3$ (Hooputra et al., 2004). Damage starts to develop as the conditions below are fulfilled:

$$\omega_s = \int \frac{d\bar{\varepsilon}^{pl}}{\bar{\varepsilon}_s^{pl}(\theta_s, \dot{\bar{\varepsilon}}^{pl})} = 1 \qquad (5.12)$$

where ω_s is a state variable that is increased in a monotonic manner with plastic deformation and is relative to the incremental change in equivalent plastic strain. During the analysis, at each increment, the incremental increase in ω_s is computed as:

$$\Delta\omega_s = \frac{\Delta\bar{\varepsilon}^{pl}}{\bar{\varepsilon}_s^{pl}(\theta_s, \dot{\bar{\varepsilon}}^{pl})} \geq 0 \qquad (5.13)$$

The definition of damage evolution is the degradation of the material that occurs after one or more of the criteria for the initiation of damage are satisfied. The effective plastic displacement, $\bar{u}^{pl}$, is defined using an evolution equation:

$$\dot{\overline{u}}^{pl} = L\,\dot{\overline{\epsilon}}^{pl} \tag{5.14}$$

where L is the characteristic length of the element. Here, two failure models for the aluminium matrix syntactic foam were considered, i.e. the ductile and shear failure models. Both failure models are applicable to high strain-rate dynamic problems. The shear failure model is based on the value of the equivalent plastic strain. The shear failure damage parameter, ω, is calculated by:

$$\omega = \frac{\overline{\varepsilon}_0^{pl} + \sum \Delta\overline{\varepsilon}^{pl}}{\overline{\varepsilon}_f^{pl}} \tag{5.15}$$

where $\overline{\varepsilon}_f^{pl}$ is the equivalent plastic strain at the point of failure and $\Delta\overline{\varepsilon}^{pl}$ is an increment of the equivalent plastic strain. Failure is presumed to occur when the damage parameter exceeds one.

5.2 Materials

The materials investigated in this study were the previously discussed aluminium matrix syntactic foams. This type of the material behaves in an elasto-plastic manner and can undergo damage due to nucleation, shear band formation or a combination of the two. The mechanical properties of aluminium matrix syntactic foams were obtained from a series of tests, as discussed in Chapter Four. Table 5.1, 5.2 and 5.3 summarise the elastic properties, plastic properties and damage parameters for the aluminium matrix syntactic foams obtained from the quasi-static test data as required for the FE analysis.

Table 5.1. Summary of the elastic properties of the aluminium matrix foam material.

ID	Density (kg/m^3)	Young's modulus (GPa)	Possion's ratio*
CM (I)	2388	3.22	0.29
CM (II)	2321	2.83	0.29
CM (III)	2250	2.42	0.29

*experimental results.

Table 5.2. Summary of the plasticity properties of the aluminium matrix syntactic foams.

CM(I)	Yield stress (MPa)	200	205	214	225	229	235	246	257	279	300
	Plastic strain	0	0.10	0.16	0.19	0.3	0.33	0.47	0.48	0.49	0.52
CM(II)	Yield stress (MPa)	150	165	185	145	191	209	211	215	225	248
	Plastic strain	0	0.10	0.16	0.19	0.3	0.33	0.47	0.48	0.49	0.52
CM(III)	Yield stress (MPa)	130	135	141	145	149	151	165	175	179	200
	Plastic strain	0	0.10	0.16	0.19	0.3	0.33	0.47	0.48	0.49	0.52

Table 5.3. Summary of ductile and shear damage behaviout for the aluminium matrix syntactic foams.

		Compression ductile damage	Shear damage
CM (I)	Fracture strain	0.052	0.053
	Stress triaxially and	0.333	-
	shear stress ratio		3.2
	Strain rate (s^{-1})	.0001	.0001
	Fracture energy(kJ/m^2)	179	31.2
CM (II)	Fracture strain	0.050	0.050
	Stress triaxially and	0.333	-
	shear stress ratio		3.2
	Strain rate (s^{-1})	.0001	.0001
	Fracture energy (kJ/m^2)	167	26.81
CM (III)	Fracture strain	0.050	0.048
	Stress triaxially and	0.333	-
	shear stress ratio		3.2
	Strain rate (s^{-1})	.0001	.0001
	Fracture energy (kJ/m^2)	163	24.22

5.3   FE Modelling at Quasi-static rates

This section presents details of the FE simulation procedures for the aluminium matrix syntactic foams under quasi-static compressive, three-point bending and shear loading conditions. The objective of this section is to simulate the experimental tests presented in Chapter Four using the Finite Element Method (FEM). Three dimensional quasi-static FE models were implemented using the commercial code Abaqus/Standard (Hibitt, 2012).

5.3.1 Simulation of the Compression Tests

5.3.1.1 Geometry, loading and boundary conditions

The configuration of the quasi-static compression model are shown in Figure 5.1. The overall dimensions of the aluminium matrix syntactic foam sample are L = 20 mm, W = 20 mm and H = 20 mm.
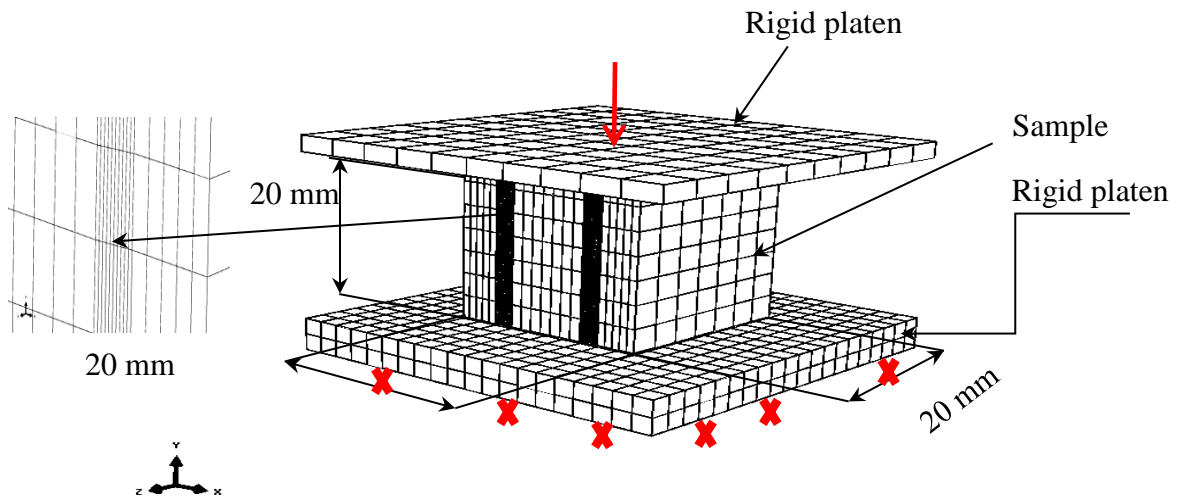
Figure 5.1. Mesh, boundary and loading conditions used in modelling compression testing on the aluminium syntactic foam.

In the quasi-static compression simulation, the bottom surface of the bottom-platen was fully constrained and the top surface of the sample was subjected to a vertical displacement boundary condition by a planar rigid platen. At the centre of the top rigid platen, a reference point was used to assign the boundary conditions of the vertical displacement and constraints in other directions. The load was calculated by considering the interaction between the top platen and the sample.

5.3.1.2   Element types

The responses of the aluminium matrix syntactic foam to quasi-static compression (and later on dynamic loading) were modelled using a linear brick element (C3D8R). C3D8R is eight-noded, reduced integration with hourglass control. C3D8R elements use few integration points and reduce shear locking problems due to the elimination of some terms in Gauss integration. The reduced integration elements are used with a low order of integration to form element stiffness, which leads to reduced CPU (Central Processing Unit) time consumption (Hibbit et al., 2012).

C3D8R elements have one integration point, which can possibly lead to uncontrolled distortion of the mesh. A fine mesh is the recommended solution for this problem as C3D8R elements are not very useful without hourglass control.

5.3.1.3   Mesh dependency

A mesh sensitivity study was executed on the 3D brick element models. A mesh sensitivity study revealed that the structural stiffness is dependent on both the size of the element and the properties of the material used. In this research, the same element size was used in all models (1 mm) with an optimum processing time in order to keep the models consistent during the study. The effect of element size on the plateau stress is obvious. The plateau stress increases as the size of the element increases. On the other hand, the CPU time increases rapidly as the size of the element is decreased and the total number of elements within the model is increased.

5.3.1.4   Modelling interaction

A surface to surface contact algorithm was used to model interaction in the FE models, which has many restrictions on the types of surface involved. Surface to surface contact allows defining contact between the sample and the loading platen. Such contact interaction is related to contact properties. Both normal behaviour (contact pressure–clearance relationship) and tangential behaviour (friction formulation) are defined by the corresponding contact properties. Figure 5.2 summarises the contact pressure over-closure relationship.
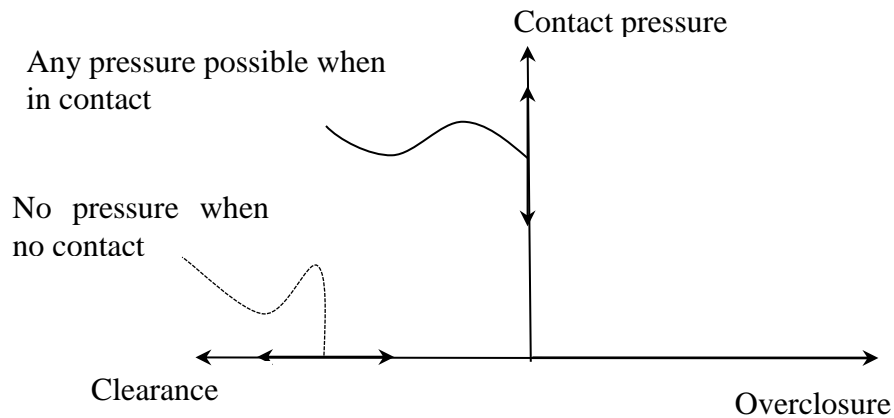
Figure 5.2. Hard contact pressure–overclosure relationship.

The penetration of the slave surface, at constraint locations, into the master surface is minimised by the contact relationship. The hard contact relationship is used when the surfaces are used in contact with each other. Any contact pressure can be transferred between them. When the clearance between them has a value of zero, surfaces come into contact with each other. The surfaces separate from each other when the contact pressure has a value of zero.

There are three forms of contact relationship that are often found in nature in addition to the hard contact pressure–overclosure relationship. These describe the relationship between clearance and contact pressure between surfaces using an exponential law, a tabular piecewise-linear law and a linear law.

The concept of the Coulomb friction model is defined as the relationship between permissible frictional shear stress across an interface and contact pressure. In Abaqus, no relative motion occurs if the equivalent stress is equivalent to:

$$\tau_{eq} = \sqrt{\tau_1^2 + \tau_2^2} \qquad (5.16)$$

Sliding between surfaces remains zero until the surface traction reaches a critical shear stress value, τ_{crit}, which is defined as:

$$\tau_{crit} = \mu P \qquad (5.17)$$

where μ is the coefficient of friction and P is the constant pressure between two surfaces. When the value of μ is zero, the modelling is frictionless and surfaces are free to slide across one another (Hibbit et al., 2012).

5.3.1.5   Process simulation output

The data output from the simulation can be designated by creating output requests. At each step, Abaqus creates a lot of data for different variables, but it can be managed and controlled by the user. An output request defines the analysis output for the variable components of interest. There are two ways to request data output: history output and field output.

Here, the history output is generated at specific points or interfaces in a model. The output frequency is specified in equally spaced time intervals. Output frequency is assigned using increments that depend on the last increment of each step, or according to a set of time points in Abaqus/Standard. The displacement data along the relevant direction for the rigid loading platen and the corresponding interaction force are required in a history output.

5.3.2   Three-point bending simulation

The geometrical configuration used for the quasi-static for three-point bending model is shown in Figure 5.3.
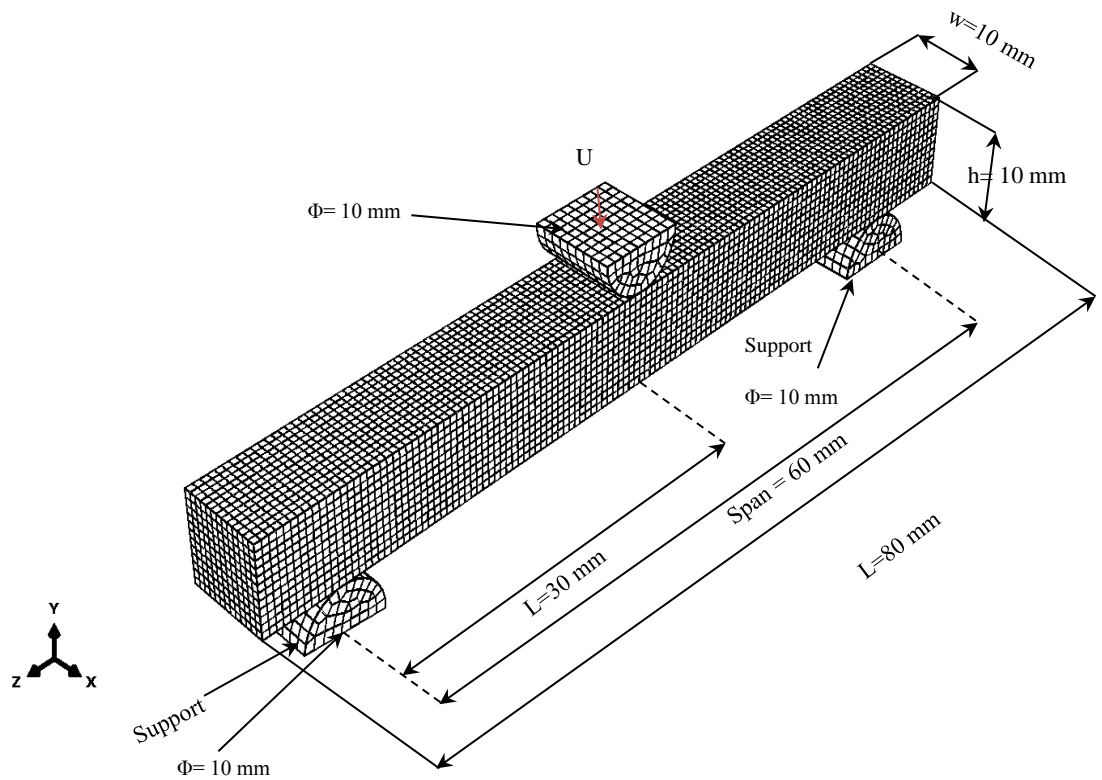
Figure 5.3. Mesh and loading conditions used in modelling the three-point bending test on the aluminium syntactic foam.

134

The overall dimensions of the foam model are L = 80 mm, span = 60 mm, w = 10 mm and h =10 mm. In the three-point bending simulation, the support is specified by applying a zero displacement boundary condition on the respective node in the x ,y and z directions. Also, a vertical displacement boundary condition was applied at the middle top surface to gradually bend the beam, which was constrained except in the y direction ($U_y \neq 0$). Finer meshes were used in the area of loading than in other regions of the beam. The size of the element in the middle of the beam was 1 mm, while it was 1.25mm or 1.5 mm at the support and other regions of the beam to reduce the consumption of CPU time.

5.3.3 Simulation of the shear tests

The configuration of the shear test model is shown in Figure 5.5.
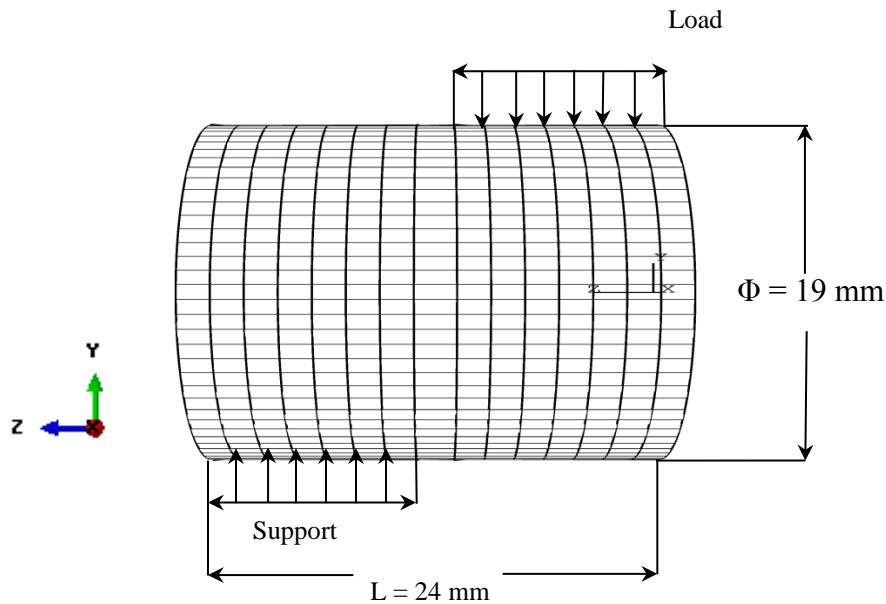
Figure 5.4. Mesh, boundary and loading conditions used in shear modelling of the foam.

In the shear test simulation, the foam cylinder was modelled according to its experimental shape and size. The overall dimensions of the foam cylinder are L = 24 mm and Φ = 19

135

mm. In the shear test simulations, the foam cylinder was fixed over one half of its length and the other half was displaced in the y direction to ensure that shear fracture occurs in the middle plane of the sample. A displacement boundary condition was applied to the right half of the cylinder to gradually shear the cylinder downwards. The force-displacement curves were then compared to the respective experimental curves, presented in Chapter Six.

5.4   Dynamic FE Modelling Procedures

This section describes the FE simulation procedures for aluminium matrix syntactic foams subjected to low (drop-weight) and high velocity impact (Split Hopkinson Pressure Bar), terminal ballistic and blast loading conditions. The objective of this section is to simulate the dynamic experimental tests presented in Chapter Three using the FE modelling. 3D dynamic models were implemented using Abaqus/Explicit (Hibbit et al., 2012).

5.4.1   Simulation of the drop-weight tests

Drop-weight tests were simulated on the aluminium matrix syntactic foam. Here, the same conditions that were used in the experimental tests were applied. The drop-weight FE model is similar to that shown in Figure 5.1, however, the downward displacement, U_y, is now replaced by an initial velocity on the top platen.

In the drop-weight simulations, the bottom surface of the platen was fully constrained and the top surface of the sample was subjected to an instantaneous velocity by a planar rigid impactor. A point mass was specified on a reference point that was located at the centre of the top platen. An initial velocity was defined at the reference point using the initial

condition. The reference point also was used to record displacement, and the interaction between the top platen and the sample was used to record contact force. A series of drop-weight simulations were carried out to compare the FE simulations predicted to the corresponding experimental results at various strain-rates. Here, the explicit C3D8R elements were used to model aluminium syntactic foams at high strain-rate loading. In Abaqus/Explicit, the rate-dependent elastic-plastic model was used to model aluminium syntactic foam under drop-weight loading conditions. In addition, the equivalent strain rate and the yield stress ratio were used to describe the dynamic loading effect. Tables 5.4 to 5.7 show the input dynamic material properties that were used to model aluminium syntactic foam under drop-weight loading. Table 5.5 shows the yield stress of aluminium syntactic foam CM (I) higher than CM (II) and CM (III) due to strain rate sensitivity of the material at high strain-rate impact. These data were inputted to reflect the rate dependent dynamic material properties of the material in the Abaqus/Explicit FE model.

Table 5.4. Summary of the elastic properties of the aluminium matrix foams used in the drop-weight modelling.

ID	Density (kg/m^3)	Young's modulus (GPa)	Possion's ratio
CM (I)	2388	4.50	0.29
CM (II)	2321	2.94	0.29
CM (III)	2250	2.51	0.29

Table 5.5. Summary of the plasticity properties of the aluminium matrix syntactic foams used in the drop-weight modelling.

CM(I)	Yield stress (MPa)	270	272	273	275	276	277	279	280	290
	Plastic strain	0	0.10	0.16	0.19	0.30	0.33	0.48	0.49	0.52
CM(II)	Yield stress (MPa)	225	227	232	250	254	255	256	260	262
	Plastic strain	0	0.04	0.08	0.12	0.18	0.24	0.26	0.28	0.32
CM(III)	Yield stress (MPa)	200	250	270	300	325	330	340	345	400
	Plastic strain	0	0.27	0.31	0.34	0.35	0.36	0.42	0.45	0.49

Table 5.6. Summary of ductile and shear damage parameters for the aluminium matrix syntactic foams used in the drop-weight modelling.

		Compression ductile damage	Shear damage
CM (I)	Fracture strain	0.04	0.04
	Stress triaxially and shear stress ratio	0.333	- 10.2
	Strain rate (1/s)	200	200
	Energy fracture (kJ/m^2)	364.59	31.20
CM (II)	Fracture strain	0.050	0.050
	Stress triaxially and shear stress ratio	0.333	- 10.2
	Strain rate (1/s)	130	130
	Energy fracture (kJ/m^2)	351.4	26.80
CM (III)	Fracture strain	0.050	0.048
	Stress triaxially and shear stress ratio	0.333	- 10.2
	Strain rate (1/s)	100	100
	Energy fracture (kJ/m^2)	317.22	24.22

Table 5.7. Summary of rate dependent of hardening yield ratio for the aluminium matrix syntactic foams used in the drop-weight modelling.

	R (yield stress ratio)	strain rate (1/s)
	1	0
	1.30	91
CM (I)	1.37	120
	2.58	199
	1	0
	1.42	96
CM (II)	1.87	130
	3.35	202
	1	0
	1.23	100
CM (III)	1.87	136
	3.20	204

5.4.2   Split Hopkinson Pressure Bar simulation

The Split Hopkinson Pressure Bar (SHPB) test was modelled to simulate the response of the material at a high strain-rate. The exact conditions applied in the experimental work were used to undertake the SHPB simulation.

5.4.2.1   Geometry, boundary and loading conditions

The configurations of the SHPB model are shown in Figure 5.6.
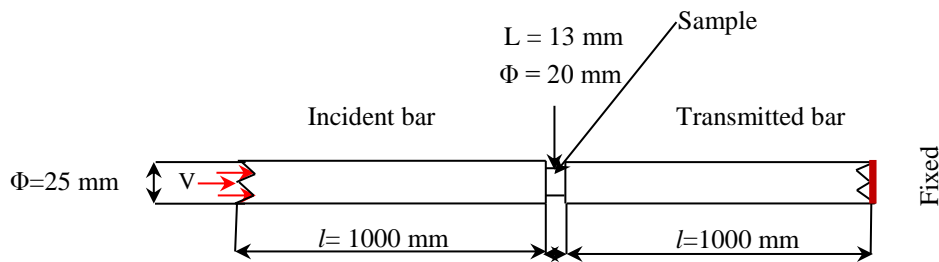
Figure 5.5. Boundary and loading conditions used in the SHPB test of aluminium syntactic foam.

The overall dimensions of the aluminium matrix syntactic foam sample are L = 13 mm and the diameter = 20 mm, while the length of the incident and transmitted bars is l =1000 mm with a diameter (Φ) of 25 mm. In the SHPB simulation, the right surface of the transmitted bar was fully constrained, while the left surface of the sample and the transmitted bar were subjected to an instantaneous velocity by the incident bar. An initial velocity was defined at the incident bar, which was equal to the impact velocity appointed in the SHPB test using the velocity initial condition to move the incident bar to the right. The reaction force and displacement at the left surface of the sample were recorded.

The influence of the strain-rate effect was examined at impacts with different velocities. The models were run to seek the strain-rate sensitivity of aluminium syntactic foams.

The material input dynamic properties are presented in Tables 5.8–5.11. In Abaqus/Explicit, the elastic-plastic model was incorporated with dynamic data and rate-dependent hardening tabular input data. A typical stress yield ratio model with the related strain-rate can be used to illustrate the strain-rate effect. A failure model was defined that included both the ductile and the shear damage. The explicit C3D8R elements and surface to surface contact were used to model the sample at SHPB simulation.

Table 5.8. Summary of the elastic properties of the aluminium matrix foams used in the SHPB modelling.

ID	Density (kg/m^3)	Young's modulus (GPa)	Possion's ratio
CM (I)	2388	14.22	0.29
CM (II)	2321	13.95	0.29
CM (III)	2250	13.86	0.29

Table 5.9. Summary of the plasticity properties of the aluminium matrix syntactic foams used in the SHPB modelling.

CM (I)	Yield stress (MPa)	520	530	540	546	548	555	562	566
	Plastic strain	0	0.02	0.04	0.07	0.09	0.12	0.13	0.15
CM (II)	Yield stress (MPa)	475	477	478	479	480	481	482	520
	Plastic strain	0	0.02	0.04	0.05	0.06	0.07	0.09	0.12
CM (III)	Yield stress (MPa)	255	257	258	260	261	262	263	265
	Plastic strain	0	0.02	0.03	0.04	0.09	0.16	0.17	0.18

Table 5.10. Summary of ductile and shear damage parameters for modelling the aluminium matrix syntactic foams under SHPB testing.

		Compression ductile damage	Shear damage
CM (I)	Fracture strain	0.017	0.004
	Stress triaxially and shear stress ratio	0.333	- 10.9
	Strain rate (1/s)	1578	1578
	Energy fracture (kJ/m^2)	412.5	31.20
CM (II)	Fracture strain	0.016	0.005
	Stress triaxially and shear stress ratio	0.333	- 10.9
	Strain rate (1/s)	1273	1273
	Energy fracture (kJ/m^2)	353.0	26.80
CM (III)	Fracture strain	0.050	0.004
	Stress triaxially and shear stress ratio	0.333	- 10.9
	Strain rate (1/s)	1263	1263
	Energy fracture (kJ/m^2)	210	24.22

Table 5.11. Summary of rate dependent of hardening yield ratio for the aluminium matrix syntactic foams used in the SHPB modelling.

ID	R (yield stress ratio)	strain rate (1/s)
	1	0
	3.30	1578
CM (I)	3.35	1562
	3.44	1547
	1	0
	3.07	1517
CM (II)	3.16	1395
	3.25	1273
	1	0
	1.37	1263
CM (III)	1.62	1070
	1.79	882

5.4.3   Simulation of the terminal ballistic tests

Terminal ballistic simulations were carried out to model the related impact response of the aluminium matrix syntactic foams and to find the strength of material required to prevent the perforation of the bullet. Conditions similar to the experiments were set in the modelling to simulate the sample under terminal ballistic loading. The mesh size in the central area of the sample was finer than that at the outer regions. Elements in the central area that failed were allowed to be removed from the model during the penetration. The explicit C3D8R elements and surface to surface contact were used to model the sample at terminal ballistic simulation. Force-displacement histories were recorded from this model. The configurations of the terminal ballistic model are shown in Figure 5.7.
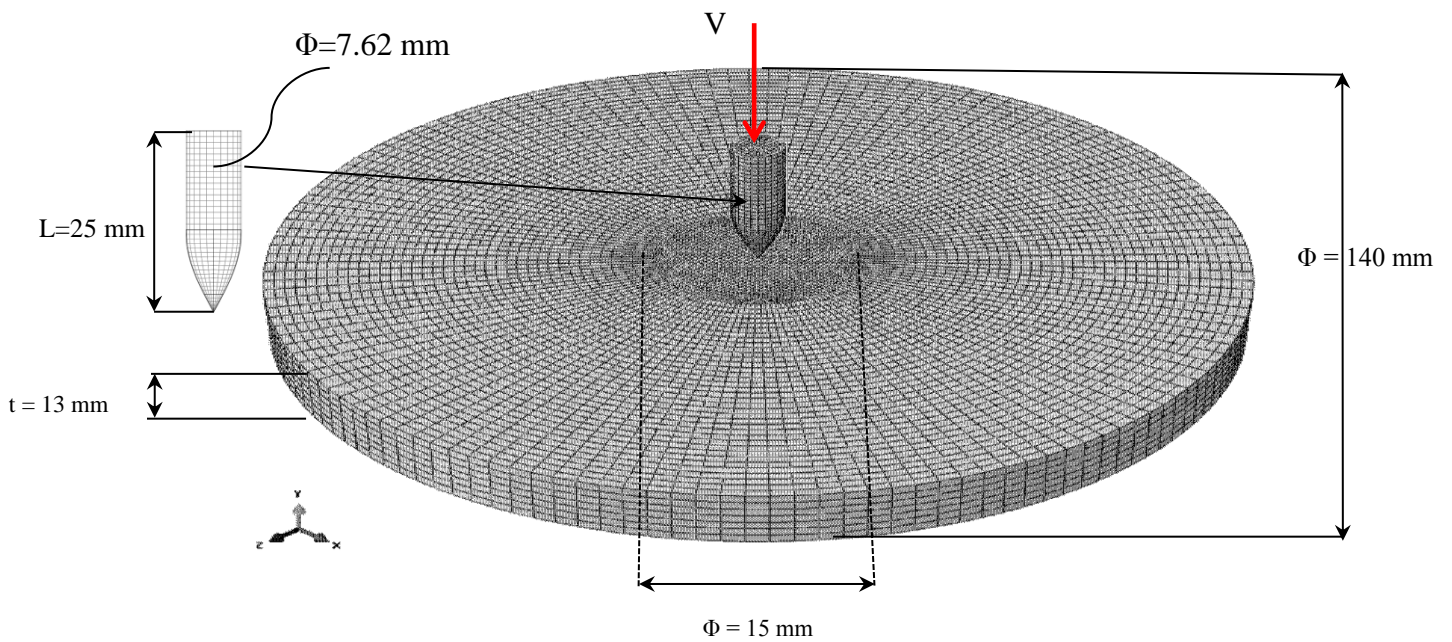
Figure 5.6. Mesh and loading conditions used in the terminal ballistic test on aluminium syntactic foam.

The overall dimensions of the aluminium matrix syntactic foam sample are diameter (Φ) 140 mm, thickness (t) 13 mm, length of the bullet (L) 25 mm and diameter (Φ) 7.62 mm. In the terminal ballistic simulation, the peripheral surface of the sample was fully constrained. An initial velocity was defined on the bullet, which was equal to the impact velocity appointed in the terminal ballistic test. The residual velocity and depth of penetration were recorded from the modelling. Material properties listed in Tables 5.8-5.11 were used here.

5.4.4   Blast test simulation

The Blast responses of the aluminium matrix syntactic foams were modelled to investigate the capability of the material to absorb shock loading. Conditions similar to the experiment were applied. The charge was located at a stand-off distance of 50, 100

and 180 mm from the front surface of the sample. The configurations of the blast model are shown in Figure 5.8.
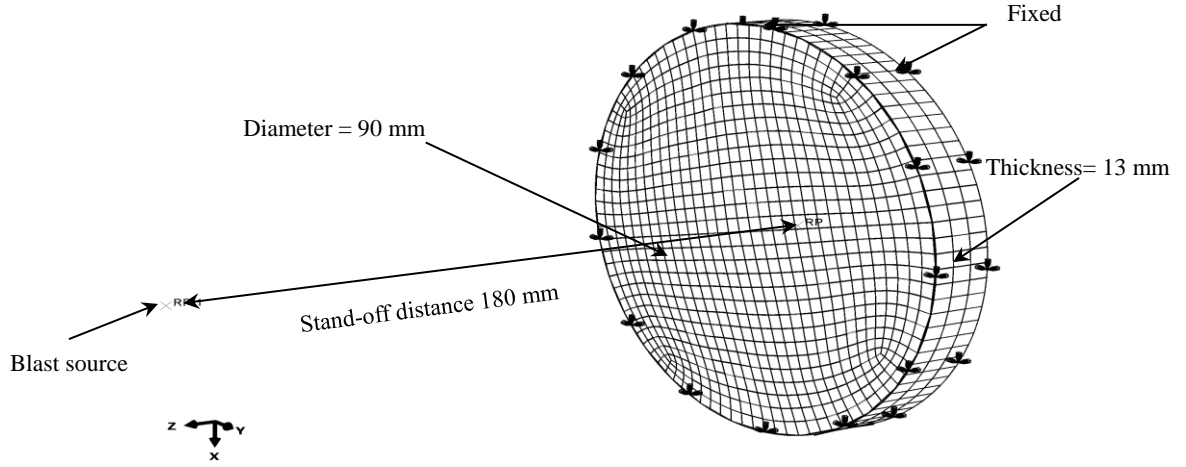
Figure 5.7. Boundary, geometry and loading conditions used in the blast modelling of the aluminium syntactic foam.

The size of the aluminium matrix syntactic foam model is 90 mm in diameter with a thickness of 13 mm. In the blast simulation, the peripheral surface of the sample were fully constrained. The CONWEP (Conventional Weapon Effects) blast load was applied on the top surface of the sample. In the model, pressure loading was imposed due to an air explosion, which is defined by detonation time, loading surfaces and location of the explosion. The blast charge properties were defined in relation to CONWEP charge properties. The CONWEP model can be described using the modified expression of the pressure–time response (Dharmasena et al., 2008):

$$p(t) = (p_{max} - p_{atm})\left[1 - \frac{t-t_a}{t_d}\right]e^{-\frac{a(t-t_a)}{t_d}} \qquad (5.18)$$

$$I = \int_{t_a}^{t_a+t_d} p(t)Ad(t) \qquad (5.19)$$

where p_{atm} is the atmospheric pressure, $(p_{max} - p_{atm})$ is the overpressure, t_d is the duration of the positive phase, t_a is the time of arrival of shock front, a is the decay constant that can be iteratively calculated from the impulse and A is cross sectional area. Here, the influence of the charge mass, thickness and stand-off distance on the material responses were investigated. Also, the velocity and displacement-time histories were numerically recorded.

5.5 Summary

Finite element models have been developed to model the behaviour of aluminium matrix syntactic foams under static and dynamic loading conditions. An elasto-plastic model was used to model aluminium syntactic foams. The damage evolution of aluminium matrix syntactic foams was described using ductile and shear damage failure. In addition, the rate-dependent model was used to designate the material yield behaviour with strain-rate effects. Quasi-static compression, three-point bending and shear tests were modelled to compare the FE simulations with the corresponding experimental results. In the quasi-static model, standard C3D8R elements were used, while explicit C3D8R elements were applied in the drop-weight, SHPB, terminal ballistic and blast models. In addition, the standard surface to surface contact was applied for the quasi-static modelling, while the explicit surface to surface contact was utilised in drop-weight, SHPB, terminal ballistic and blast models. The FE predictions are presented and compared with corresponding experimental results in the following chapter.

CHAPTER 6: FINITE ELEMENT SIMULATION RESULTS AND DISCUSSION

This chapter presents the finite element simulation results of aluminium matrix syntactic foams subjected to quasi-static compression, flexural and shear loads, followed by drop-weight, SHPB, terminal ballistic impact and blast. The modelling results obtained are compared with the experimental results presented in Chapter Four. The simulations presented here are valid only for aluminium matrix syntactic foam specimens. The FE simulations results were focused on aluminium syntactic foams based on Al 7075-T6 only, since it is found that this type of aluminium foam system has a higher energy absorption capability.

6.1   Modelling the Quasi-static Compression

To ensure that the FE models developed are sufficiently accurate, they need to be validated against experimental results of aluminium syntactic foams. The validations were carried out by comparing the load-displacement traces, plateau stress and failure modes. Figure 6.1 gives comparisons of the simulated and experimental load-displacement traces for the aluminium matrix syntactic foams with different ceramic micro-spheres sizes subjected to compression. As can be seen in Figures 6.1 (a), (b) and (c), the numerical predictions related to CM III (25-75 μm), CM II (150-250 μm) and CM I (250-500 μm) show a reasonably good agreement with the experimental load-displacement traces. The FE models capture well the initial stiffness, the first peak load, as well as the subsequent plateau. In addition, the deformation and failure modes are simulated reasonably well, as shown in Figure 6.2.

(a)

(b)

147
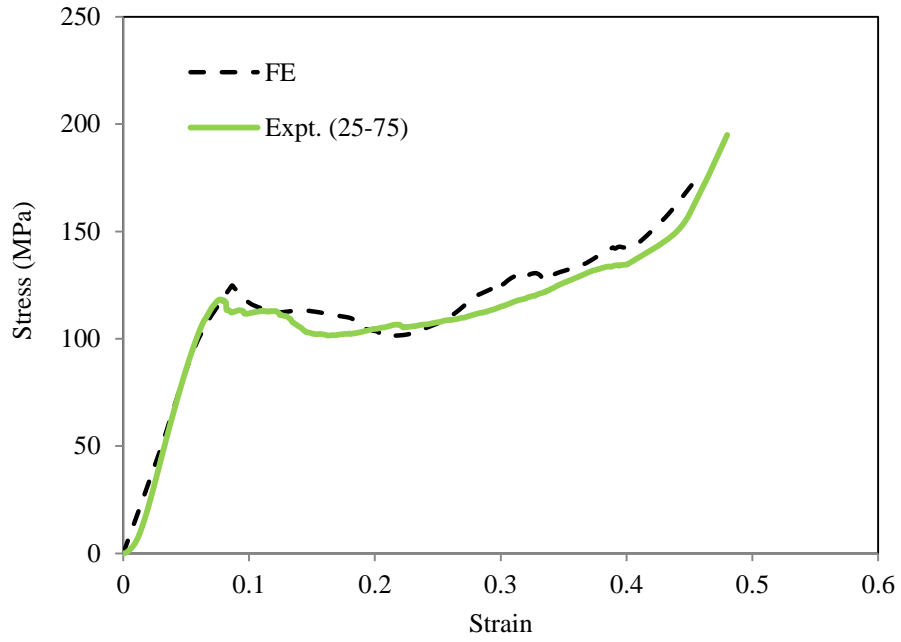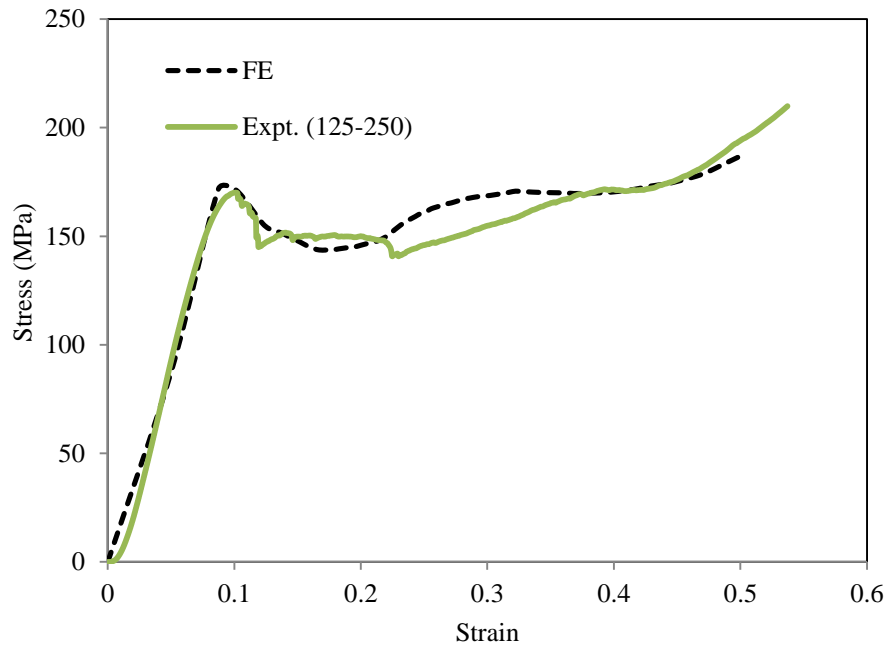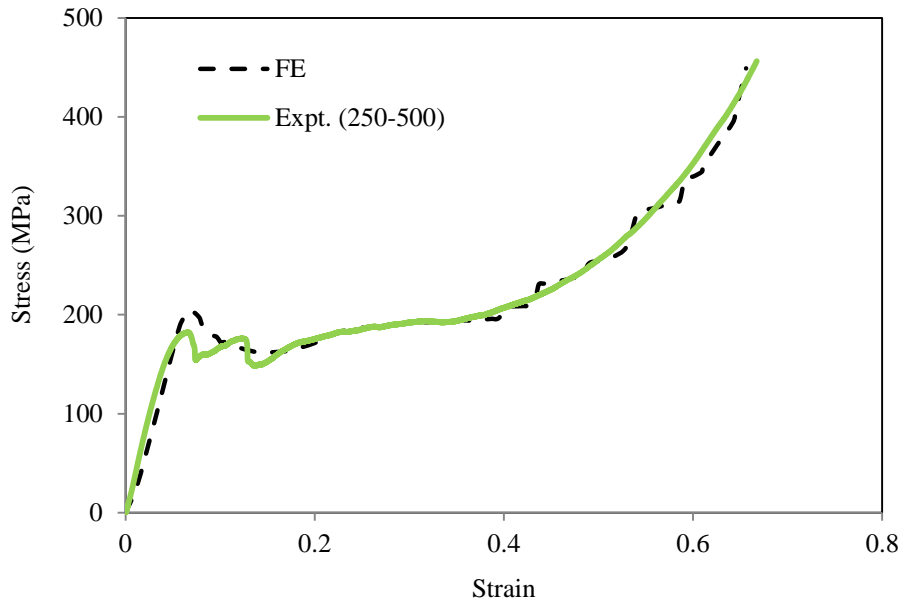
(c)

Figure 6.1. Stress-strain traces for the aluminium matrix syntactic foam Al 7075-T6 with different sizes of ceramic mirco-spheres under quasi-static compression loading: a) 25-75 μm, b) 125-250 μm, c) 250-500 μm (the solid line represents experimental results and the dashed line represents FE simulation).
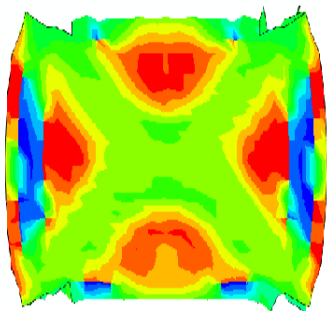
(a)   (b)

Figure 6.2. Comparison of the tested foam (Al 7075-T6 with 125-250 μm ceramic microspheres) with the simulated foam.

148

6.2   Simulation of the Three Point Bending

The FE models of aluminium syntactic foam beams under three point bending were validated using experimental results. Figures 6.3(a), (b) and (C) show comparisons between the FE simulations and the corresponding experimental load-deflection responses of the beam specimens.

The predicted peak loads for the CM (III), CM (II) and CM (I) foams are 7.06, 7.23 and 7.35 kN, which are 7.7, 6.0 and 6.2 % lower than the corresponding experimental results. The predicted initial stiffness shows a good correlation with the experimental data except CM (III) which is lower by 26.5%. The predicted displacements at peak load show higher values than the experimental data for the CM (I) and CM (II) foams, while CM (III) shows a lower predicted displacement. Despite the difference between the simulated values and the experimental results, the correlation is reasonably good.
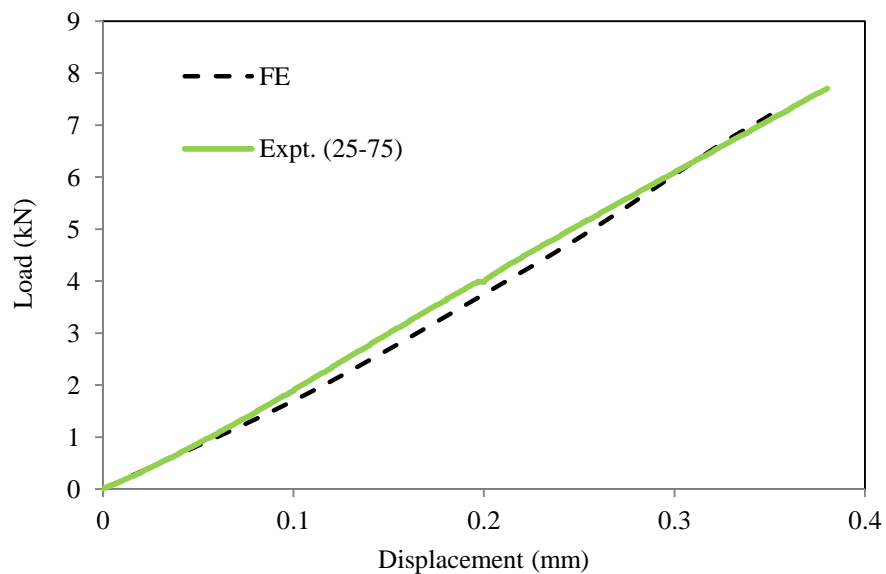

(a)
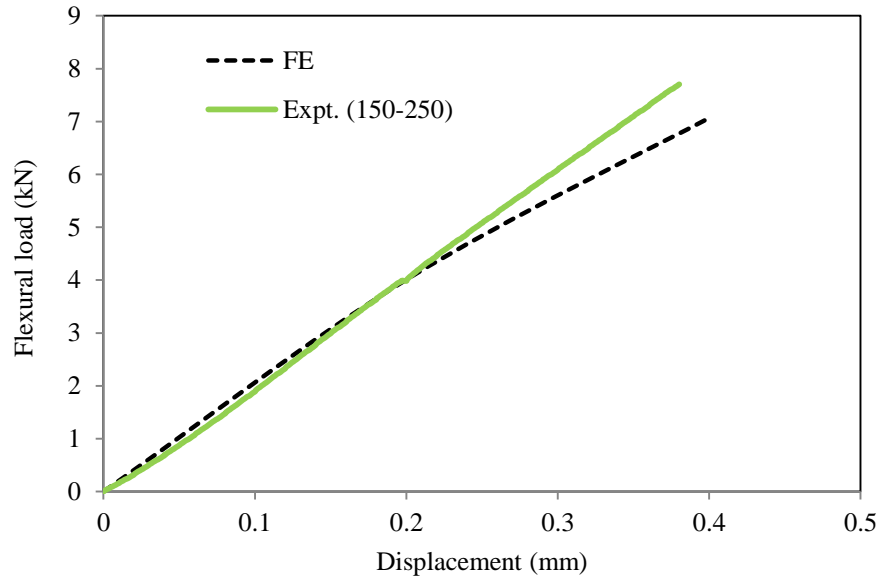
(b)
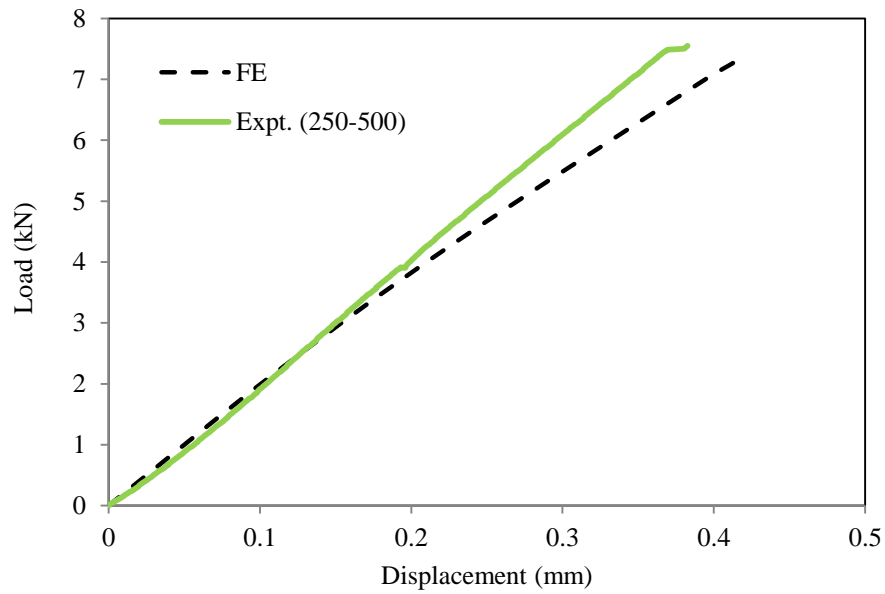
(c)

Figure 6.3. Load-displacement traces for the aluminium matrix syntactic foam Al 7075-T6 with different sizes of ceramic micro-spheres under three point bending loading: a) 25-75 μm, b) 125-250 μm, c) 250-500 μm (the solid line represents experimental results and the dashed line represents FE simulation).

6.3   Modelling the Shear Tests

Figures 6.4 (a), (b) and (c) present the numerical predictions of load-displacement plots for shear tests on the three types of the same foam. For a better comparison, the corresponding experimental results are shown in the same diagrams. The numerical simulations generally correlated with the experimental trends. The predicted peak loads for these three foams are 18.2, 18.2 and 17.6 kN, which are 5, 15 and 16.7% higher than experimental measurements, respectively. Here, the predict displacements at peak load show a good agreement with the corresponding experimental results. Here, the predicted initial stiffness are 17.8, 18.1 and 21.15 kN/mm, which are 3.8, 6.0 and 23.5% higher than test ones, respectively. Figure 6.5 shows the numerically and experimentally-obtained failure modes. The numerical simulation shows that the von Mises stress exceeds the critical stress level at the middle of the specimen where failure occurred. In general, the FE models offer reasonable predictions of the essential features of experimental load-displacement curves and failure modes.

(a)

151

(b)
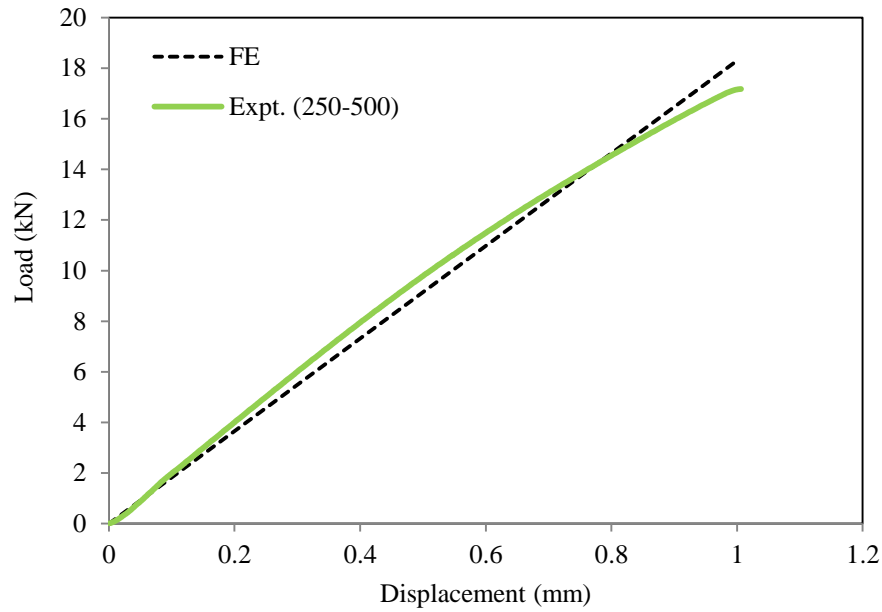
(c)

Figure 6.4. Load-displacement traces for the aluminium matrix syntactic foam Al 7075-T6 with different sizes of ceramic micro-sphere under shear loading: a) 25-75 μm, b) 125-250 μm, c) 250-500 μm (the solid line represents experimental results and the dashed line represents FE simulation).

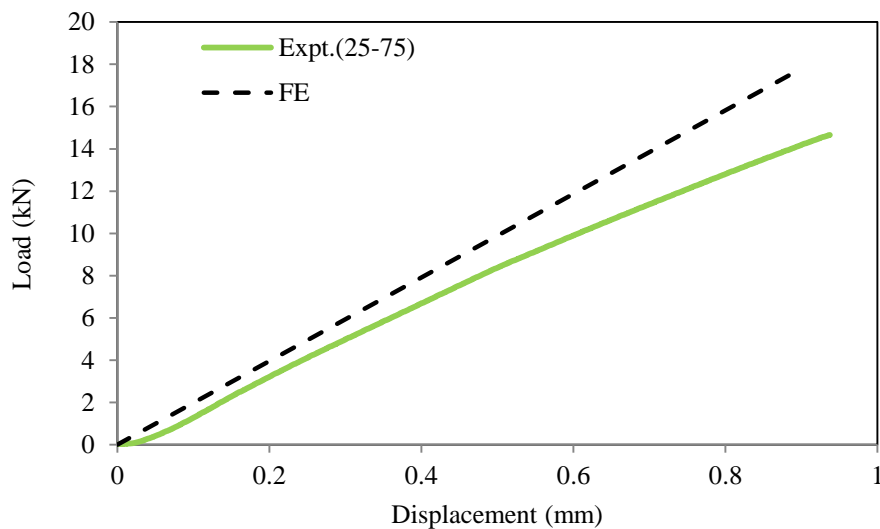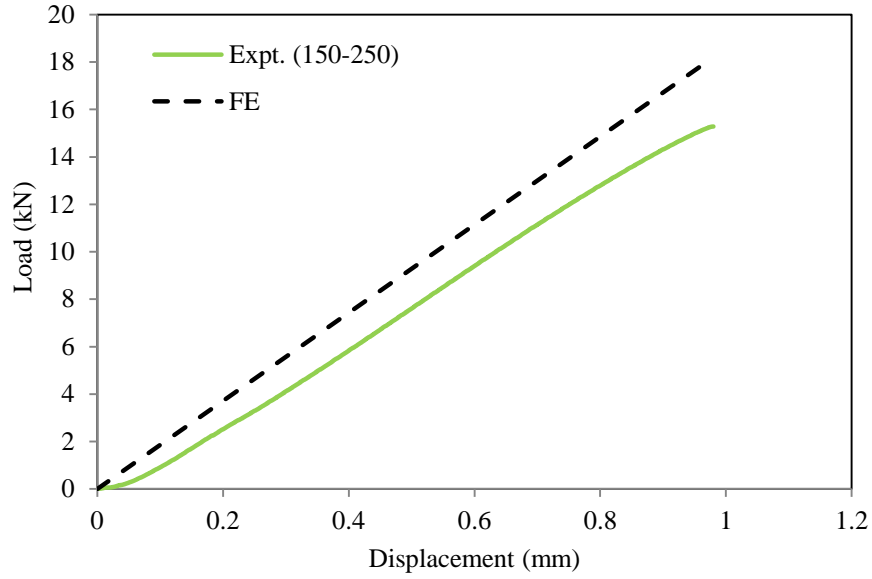Figure 6.5. Comparison of the tested foam (Al 7075-T6 with 125-250 μm ceramic microspheres) with Von Mises stress distribution, (in MPa), for the simulated foam.

6.4   Modelling the Drop-weight Impact Response

Figure 6.6 shows the simulated load-displacement traces for the three types of the aluminium matrix syntactic foam based on Al 7075-T6 subjected to impact at different strain-rates (drop-weight heights). For a better comparison, the corresponding experimental results are shown in the same diagram. The predicted peak stresses for these three foams at different strain-rates were 191.5, 206.4 and 380.2 MPa for CM (III), 215.8, 283.6 and 539 MPa for CM (II) and 226.3, 340.6 and 580.4 MPa for CM (I), which were 4.0% higher than experimental results. In addition, the predicted plateau stresses are higher by 13.1, 7.5 and 4.0% in comparison to the experimental results. The predicted specific energy absorption for these three foams at different strain-rates were 217.5, 296.2 and 337.3 kJ/kg, which were 1.0, 3.3 and 10.5% higher than the corresponding

experimental results, respectively. It is clear that good correlation is obtained between the simulations and the experimental results.

The failure mode of the foam CM (I) is compared with the simulation one in Figure 6.7. It is clear that basic features, such as the threshold for significant densification, the edge and corner configurations, are captured by the finite element modelling. Together with the well simulated load-displacement traces, the finite element models developed are ready to be used for further parametric studies to assist designing with this type of the foam.

(a)
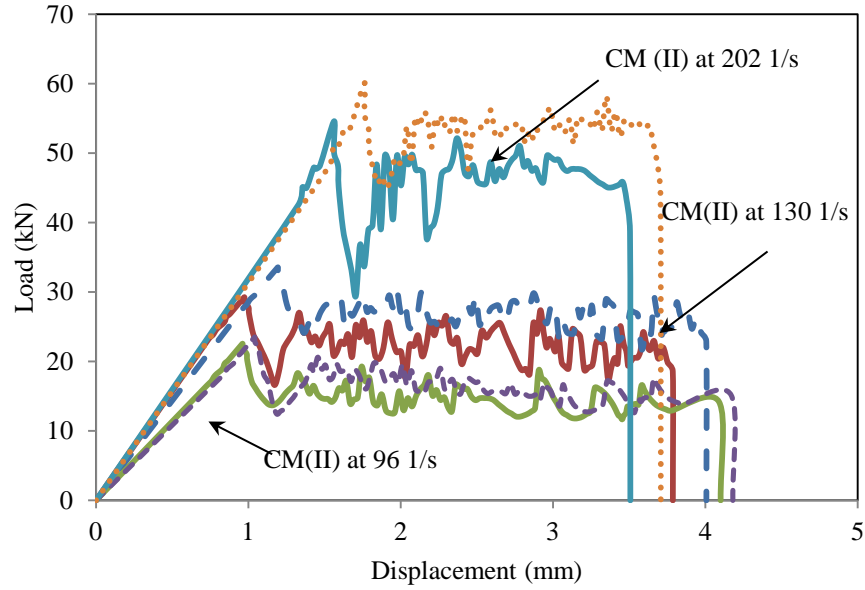
(b)
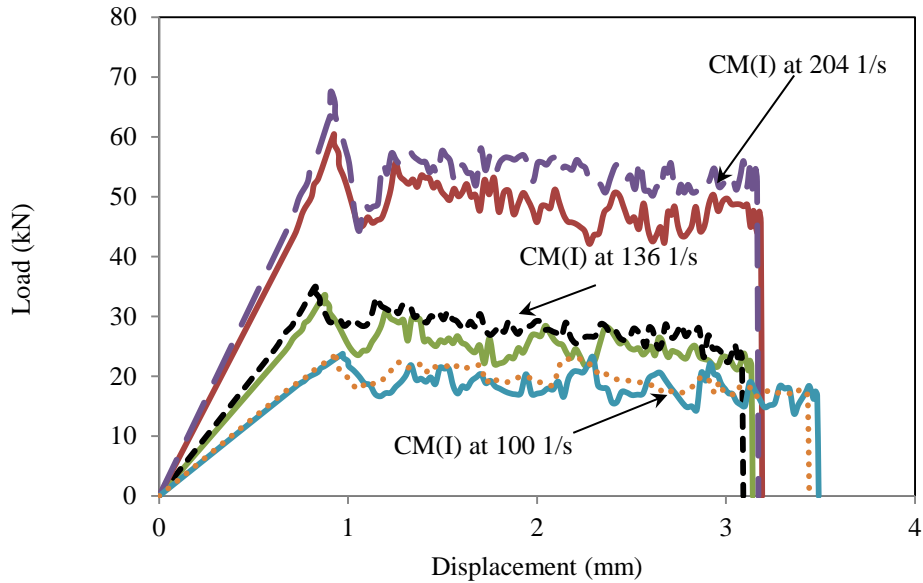
(c)

Figure 6.6. Load-displacement traces for the aluminium matrix syntactic foam Al 7075-T6 with different sizes of ceramic micro-spheres under dynamic loading at different strain rates: a) 25-75 μm, b) 125-250 μm, c) 250-500 μm (the solid line represents experimental results and the dashed line represents FE simulation).

155

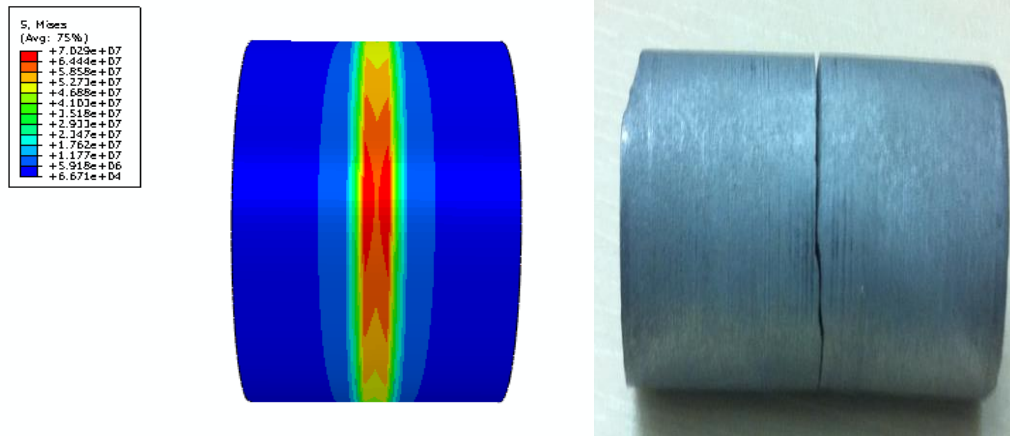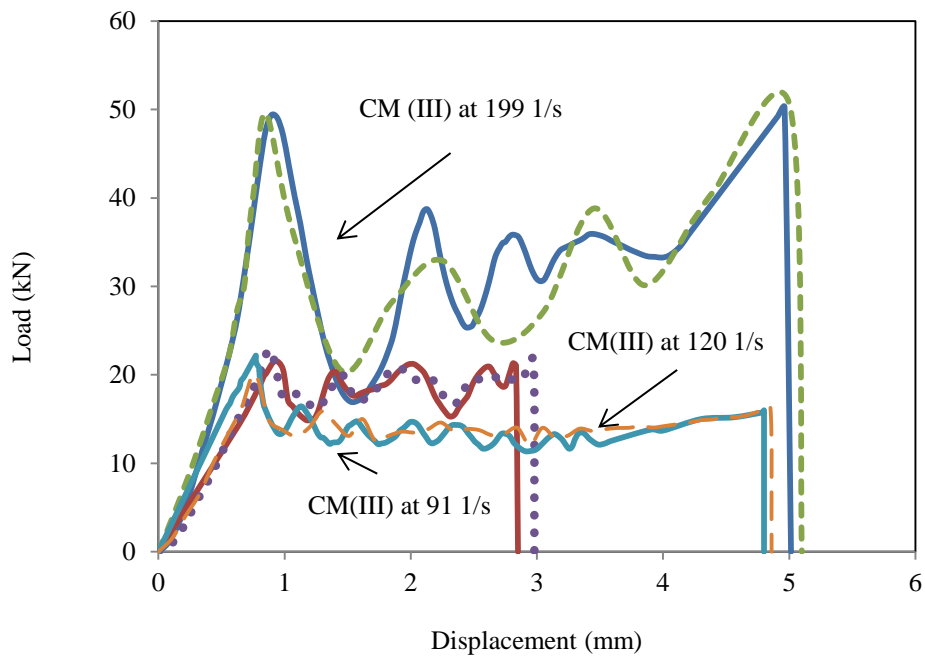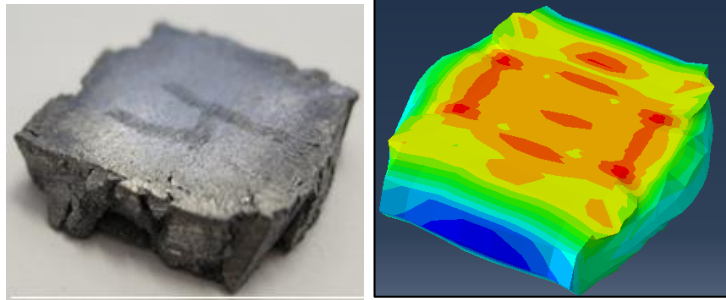Figure 6.7. Comparison of the tested foam (Al 7075-T6 with 250-500 μm ceramic microspheres at strain rate of 204 1/s) with the simulated foam.

6.5 Modelling Results of the Split Hopkinson Pressure Bar

Figures 6.8 (a), (b) and (c) shows the simulated stress-strain curves for the syntactic foams under high strain-rate loading. The predictions give reasonably good agreements with the corresponding experimental results. The predicted peak stresses for these three foams at different strain-rates are 595.9, 523.9 and 443.5 MPa for CM (I), which are 12.6, 11.1 and 2.3% higher than the corresponding experimental results. In addition, the FE simulations show a higher initial stiffness in comparison to the experimental results, which are 1.9, 5.0 and 4.5% higher.
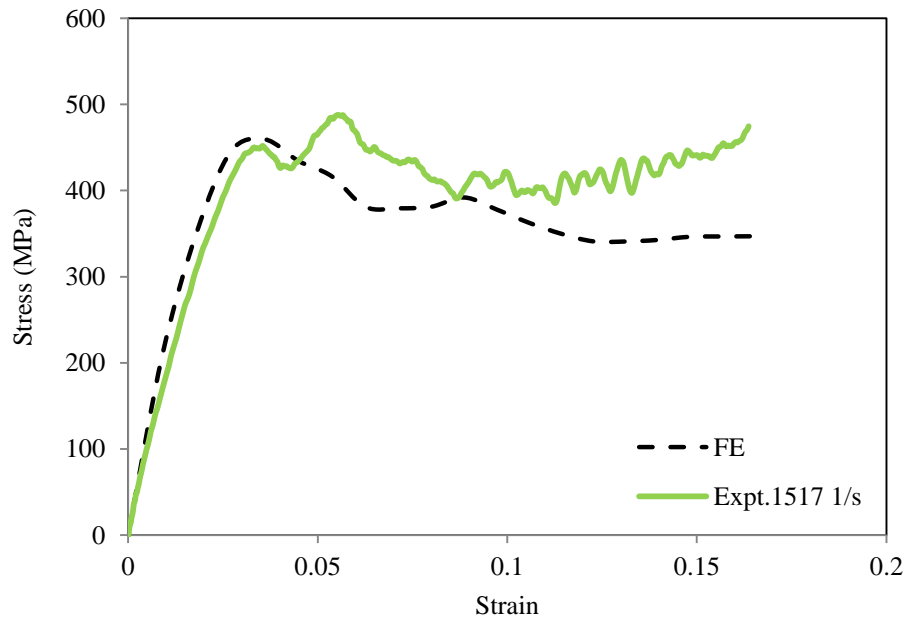
(a)
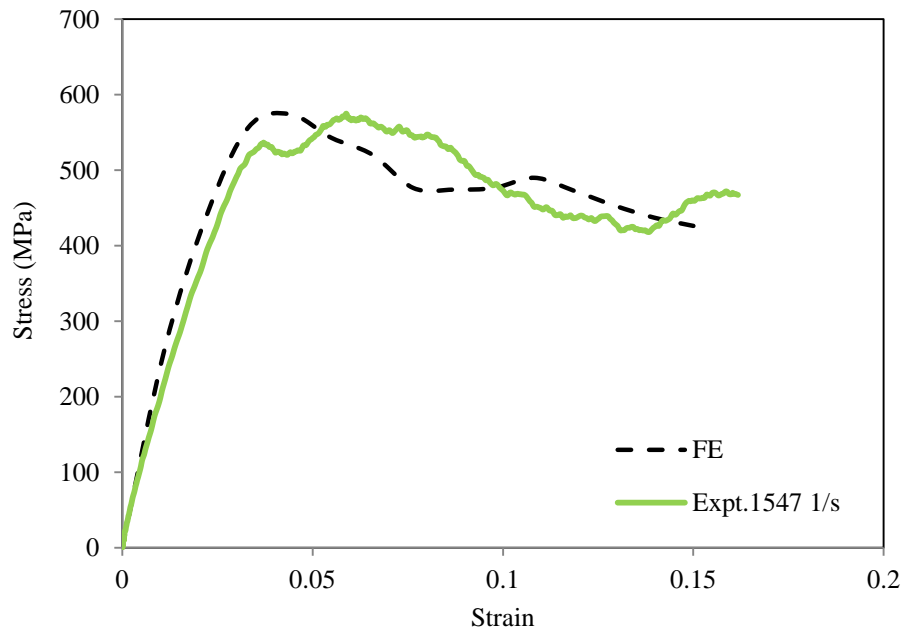
(b)
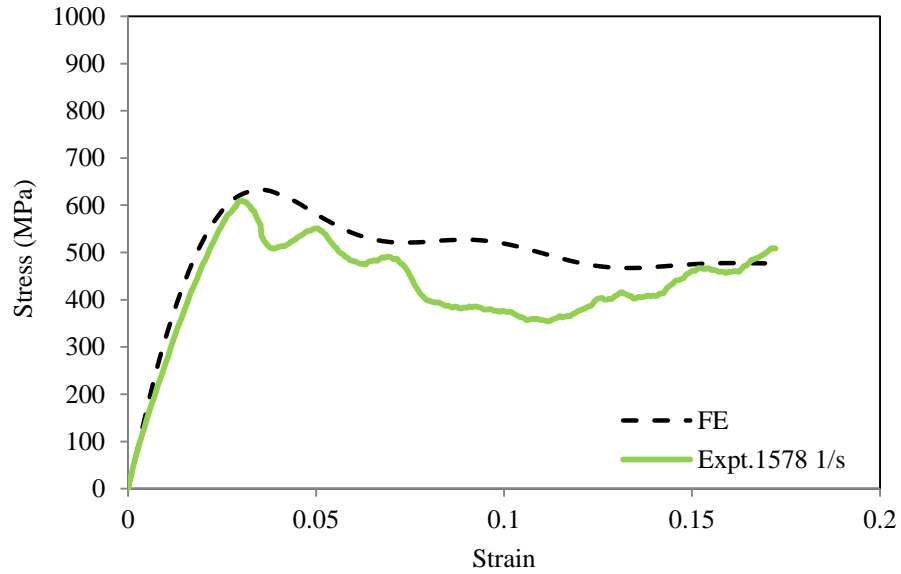
(c)

Figure 6.8. Stress-strain traces for aluminium matrix syntactic foam CM (I) under dynamic loading of SHPB at different strain rates: a) 1517 1/s, b) 1547 1/s, c) 1578 1/s (the solid line represents experimental results and the dashed line represents FE simulation).

6.6 Simulation of the Terminall Ballistic

The six experimental ballistic tests on the aluminium syntactic foam (CM I) based on Al7075-T6 were simulated using FE models. The models predicted the partial and full perforation tests accurately. In Chapter Four, the experimental results show that the material is able to resist a bullet at a velocity up to 120 m/s and it will be peforated at a higher impact velocity. Figure 6.9 shows the predicted velocity-time histories of the impact and residual velocities. V_R is plotted against V_I in Figure 6.10, V_{50} is the velocity where V_R became zero. Figure 6.11 shows the energy-time histories of the projectile. The FE results show energy-time histories with three regions. The beginning of the energy

histories represents the impact energy (E_I). After the projectile impacts the aluminium syntactic foam, it will transfer energy to the foam, called absorbed energy (E_a), and continously travel with the residual energy (E_R). Figures 6.12 illustrates the energy absorption per unit thickness and the ballistic limit (V_{50}) versus t/d for different sample thicknesses (t) at an impact velocity (V_I) of 550 m/s (d is the projectile diameter). The results show that the increase in the ballistic limit (V_{50}) follows with the increase in energy absorption per unit thickness (E_h). The ballistic limit and the energy absorption per unit thickness can be calculated using following equations (Lee et al., 1994):

$$V_{50} = \sqrt{(v_I^2 - v_R^2)} \tag{6.1}$$

$$E_h = \frac{\frac{1}{2}mv_I^2 - \frac{1}{2}mv_R^2}{t} \tag{6.2}$$

The experimental and FE predicted penetration of ballistic impact tests on aluminum syntactic foams at velocities above the ballistic limit and the velocities below the ballistic limit are illustrated in Figures 6.13 and 6.14, respectively. Similar to the experiments, the FE modelling was carried out on a 10 mm thick aluminium matrix syntactic foam with impact velocities of 550 m/s and 100 m/s, respectively. In the high velocity calculations, the ductile mode becomes fully established, as the projectile pushes the material sideways by applying a constant pressure through the nose of the projectile, accompanied by plastic flow. Figures 6.13 (c) and 6.13 (d) show good agreement between the experimental and FE results, while at low velocities the intial plastic deformation is confined to a circular region bounded by a circular hinge. At later time intervals, localized plastic failure appears around the boundary of the contact area. A comparison of Figures 6.14 (c) and 6.14 (d) shows good agreement between the FE predictions and the experimental results.
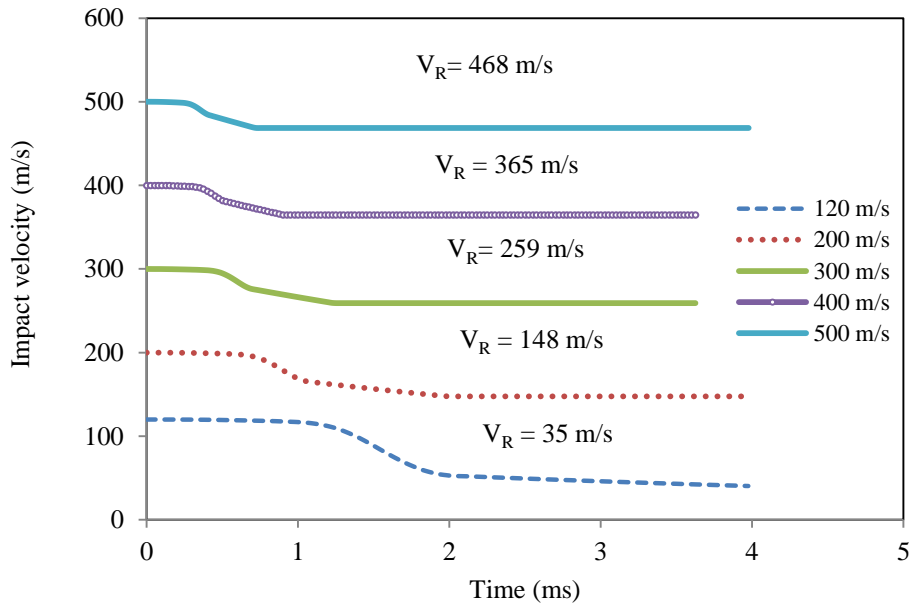
Figure 6.9. Predicted velocity time histories for the aluminum matrix syntactic foam impacted above V_{50}.
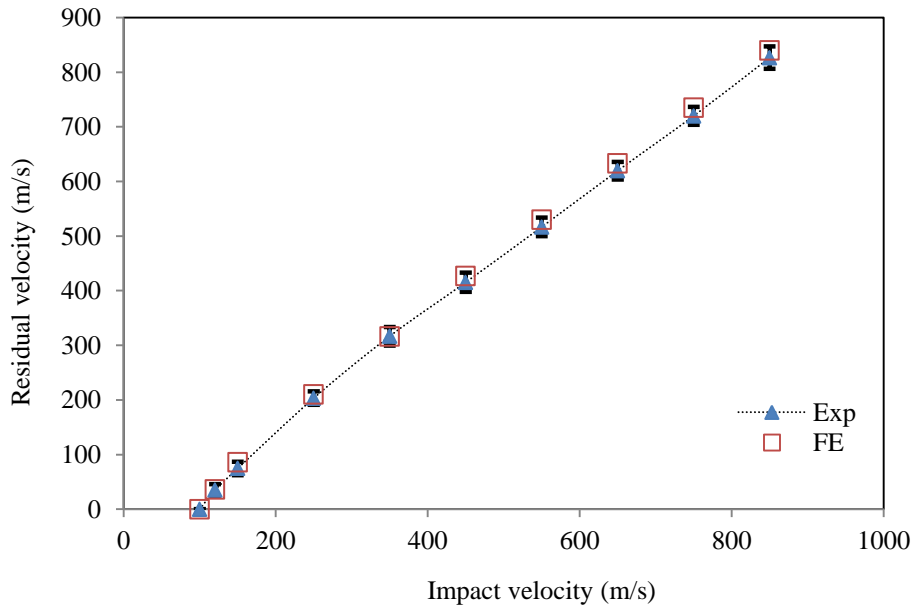
Figure 6.10. Experimental and FE predions results of V_R vs. V_I.
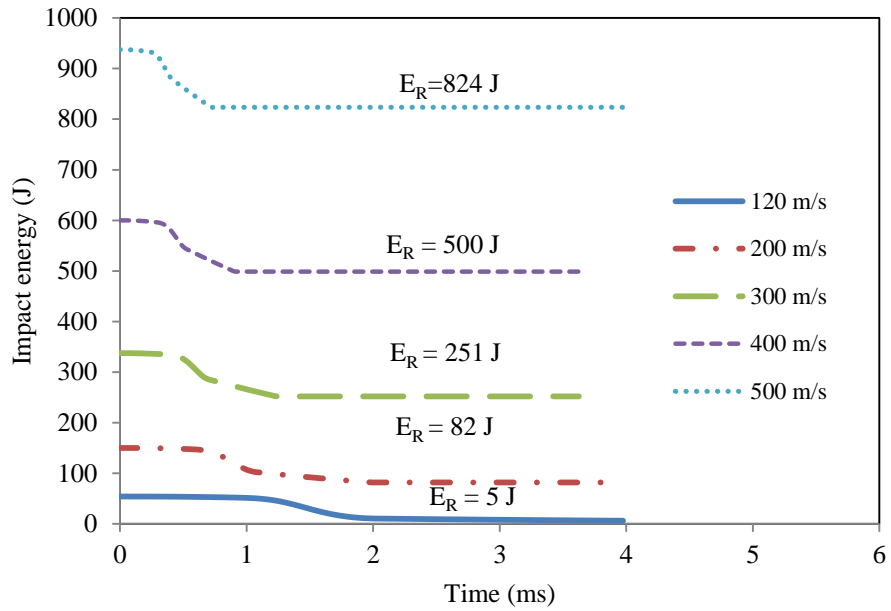
Figure 6.11. FE predicted energy histories for the aluminum matrix syntactic foam impacted above V_{50}.
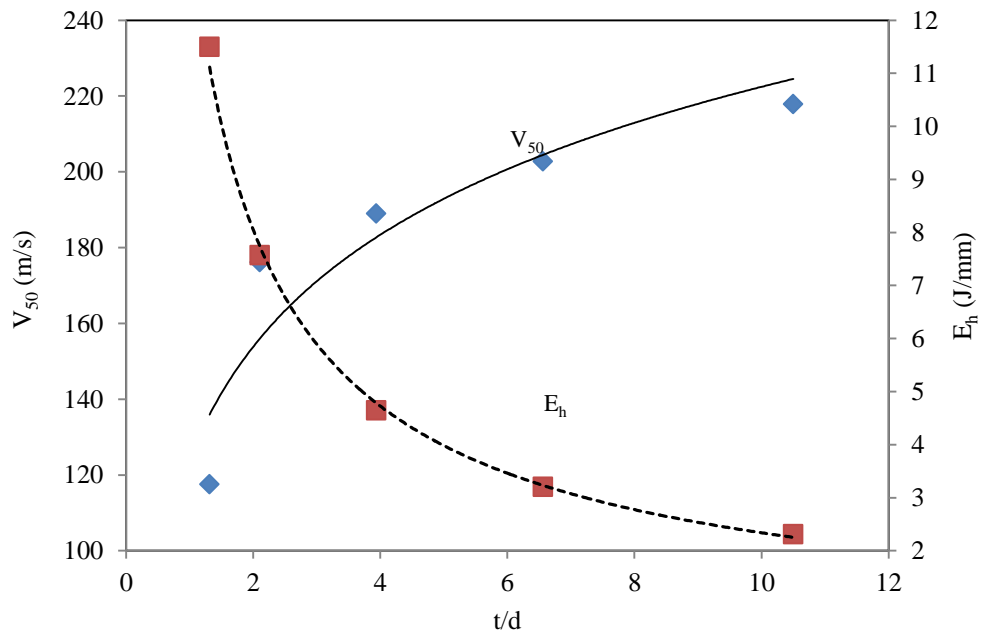
Figure 6.12. Energy absorption per thickness and ballistic limit versus the ratio of sample thickness to projectile diameter.

a

b

t = 2.5 ms

t = 5 ms

c

d

t = 7.5 ms

experiment sample
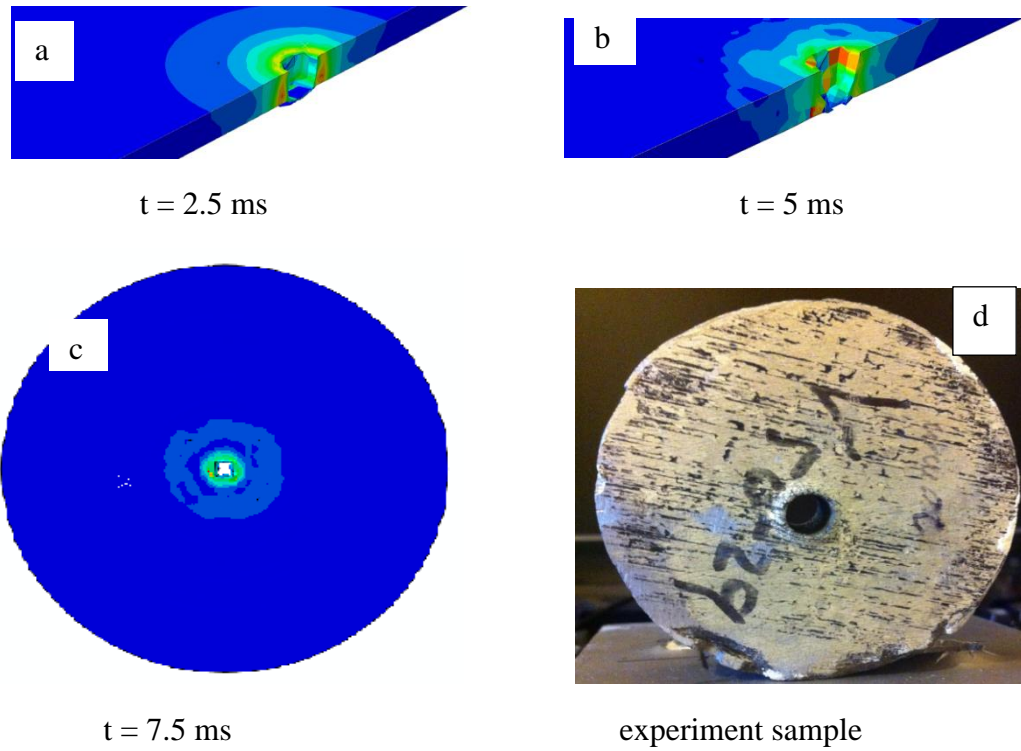
Figure 6.13. Perforation of a 10 mm aluminium matrix syntactic foam at an impact velocity 550 m/s.

(a)   (b)

Reference configuration

t = 2.25 ms

(c)

(d)

t = 7.5 ms

experiment sample
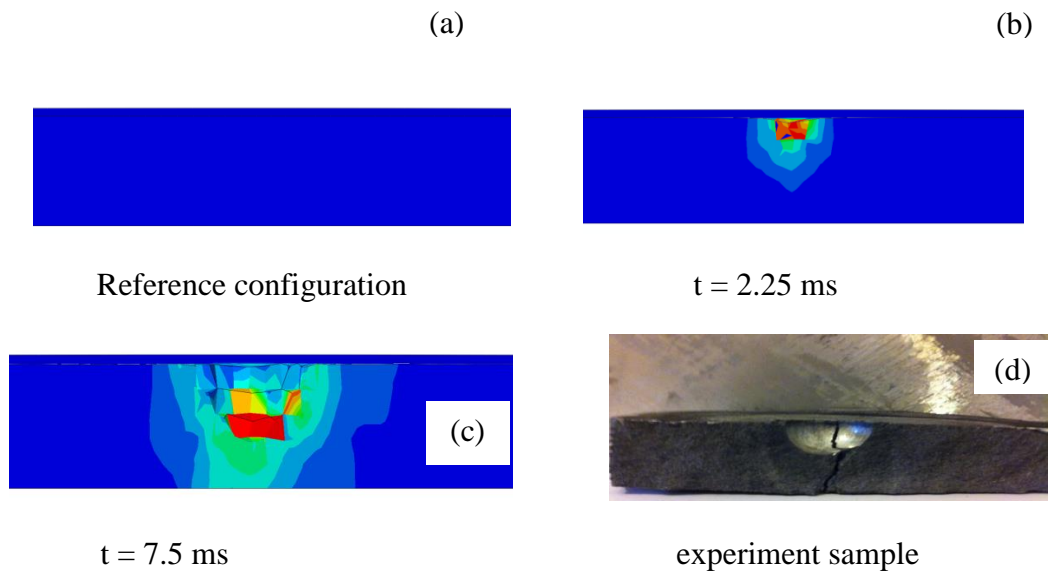
Figure 6.14. Penetration of a 10 mm aluminium matrix syntactic foam at an impact velocity of 120 m/s.

6.7   Blast Modelling

A series of simulations were carried out to model the blast response of the aluminium syntactic foams. The displacements on the front and back faces obtained from the simulations were compared with the experimental data, as shown in Figure 6.15. Here, the influence of the stand-off distance and the thickness of the sample were investigated. The results show that the displacement increases with an increase in the charge mass. The results also show that the target explodes with a load of 3g of PE4 except for a sample for the 20 mm thick sample. In addition, the results show the influence of stand-off distance on the response of the targets. The displacement of the sample increases with decreasing stand-off distance, as expected. The stand-off distance necessary to avoid hardening the target is a function of the type and mass of the explosive, the type of the target material and the desired level of protection. The results indicate that an aluminum syntactic foam with a thickness of 20 mm can accommodate a blast load of 3g charge mass at 180 mm stand-off distance. The centre displacement and velocity history of the aluminum matrix syntactic foam at a 180 mm stand-off distance are shown in Figure 6.16. Initially, the same velocity was obtained on the front and back faces until cracking appeared. Then, the acceleration of the back face reduced. At 0.15 ms, the velocity of the front face started to decrease, whilst the back face had the same sequence as the front face. At t= 0.25 ms, the front and back faces show an equal velocity, due to compaction of the material. Figure 6.17 shows the predicted FE response of the aluminum syntactic foam with a 3 mm thickness at 2 Ns impulse. Figure 6.18 shows the response of the 14 mm thick foam subjected to 4.82 Ns that is sustained by the target with cracks on the front and back faces. The results show that the basic features, such as the significant stress concentration

163

in the centre of the front and back faces and the peripheral crack configurations, are captured by the finite element modelling.
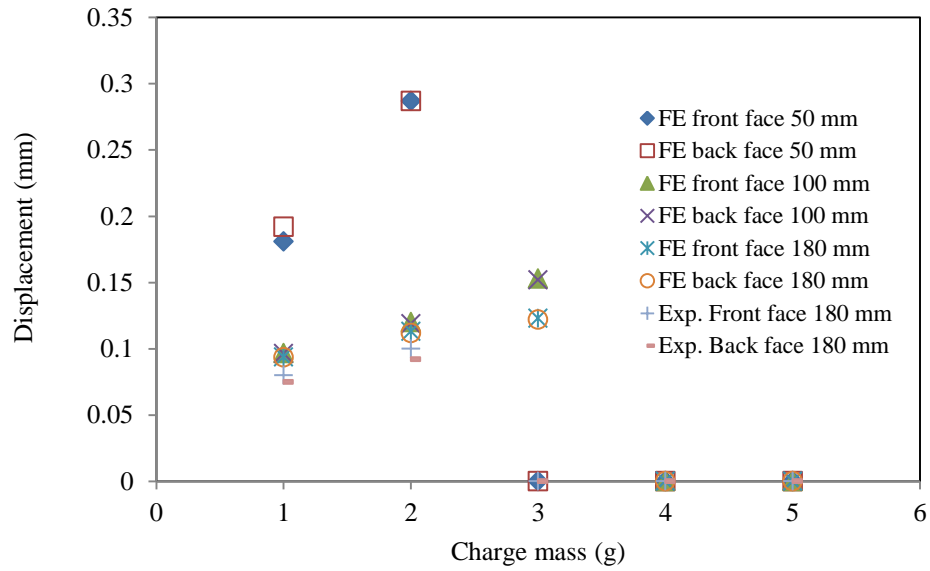
a) thickness 5mm
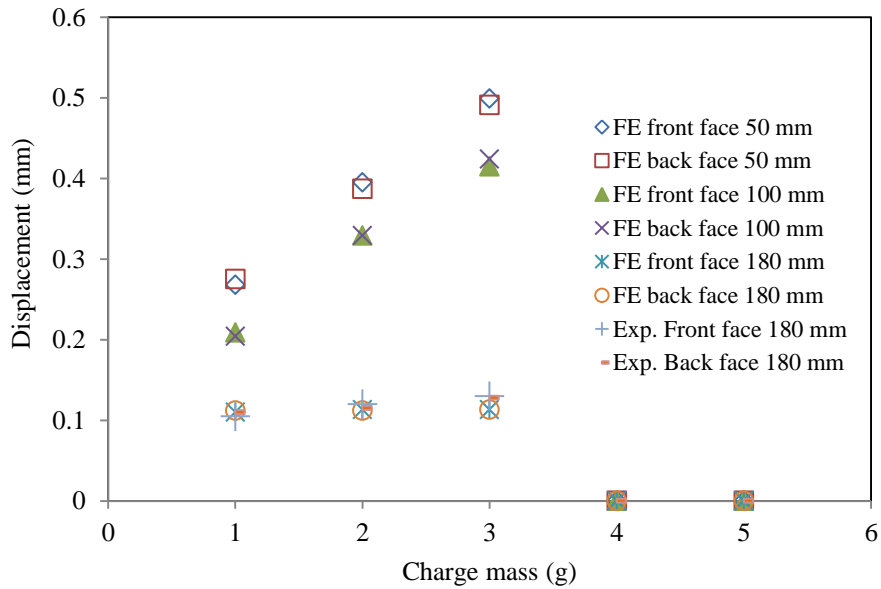
b) thickness 10 mm
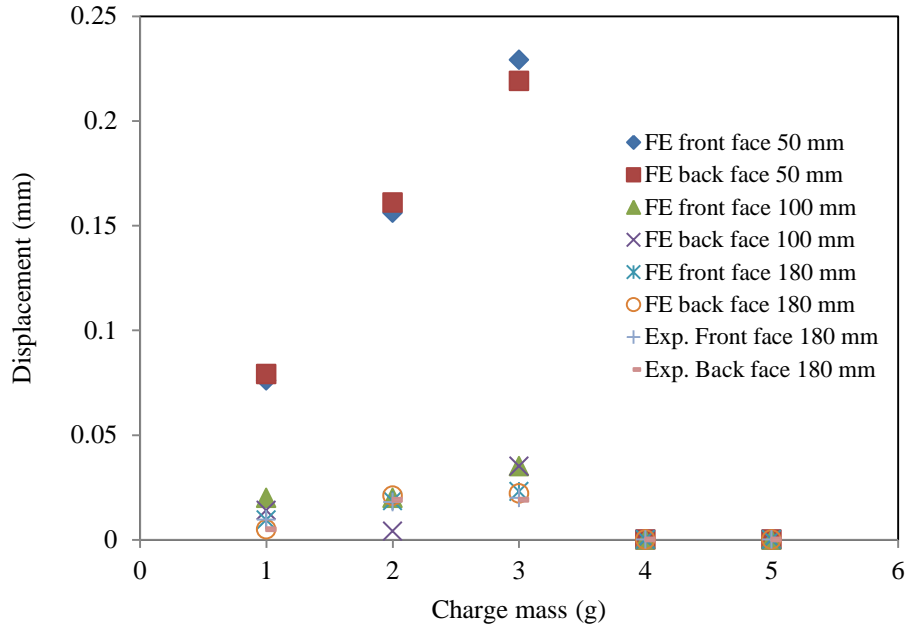
c) thickness 20 mm

Figure 6.15. Comparison of the predicted centre deflection with the experimental results for different blast charges at different sample thickness (zero deflection represents the explode material).
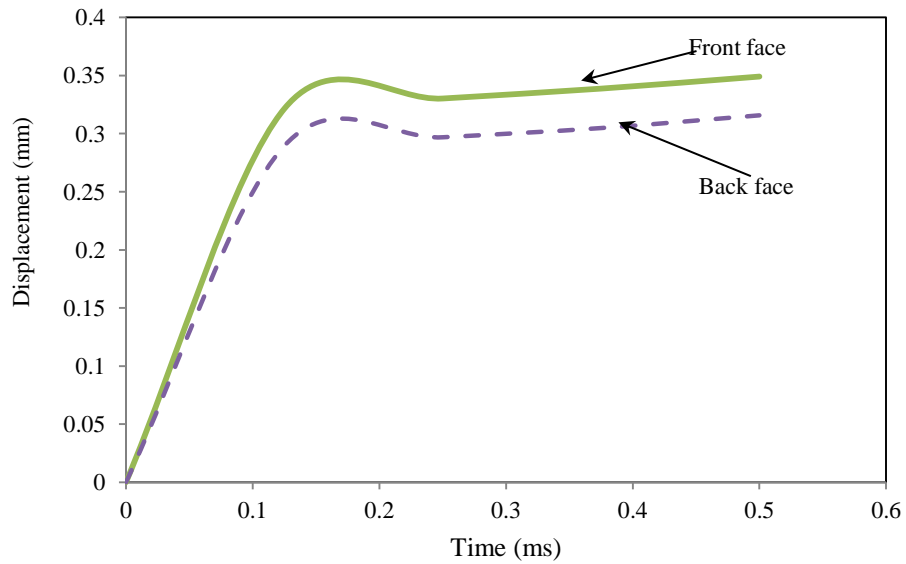
(a)
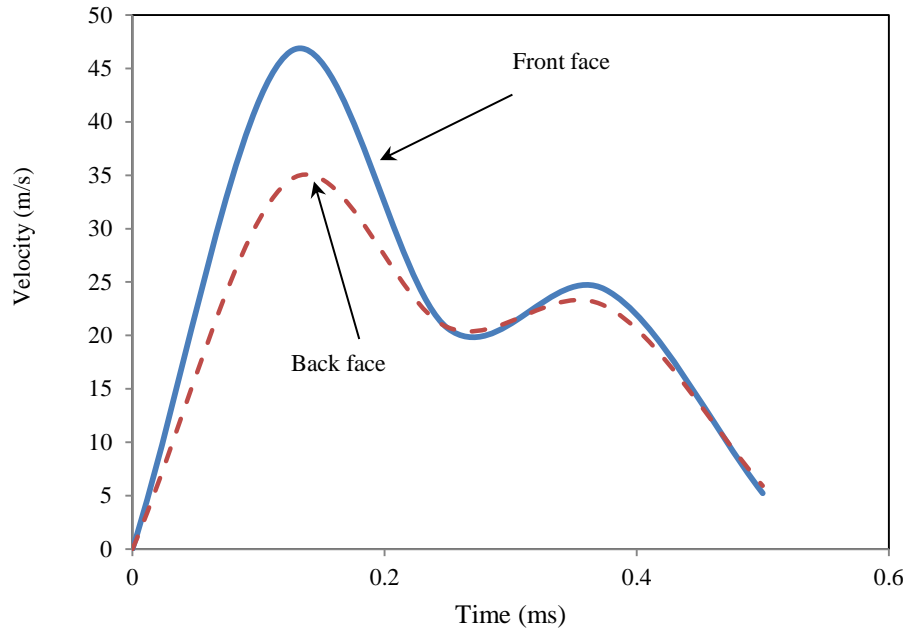
(b)

Figure 6.16. (a) Centre displacement and (b) velocity on the front and back faces of 10 mm the aluminum syntactic foam CM (I).
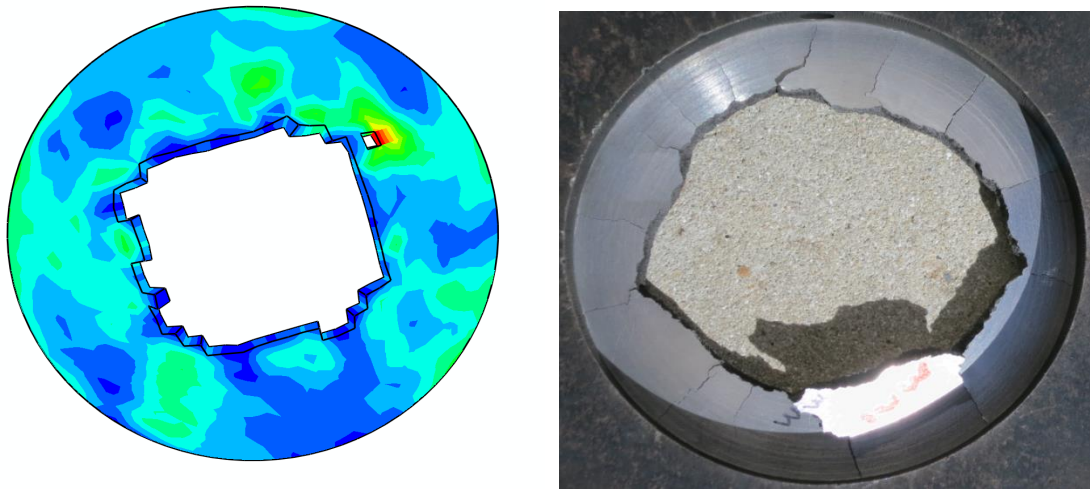
Figure 6.17. Comparison between the experiments and numerical simulations for 3 mm thickness of aluminum syntactic foams at 2 Ns.
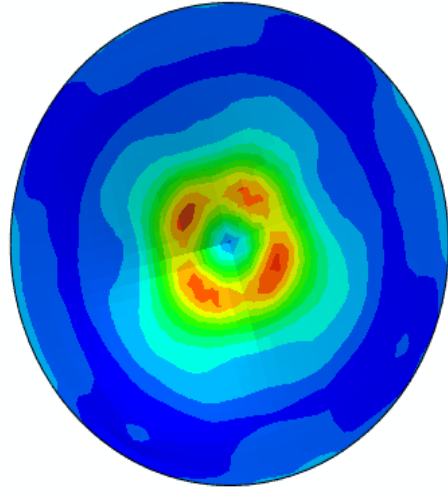
(a) Front face
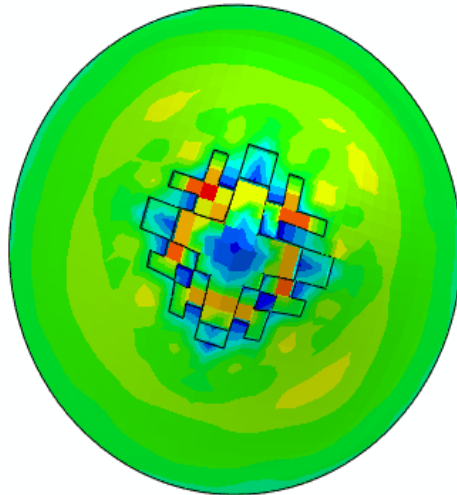
(b) Back face

Figure 6.18. Comparison between the experiments and numerical simulations for the 14 mm thick of aluminum syntactic foam CM (I) at an impulse of 4.82 Ns.

6.8   Summary

Finite element models were carried out for use in further parametric studies to optimise the structural behaviour of syntactic foams. FE results have been presented to firstly model the quasi-static compression, three point bending and shear tests. Then, simulations of drop-weight, SHPB, terminal ballistic and blast tests were conducted, which are compared with the corresponding experimental results. In quasi-static compression, the FE models capture the essential deformation features of the samples, which correlate well with the experimental load-displacement relationship. The FE predictions of the three-point bending tests also agree well with the corresponding experimental results, in terms of the load-deflection curves. In addition, the output of the shear modelling offers reasonable predictions of the experimental load-displacement traces, exhibiting similar failure modes to those observed following testing. The FE predictions of the drop-weight tests also reproduce the experimental load-displacement traces reasonably well, together with the basic features, such as significant densification, the edge and corner configurations. However, when modelling the SHPB tests, the FE simulations give an overestimation of the experimental results. Furthermore, the FE model of the ballistic tests showed good agreement with the corresponding experimental results. Parametric studies were carried out to investigate the influence of target thickness on the terminal ballistic response, which show that an increase in the target thickness leads to an increase in the peak load and the ballistic limit. The local damage and overall deformation modes were also predicted with success. Finally, comparisons of the FE predictions and the experimental results are made involving samples subjected to different charge masses, stand-off distances and with different target thicknesses. The

essential features of the experimental failure modes were captured by the FE models. Reasonably good correlation was obtained between the failure mechanisms observed in the experimental targets and the numerical models. This information is useful to be used in the design of the armoured vehicle or any applications that need a material which has high energy absorption capability.

CHAPTER 7: Conclusions and Recommendations for Future Work

7.1 General Summary

The objective of this study was to present a detailed investigation on the quasi-static and dynamic response of aluminium matrix syntactic foams under compression, three-point bending, shear, drop-weight impact, Split Hopkinson Pressure Bar, terminal ballistic and blast loading in order to characterise the mechanical properties of the foams. In addition, the Finite Element Method has been used to model the response of the foams under those loading regimes. The research has been executed to achieve these aims and the following conclusions can be drawn:

- Following the quasi-static compression tests on aluminium matrix syntactic foams, it has been shown that the yield strength, plateau strength and densification strain are sensitive to the foam density.

- The energy absorption of aluminium matrix syntactic foams is determined by densification strain and plateau stress. The former is determined by the porosity of the syntactic foam, while the latter is dependent on the compressive strength and the mode of plastic deformation.

- A series of three-point bending tests have shown that the flexural strength increases with foam density. The syntactic foams failed in a brittle fracture manner at the centre of the sample. In addition, it was shown that the specific energy absorption capacity during three-point bending tests is higher than that measured during shear tests.

- The results of shear tests have shown an increase in foam density leads to an increase in specific energy absorption, shear modulus and shear strength.

- Both yield strength and specific energy absorption of the aluminium matrix syntactic foams under drop-weight loading have been found to be sensitive to foam density and strain-rate, tending to an increase with increasing of the strain-rate.

- The SHPB results have also shown that both the yield strength and the dynamic Young's modulus of the aluminium syntactic foams are rate-dependent. There are increases in yield strength and the dynamic Young's modulus with increasing strain-rate.

- The results of terminal ballistic tests have indicated that 13 mm thick aluminium syntactic foams have an ability to stop a projectile at a velocity of 120 m/s. In addition, the results have shown the ballistic limit velocity (V_{50}) increases with an increase in target thickness.

- Blast test results have shown that foams with thickness of 14 mm are able to sustain a small blast load of 4.82 Ns. In general, aluminium syntactic foam is too brittle to sustain a higher blast loads, unless it is used as a core material in a sandwich structure.

- The Finite Element package, Abaqus/Standard, was used to model the response of the aluminium matrix syntactic foams under quasi-static compression, three-point bending and shear loading. The FE predictions from those models have given a good agreement with their corresponding experimental results.

- Abaqus/Explicit was used to model drop-weight, SHPB, terminal ballistic and blast tests. The simulations have shown that the FE models have captured the essential features of the foams tested, such as the significant densification, perforation failure, deformation modes on the edges and corners.

- The FE predictions of the quasi-static compression peak load, Young's modulus and densification strain overestimate the corresponding experimental results.

- Three-point bending and shear modelling simulations have shown good agreement with the corresponding experimental results.

- The drop-weight peak stress, plateau stress and energy absorbed by the aluminium syntactic foams were predicted to within 4.0, 4.0 and 10.5% of the experimental values, respectively. These values fall within the range of variation in the mechanical properties found experimentally.

- The FE predictions of the SHPB test results have shown a higher peak stress, plateau stress and dynamic Young's modulus, which also indicate that these mechanical properties increase with the strain-rate.

- The ballistic impact models are capable of accurately predicting partial and full perforation of the samples. Parametric studies have been carried out to establish the influence of sample thickness on the ballistic limit velocity.

- The FE predictions from the blast models have shown that the sample deflection increases with increasing charge mass, as expected. Furthermore, it has been shown that a 20 mm thick sample can withstand a mass of 3 g of PE4 at a 180mm stand-off distance.

7.2   Recommendations for Future Work

Based on the conclusions above the following recommendations are made.

- It would be valuable to investigate the response of the material under multi-axial loads (e.g. through the use of an Arcan rig).

- It would be interesting to investigate the responses of the aluminium syntactic foams under oblique impact testing.

- It would be of interest to conduct additional terminal ballistic and blast tests on a sandwich structure, where the aluminium syntactic foam is used as a core, to investigate the possibility of using aluminium matrix syntactic foams as military vehicle armour.

- Modelling the response of a single unit cell using the multi-scale modelling approach would be worthy of investigation, so as to assess the response of the foam from meso scale to micro scale in terms of deformation and failure mechanisms.

REFERENCES

Aalco. Aluminium Alloy 6082 – T6 – T651; 2013.

Al Bakri F. Investigation of the Effect of Pressing Condition on the Physical, Mechanical and Ballistic Properties of Ultra-high Molecular Weight Polyethylene Composite – Dyneema, MSc Thesis, Cranfield University; 2001.

Alonso M, Auad M and Nutt S. Short-fibre-reinforced epoxy foams. Composites. 2006; 37:1952-1960.

Altenaiji M, Schleyer G and Zhao Y. Characterisation of Aluminium matrix syntactic foams under static and dynamic loading. Applied Mechanics and Materials. 2012; 82:142-147.

Ashby F, Evans A, Fleck A, Gibson L, Hutchinson J and Wadley H. Metal Foams: A Design Guide, Butterworth Heinemann, Oxford, UK; 2000.

Autonomous Underwater Vehicles-www.esyntactic.com/auv-autonomous-underwater-vehicles, Trelleborg AEM.

Babcsan N, Garcia Moreno F and Banhart J. Metal foams – high temperature colloids: part II: In situ analysis of metal foams. Colloids and Surface A: Physicochemical and Engineering Aspects. 2007; 309:254–263.

Balch D, O'Dwyer J, Davis G, Cady C, Gray III G and Dunand D. Plasticity and damage in aluminium syntactic foams deformed under dynamic and quasi-static conditions. Materials Science and Engineering. 2005; 391:408–417.

Balch K and Dunand C. Load partitioning in aluminium syntactic foams containing ceramic micro-spheres. Acta Materialia. 2006; 54:1501–1511.

Banhart J. Manufacture, characterisation and application of cellular metals and metal foams. Progress in Materials Science. 2001; 46:559–632.

Borvik T, Hopperstad O, Langseth M and Malo K. Effect of target thickness in blunt projectile penetration of weldex 460 E steel plates. International Journal of Impact Engineering. 2002; 28:413–464.

BS EN 2746. Flexural test-Three point bend method. British Standards Institution. London, 1998.

Calladine C and English W. Strain rate and inertia effects in the collapse of two types of energy absorbing structure. International Journal of Mechanical Science. 1984; 26:689–701.

Cantwell W and Morton J. The impact resistance of composite materials-a review. Composites. 1991; 22:348–349.

Castro G and Nutt S. Synthesis of syntactic steel foam using gravity-fed infiltration. Materials Science and Engineering A. 2012; 553:89–95.

Castro G, Nutt S and Wenchen X. Compression and low velocity impact behaviour of aluminium syntactic foam. Materials Science and Engineering A. 2013; 578: 222–229.

Cebon D, Ashby F and Lee-Shothaman L. Cambridge Engineering Selector Version 3.2, First Edition. Cambridge University Press;2001.

Chou K and Song M. A novel method for making open-cell aluminium foams with soft ceramic balls. Scripta Materialia. 2002; 46:379–382.

Clyne W. Metal matrix composites: matrices and processing. Encyclopaedia of Materials: Science and Technology (ed.) A Mortensen (Elsevier);2001.

Cookson E, Floyd D, and Shih A. Design, manufacture and analysis of metal foam electrical resistance heater. International Journal of Mechanical Science. 2006; 48: 1314–1322.

Dannemann A and Lankford J. High strain rate compression of closed-cell aluminium foam. Materials Science and Engineering A. 2000; 293:157–164.

Davies G and Zhen S. Review metallic foams: their production, properties and applications. Journal of Materials Science. 1983; 18:1899–1911.

De Carli P and Meyers M. Design of uniaxial strain shock recovery experiments. In Shock Waves and High-Strain-Rate Phenomena in Metals. United States Army Research Office, New Mexico;1981.

Deshpande V and Fleck N. High strain rate compressive behaviour of aluminium alloy foams. International Journal of Impact Engineering. 2000; 24:227–298.

Dharmasena P, Wadley H, Xue Z, and Hutchinson J. Mechanical response of metallic honeycomb sandwich panel structures to high-intensity dynamic loading. International Journal of Impact Engineering. 2008; 35:1063–1074.

Dung L, Gupta N and Rohatgi P. The high strain rate compressive response of Mg-Al alloy/ fly ash ceno-sphere composites. Journal of the Minerals, Metals and Materials Society. 2011; 63:48–52.

Evans A, Marchi C and Mortensen A. Metal Matrix Composites in Industry (an Introduction and a Survey), Kluwer Academic, Massachusetts, USA; 2003:1-2.

Fan J. Investigation of the behaviour of fibre metal laminates subjected to low velocity impact, PhD thesis, Liverpool University, 2010.

Follansbee S and Frantz C. Wave propagation in the split pressure Hopkinson pressure bar. Journal of Engineering Materials and Technology. 1983; 105:61–66.

Gibson L and Ashby M. Cellular Solids: Structure and Properties. 2nd edition: Cambridge Solid State Science Series; 1999.

Gibson L. Mechanical behaviour of metallic foams. Annual Review of Materials Science. 2000; 30:191–227.

Goel M, Peroni M, Solomos G, Mondal D, Matsagar V, Gupta A, Larcher M and Marburg S. Dynamic compression behaviour of cenosphere aluminium alloy syntactic foam. Materials and Design. 2012; 42:418–423.

Goldsmith W and Sackman L. An experimental study of energy absorption in impact on sandwich plates. International Journal of Impact Engineering. 1992; 12:241–262.

Graff K. Wave Motion in Elastic Solids. Clarendon Press. Oxford, UK; 1991.

Grenestedt J. Influence of imperfection on effective properties of cellular solids. Material Symposium Proceedings. 1998; 1521:3929–3935.

Gubicza J, Juhasz A, Tasnadi P, Arato P. and Voros G. Determination of the hardness and elastic modulus from continuous Vickers indentation testing. Journal of Materials Science. 1996; 31:3109–3114.

Gupta N and Woldesenbet E. Micro-balloon wall thickness effects on properties of syntactic foams. Journal of Cellular Plastic. 2004; 40:461–480.

Gupta N and Ricci W. Comparison of compressive properties of layered syntactic foams having gradient in microballoon volume fraction and wall thickness. Materials Science and Engineering A. 2006; 427:331–342.

Gupta N, Raymond Y and Maurizio P. Comparison of tensile and compressive of vinylester /glass microballoon syntactic foams. Composites B. 2010; 4:236–245.

Hanssen G, Enstock L and Langseth M. Close-range blast loading of aluminium panels. International Journal of Impact Engineering. 2002; 27:593–618.

Hassan M, Guan Z, Cantwell W, Langdon G and Nurick G. The influence of core density on the blast resistance of foam-based sandwich structures. International Journal of Impact Engineering. 2012; 50:9-16.

Hibbitt, Karlsson, Sorensen. Abaqus/CAE user's Manual (6.12): Dassault Systèmes Simulias Corp., Providence, RI, USA; 2012.

Hibbitt, Karlsson, Sorensen. Abaqus theory Manual (6.12): Dassault Systèmes Simulias Corp., Providence, RI, USA; 2012.

Hopkinson B. A method of measuring the pressure in the deformation of high explosives or by the impact of bullets. Philosophical Transactions of the Royal Society. 1914; A213:437–452.

Hsiao M. and Daniel M. Strain rate behaviour of composite materials. Composites B. 1998; 29:521–533.

Iannace F, Iannace S, Caprino L and Nicolas L. Prediction of impact properties of polyolefin foams. Polymer Testing. 2001; 20:643–647.

Igra O, Falcovitz J, Houas L and Jourdan G. Review of methods to attenuate shock/blast waves. Progress in Aerospace Science. 2013; 58:1–35.

Jacob N., Yuen S, Nurick G, Bonorchis D, Desai S, Tait D. Scaling aspects of Quadrangular plates subjected to localised blast loads – experiments and predictions. International Journal of Impact Engineering. 2004; 30:1179–1208.

Kaiser M. Advancements in the split Hopkinson bar test. Polytechnic institute and state. 1998:1–79.

Kiser M, He M and Zok F. The mechanical response of ceramic micoballoon reinforced aluminium matrix composites under compressive loading. Acta Materialia. 1999; 47:2685–2694.

Kolsky H. An investigation of the mechanical properties of materials at very high rates of loading. Proceedings of the Physical Society. 1949; 62:676–700.

Kudo K. Overseas trends in the development of human occupied deep submersibles and a proposal for Japan's way to take. Science and Technology Trends Quarterly Review. 2008; 26:104–123.

Langdon G, Karagiozova D, Theobald D, Nurick G, Lu G and Merrett P. Fracture of aluminium foam core sacrificial cladding subjected to air-blast loading. International Journal of Impact Engineering. 2010; 37:638–651.

Lee B, Song J and Ward J. Failure of Spectra Polyethylene Fiber-Reinforced Composites under Ballistic Impact Loading. Journal of Composite Materials. 1994;28:1202-1226.

Li Z and Lambros J. Determination of the dynamic response of brittle composites by the use of the split Hopkinson pressure bar. Composites Science and Technology. 1999; 59:1097–1107.

Loehnert S, Krstulovic-Opara L, Vesenjak M and Muller-Hoeppe D. Homogenization principle based multi-scale modelling of cellular structures. Journal of the Serbian Society for Computational Mechanics. 2010; 4:97–109.

Lopatnikov L and Cheng H. Variational formulation of fluid infiltrated porous material in thermal and mechanical equilibrium. Mechanics of Materials. 2002; 34:685–704.

Lopatnikov S, Gama B, Haque Md, Krauthauser C, Gillespie J, Guden M and Hall I. Dynamic of metal foam deformation during Taylor cylinder-Hopkinson bar impact experiment. Composites Structures. 2003; 61:61-71.

Luong D, Strbik III O, Hammond V, Gupta N. and Cho K. Development of high performance lightweight aluminium alloy/Sic hollow sphere syntactic foams and compressive characterization at quasi-static and high strain rates. Journal of Alloys and Compounds. 2013; 550:412–422.

Maharsia R, Gupta N and Dwayne H. Investigation of flexural strength properties of rubber and nano-clay reinforced hybrid syntactic foams. Materials Science and Engineering A. 2006; 417:249–258.

Malekjafarian M and Sadrnezhaad S. Closed-cell Al alloy composite foams: production and characterization. Materials and Design. 2012; 42:8–12.

Maire E, Fazekas A, Salvo L, Dendievel R, Youssef S, Cloetens P and Letang J. X-ray tomography applied to the characterization of cellular materials- related finite element modelling problems. Composites Science and Technology. 2003; 63:2431–2443.

Matweb. Materials Property Data; 2006.

Mays G and Smith P. Blast effects on buildings: Design of building to optimize resistance to blast loading. Thomas Telford Publications, London, UK; 1995.

MCCullough K, Fleck N, Ashby M. Unaxial stress-strain behaviour of aluminium alloy foams. Acta Materialia. 1999; 47:2323-2330.

Merlen A. and Dyment A. Similarity and asymptotic analysis for gun-firing aerodynamics. Journal of Fluid Mechanics. 1991; 225:497–528.

Mills J. Polymer Foams Handbook – Engineering and Biomechanics Applications and Design Guide. Butterworth-Heinemann, Oxford, UK;2007.

Ming Y, Ping Z and Yingqi M. Effect of particle dustering on the tensile properties and failure mechanism of hollow spheres filled syntactic foams: A numerical investigation by microstructure based modelling. Materials and Design, 2013;47:80-89.

Miyoshi T, Itoh M, Mukai T, Kanahashi H, Konzu H, Tanabe S and Higashi K. Enhancement of energy absorption in a closed-cell aluminium by the modification of cellular structure. Scripta Materialia. 1999; 41:1055–1060.

Mocko W. Dynamic properties of aluminium alloys used in automotive industry. Journal of KONES Powertrain and Transport. 2012; 19:345–352.

Mohotti D, Ngo T, Mendis P and Raman S. Polyurea Coated Composite Aluminium Plates Subjected to High Velocity Projectile Impact. 2013; 52:1-16.

Mondal D, Goel M and Das S. Compressive deformation and energy absorption characteristics of closed cell aluminium fly ash particle composite foam. Materials Science and Engineering A. 2009; 507:102–109.

Montanini R. Measurement of strain rate sensitivity of aluminium foams for energy dissipation. International Journal of Mechanical Sciences. 2005; 47:26–42.

Mukai T, Kanahashi H, Miyoshi T, Mabuchi M, Nieh G and Higashi K. Experimental study of energy absorption in a closed cell aluminium foam under dynamic loading. Scripta Materialia. 1999; 40:921–927.

Mukai T, Miyoshi T, Nakauo S, Somekawa H, Higashi K. Compressive response of a closed-cell aluminium foam at high strain rate. Scripta Materialia. 2005; 54:533-537.

Neville B and Rabiei A. Composite metal foams processed through powder metallurgy. Materials and Design. 2008; 29:388–396.

Ngo T, Mendis P, Gupta A and Ramsay J. Blast loading and blast effects on structures – an overview. Electronic Journal of Structural Engineering. 2007; 7:76–91.

Nurick G, Radford A. Deformation and tearing of clamped circular plates subjected to localised central blast loads. In: Recent Developments in Computional and Applied Mechanics: A Volume in Honour of John B. Martin. International Centre for Numerical Methods in Engineering (CIMNE): Barcelona, pp. 491–499.

Orbulov I and Majlinger K. On the microstructure of ceramic hollow microspheres. Periodica Polytechnica Mechanical Engineering. 2010; 52:89–94.

Orbulov I and Ginsztler J. Compressive characteristics of metal matrix syntactic foams. Composites A. 2012; 43:553–561.

Orbulov I. Compressive properties of aluminium matrix syntactic foams. Materials Science and Engineering A. 2012; 43:52-56.

Orbulov I and Majlinger K. Microstructure of metal matrix composites reinforced by ceramic microballoon. Materials and Technology. 2012; 46:375–382.

Orbulov I. Metal matrix syntactic foams produced by pressure infiltration – the effect of infiltration parameters. Material Science and Engineering A. 2013; 583:11–19.

Ozturk U and Anlas G. Finite element anaylsis of expanded polystyrene foam under multiple compressive loading and unloading. Materials and Design, 2011;32:773-780.

Phelan R, Weaire D and Brakke K. Computation of equilibrium foam structures using surface evolver. Experimental Mathmatics. 1995; 4:181–192.

Radford D, Deshpande S and Fleck A. The use of metal foam projectiles to simulate shock loading on a structure. International Journal of Impact Engineering. 2005; 31:1152–1171.

Radford D, McShane G, Deshpande V and Fleck N. The response of clamped sandwich plates with metallic foam cores to simulated blast loading. International Journal of Solids and Structures. 2006; 43:2243–2259.

Rajendran R. and Lee J. Blast loaded plates. Marine Structures. 2009; 22:99–127.

Rajkumar G, Krishna M, Murthy H, Sharma S, Mahesh K. Investigation of repeated low velocity impact behaviour of GFRP/Aluminium and CFRP/ Aluminium laminates. International Journal of Soft Computing and Engineering. 2012; 1:50–58.

Rohatgi P, Gupta N, Schultz B and Luong D. The synthesis, compressive properties, and applications of metal matrix syntactic foams. Journal of the Minerals, Metals, and Materials Society. 2011; 63:36–42.

Rohatgi P, Kim J, Gupta N, Alaraj S, Daoud A. Compressive characteristics of A356/fly ash cenosphere composites synthesized by pressure infiltration technique. Composites part A: Applied Science and Manufacturing. 2006; 37: 430-437.

Sable A and Deshmukh S. Preparation of metal matrix composites by stir-casting method. International Journal of Mechanical Engineering and Technology. 2012; 3:404-411.

Sahu S, Barnwal A, Mondal D and Jain P. ZA27- Sicp composite foam through liquid metallurgy technique using CaH2 as a foaming agent. Indian Foundry Journal. 2013; 59:23–29.

Schneider T, Schneider G and Greil P. Numerical modelling of the strength of highly porous aerated autoclaved concrete. Materials Research Society. 1998; 521:21–26.

Schwartz D, Shih D, Evans A and Wadley H. Porous and Cellular Materials for Structural Applications. Materials Research Society. Warrendale, Pennsylvania; 1998.

Sharma P, Kaushal O and Sharma A. Manufacturing and characterization of Al-fly ash composites. National Conference on Recent Advances in Manufacturing. Surat, India; 2011.

Shen J, Lu G, Ruan D. Compressive behaviour of closed-cell aluminium foams at high strain rates. Composites B. 2010; 41:678-685.

Simone A and Gibson L. The effects of cell face curvature and corrugations on the stiffness and strength of metallic foams. Acta Materialia. 1998; 46:3929–3935.

Siu D. Tensile Response of SiC(p) Reinforced Al Based Foam Material(MSc Thesis): University of Toronto;1999.

Song B and Chen W. Dynamic stress equilibration in split Hopkinson pressure bar tests in soft material.Experimental Mechanics. 2004; 44:300–312.

Sugimura Y, Meyer J, He Y and Bart-Smith H. On the mechanical performance of closed cell Al alloy foams. Acta Materialia. 1997; 45:5245–5259.

Sun D and Zhao Y. Static and dynamic energy absorption of Al foams produced by a sintering and dissolution process. Metallurgical and Materials Transactions B. 2003; 34:69–74.

Surace R, De Fillippis L, Ludovic A and Boghetich G. Influence of processing parameters on aluminium foam produced by space holder technique. Materials Design. 2009; 30:1878–1885.

Tan J, Reid R, Harrigan J, Zou Z, and Li S. Dynamic compressive strength properties of aluminium foams. Part I Experimental data and observations. Journal of the Mechanics and Physics of Solids. 2005; 53:2174–2205.

Tan P, Reid S, Harrigan J, Zou Z and Li S. Dynamic compressive strength properties of aluminium foams. Part I – experimental data and observations. Journal of the Mechanics and Physics of Solids. 2005; 53: 2174–2205.

Tao L, Zi D and Tian L. Analytical modelling and finite element simulation of the plastic collapse of sandwich beams with pin-reinforced foam cores. International Journal of Solids and Structures, 2008;45:5127-5151.

Tao X. Fabrication and mechanical properties of metal matrix syntactic foams, PhD thesis, University of Liverpool, 2010.

Tao X, Zhang L, Zhao Y. Al matrix syntactic foam fabricated with bimodal ceramic microspheres. Materials and Designs. 2009;30: 2732-2736.

Tao X and Zhao Y. Compressive behaviour of Al matrix syntactic foams toughened with Al particles. Scripta Materialia. 2009;61: 461–464.

Tao X, Schleyer G and Zhao Y. Indentation tests on Al matrix syntactic foams. In: Zhao, H. and Fleck, N. A. (eds) Proceedings of the IUTAM Symposium on Mechanical Properties of Cellular Materials. Springer Netherlands: Cachan: 97–104.

Teeling-Smith R and Nurick G. The deformation and tearing of circular plates subjected to impulsive loads. International Journal of Impact Engineering. 1991; 11:77–92.

Udomphol T. Aluminium and its alloys. Suranaree University of Technology, 2007.

Wadley H. Cellular metals manufacturing. Advanced Engineering Materials. 2002;4: 726–733.

Walley S. Historical review of high strain rate and shock properties of ceramics relevant to their application in armour. Advances in Applied Ceramics. Maney Publishing, Leeds; 2009.

Walsh D. Preparation of porous ceramic microsphere. Bath University, 1997.

Wei Y, Yong T, Xiaojun Y and Zhenping W. Porous metal materials for polymer electrolyte membrane fuel cell – A review. Applied Energy. 2012; 94:309–329.

Weinong W and Chen S. Split Hopkinson (Kolsky) Bar Design, Testing and Application. Springer; 2011.

Wharton R, Formby S and Merrifield R. Airblast TNT equivalence for a range of commercial blasting explosives. Journal of Hazardous Materials. 2000; 79:31–39.

Wilkins L. Mechanics of Penetration and Perforation. International Journal of Engineering Sciences. 1978; 16:793-807.

Wu H, Dou Y, Sun L, Jiang T, Ding S. and He F. Compression behaviours of cenosphere pure aluminium syntactic foams. Scripta Materialia. 2007; 56:221–224.

Wu G, Dou Z, Jiang L and Cao J. Damping properties of aluminium matrix-fly ash composites. Materials Letters. 2006; 60:2945–2948.

www.fraunhofer.de/en

Yahya M. The Blast Response of Fibre Reinforced Composites and Sandwich Structures, PhD Thesis, University of Liverpool, 2008.

Yang F. Geometrical effects in the impact response of composite structures, PhD thesis, University of Liverpool, 2010.

Zhang L. Engineering plasticity and impact dynamics. World Scientific Publishing Co, Singapore;2001

Zhang L and Zhao Y. Mechanical response of Al matrix syntactic foams produced by pressure infiltration casting. Journal of Composite Materials. 2007; 41:2105–2117.

Zhang Q, Lee P, Singh R, Wu G and Lindley T. Micro-CT characterization of structural features and deformation behaviour of fly ash/ aluminium syntactic foam. Acta Materialia. 2009; 57:3003–3011.

Zhao H, Elnasri I and Abdennadher S. An experimental study on the behaviour under impact loading of metallic cellular materials. International Journal of Mechanical Sciences. 2005; 47:757–774.

Zhao Y. Metal matrix syntactic foams: manufacture, matrix material, microstructure, modulus and more. Journal of the Minerals, Metals and Materials Society. 2011; 63:35.

Zhao Y. Porous metallic materials produced by P/M methods. Journal of Powder Metallurgy and Mining. 2013; 2:e113.

Zhao Y, Han F and Fung T. Optimisation of compaction and liquid-state sintering in sintering and dissolution process for manufacturing Al foams. Materials Science and Engineering A. 2004; 364:117–125.

Zhao Y, Tao X and Xue X. Manufacture and mechanical properties of metal matrix syntactic foams. Materials Science and Technology. Pennsylvania, 2008.

Zhao Y and Tao X. Behaviour of metal matrix syntactic foams in compression. In: Proc. Materials Science and Technology (MS&T) 2009, 1785-1794.

Zhu F, Lu G, Ruan D and Wang Z. Plastic deformation, failure and energy absorption of sandwich structures with metallic cellular cores. International of Protective Structures. 2010; 1:507–541.